

**STRUCTURAL DESIGN OF COMPOSITE ROTOR
BLADES WITH CONSIDERATION OF
MANUFACTURABILITY, DURABILITY, AND
MANUFACTURING UNCERTAINTIES**

A Thesis
Presented to
The Academic Faculty

by

Leihong Li

In Partial Fulfillment
of the Requirements for the Degree
Doctor of Philosophy in the
School of Aerospace Engineering

Georgia Institute of Technology
August 2008

**STRUCTURAL DESIGN OF COMPOSITE ROTOR
BLADES WITH CONSIDERATION OF
MANUFACTURABILITY, DURABILITY, AND
MANUFACTURING UNCERTAINTIES**

Approved by:

Professor Dewey H. Hodges, Advisor
School of Aerospace Engineering
Georgia Institute of Technology

Professor Vitali V. Volovoi
School of Aerospace Engineering
Georgia Institute of Technology

Professor Andrew Makeev
School of Aerospace Engineering
Georgia Institute of Technology

Professor Olivier A. Bauchau
School of Aerospace Engineering
Georgia Institute of Technology

Professor Ellis Johnson
School of Industry System Engineering
Georgia Institute of Technology

Date Approved: June 16, 2008

ACKNOWLEDGEMENTS

I would like to express my appreciation to all who have directly or indirectly helped me complete my thesis.

First, I would like to express my sincere gratitude to my advisor, Professor Dewey H. Hodges, for his close guidance and continuously supporting my studies at Georgia Tech. He also granted me the freedom to explore and implement new ideas. His patience and advice gave me confidence in myself and guided me through difficult times. Without his assistance, I will never be able to reach this point. Dr. Hodges has been an excellent advisor in academics but also a trusted mentor in life. The working experiences with Dr. Hodges will be an invaluable wealth in my life.

Next, I would like to thank Professor Vitali V. Volovoi. His unique and brilliant way of thinking has been influential to me. He led me to right directions for several times when I lost in complicate situations. He impressed me with his great ideas and knowledge in many areas.

I am grateful to Professor Olivier A. Bauchau for inspiring teaching, serving on my committee, and providing a wealth of knowledge relevant to this dissertation. I am privileged to have the chance to learn from a researcher of such caliber and reputation.

I would also like to thank Professor Andrew Makeev and Professor Ellis Johnson for being my thesis committee members and helping to improve my dissertation with their thoughtful advice and suggestions.

I wish to acknowledge funding for portions of this work from the Center for Rotorcraft Innovation and the Georgia Institute of Technology Vertical Lift Research Center of Excellence.

I wish to thank my classmates for helping me enjoy my graduate studies. In particular, Dr. Tianci Jiang, Huiming Song, Di Yang, and Xi Liu have been my great friends during my time in Georgia Tech. I would like to thank my group members: Dr. Chang-yong Lee, Dr. Uttam Kumar Chakravarty, Dr. Haiying Liu, Dr. Jielong Wang, Zhibo Wu, Wei-En Li, Jimmy Ho, Changkuan Ju, and Zahra Sotoudeh for their willingness to help, our insightful discussions and fruitful collaborations.

My sincere thanks also go to my parents for their unconditional love, encouragement, and support.

Last but not least, I would like to express my deepest gratitude to my husband, Dr. Chunpeng Xiao, for his company during my graduate study. His love and the happiness he brings to my life give me the strength to work hard and reach for my goals. Without his understanding and support, I would not have been able to complete this work.

TABLE OF CONTENTS

ACKNOWLEDGEMENTS	iii
LIST OF TABLES	vii
LIST OF FIGURES	viii
SUMMARY	xi
I INTRODUCTION	1
1.1 Motivation	1
1.2 Previous Work	3
1.2.1 Rotor Blade Design	3
1.2.2 Modeling of Composite Blades	6
1.2.3 Fatigue of Composite Blades	9
1.2.4 Manufacturing Uncertainty of Composite Blades	11
1.2.5 Optimization Methods of Structural Design	13
1.3 Present Work	15
1.3.1 A Critique of Current Methods	15
1.3.2 Overview	17
II ROTOR BLADE STRUCTURAL DESIGN	20
2.1 Rotor Blade Structural Analysis	20
2.1.1 Sectional Properties Analysis	20
2.1.2 Parametric Geometry Generator with a Realistic Cross-Section	24
2.1.3 Aeroelastic Analysis and Load Calculation	27
2.1.4 Stress Analysis	30
2.2 Strength-Based Fatigue Analysis	31
2.3 General Optimization Model for Blade Structural Design	34
III STRUCTURAL SIZING WITH MANUFACTURABILITY CONSTRAINTS	39
3.1 Baseline Model	39
3.2 Minimizing the Distance from Shear Center to Aerodynamic Center	43

3.2.1	The Hybrid Optimization Method	44
3.2.2	Design Results	46
3.3	Locating Both Mass and Shear Centers to Aerodynamic Center . .	50
3.4	Parametric Study and Sensitivity Analysis	51
IV	STRUCTURAL DESIGN AGAINST FATIGUE FAILURE	60
4.1	Design Methodology	60
4.1.1	Cross-Section with Nonstructural Mass	60
4.1.2	Design Objectives and Constraints	61
4.1.3	Sectional Properties Analysis	64
4.1.4	Aeroelastic Analysis and Rotor Trim	65
4.1.5	Stress and Fatigue Analysis	65
4.1.6	Optimization Procedure	67
4.2	Design Results	68
V	PROBABILISTIC DESIGN	74
5.1	Probabilistic Design Approach	74
5.1.1	Mean performance and performance variation	75
5.1.2	Reliability constraints	76
5.1.3	Monte Carlo Simulation	77
5.2	Design Objectives and Constraints with Uncertainty	78
5.3	Geometrical Uncertainty Effects	80
5.4	Design Results	85
VI	CONCLUSION AND FUTURE WORK	94
6.1	Conclusion	94
6.2	Future Work	96
	REFERENCES	99

LIST OF TABLES

1	Material Properties	41
2	Geometric parameters of the baseline layout	41
3	The sectional properties of the baseline layout	42
4	The optimization results of locating shear center to aerodynamic center	48
5	The comparison of approximate computation costs between the general GA and the proposed hybrid optimization scheme	49
6	The optimization results of locating both mass and shear centers to aerodynamic center	50
7	Design variables and feasible ranges	62
8	Parameters for Fatigue Analysis	67
9	The comparison between the initial design and the optimal design . .	73
10	The comparison of optimization results between the design with and without uncertainties	88
11	The frequencies of the optimal design	89

LIST OF FIGURES

1	Concepts and relationship associated with durability and damage tolerance	9
2	Cross-section of a composite rotor blade	13
3	Overview of variational asymptotic beam modeling procedure	21
4	The decomposition of a three dimensional blade	21
5	The structural template for the blade cross-sectional “geometry generator”	25
6	Defining a curve with control points	26
7	VABS layup convention	28
8	VABS elements	28
9	The geometry layout and the mesh of the baseline cross-section	42
10	The optimization flow chart for composite blade design with mixed continuous and discrete variables due to manufacturability constraints	45
11	The cross-sectional layout and the mesh of the optimal solution with weight factors $w=(1, 0, 0, 0)$	47
12	The contribution of each design variable to mass per unit length	53
13	The contribution of each design variable to shear center	53
14	The contribution of each design variable to torsional stiffness	54
15	The contribution of each design variable to flapwise stiffness	54
16	The contribution of each design variable to chordwise stiffness	55
17	The contribution of each design variable to mass center	55
18	Mass per unit length vs. D-spar thickness and web location	56
19	Non-dimensional SC offset from AC vs. fiber orientation in the skin and the D-spar location	57
20	Torsional stiffness vs. skin thickness and D-spar location	58
21	Non-dimensional MC offset from AC vs. D-spar thickness and D-spar location	59
22	The structural template of a typical blade cross-section with a non-structural mass	61

23	A three-bladed hingeless rotor	66
24	The DYMORE topology model of the hingeless rotor	66
25	The optimization flow chart for composite blade design with durability analysis	69
26	Optimization history of the objective function	70
27	Steady-state axial loads history at the root of the blade	70
28	Steady-state shear forces history at the root of the blade	71
29	Steady-state torsion and lag moments history at the root of the blade	71
30	Steady-state flap moments history at the root of the blade	72
31	Steady-state stress history of the critical point over the root section .	72
32	The concept of reliability and the event region of failure	76
33	The normalized equivalent stress σ_{eq} distribution over a perturbed hollow cross-sections with NACA0015 airfoil. Perturbation amplitude parameters A_1 and A_2 are 3% and 7% skin thickness, respectively. Frequency parameters f_1 and f_2 are 78.8 and 7.88, respectively. Phase angle ϕ is zero.	81
34	The normalized equivalent stress σ_{eq} distribution over the perfect section with NACA0015 airfoil	81
35	The normalized equivalent stress σ_{eq} distribution over a perturbed hollow cross-sections with NACA1415 airfoil. Perturbation amplitude parameters A_1 and A_2 are 3% and 7% skin thickness, respectively. Frequency parameters f_1 and f_2 are 78.8 and 7.88, respectively. Phase angle ϕ is zero.	82
36	The normalized equivalent stress σ_{eq} distribution over a perfect section with NACA1415 airfoil	82
37	The histogram of the minimum safety factors g_{min} of perturbed cross-sections normalized with respect to that of the perfect section (vertical thin lines are mean values 0.969 and 0.984 for sections with NACA0015 and NACA1415 airfoils, respectively.)	83
38	Possible locations of point with minimum safety factor g , mass center, and shear center for perturbed hollow cross-sections with NACA0015 airfoil	84
39	Possible locations of point with minimum safety factor g , mass center, and shear center for perturbed hollow cross-sections with NACA1415 airfoil	84

40	The flow chart of probabilistic approach for composite blade structural design	87
41	Optimization history of the objective function	89
42	Probability histogram of sectional stiffness(thick black solid line is fitted normal distribution; vertical thin dash line is mean value of the design with introduced uncertainties)	91
43	Probability histogram of the first six nonrotating natural frequencies (thick black solid line is fitted normal distribution; vertical thin dash line is mean value of the design with introduced uncertainties)	92
44	Probability histogram of the first six rotating natural frequencies (thick black solid line is fitted normal distribution; vertical thin dash line is mean value of the design with introduced uncertainties)	93

SUMMARY

A modular structural design methodology for composite blades is developed. This design method can be used to design composite rotor blades with sophisticated geometric cross-sections. This design method hierarchically decomposed the highly-coupled interdisciplinary rotor analysis into global and local levels. In the global level, aeroelastic response analysis and rotor trim are conducted based on multi-body dynamic models. In the local level, variational asymptotic beam sectional analysis methods are used for the equivalent one-dimensional beam properties. Compared with traditional design methodology, the proposed method is more efficient and accurate.

Then, the proposed method is used to study three different design problems that have not been investigated before. The first is to add manufacturing constraints into design optimization. The introduction of manufacturing constraints complicates the optimization process. However, the design with manufacturing constraints benefits the manufacturing process and reduces the risk of violating major performance constraints. Next, a new design procedure for structural design against fatigue failure is proposed. This procedure combines the fatigue analysis with the optimization process. The durability or fatigue analysis employs a strength-based model. The design is subject to stiffness, frequency, and durability constraints. Finally, the manufacturing uncertainty impacts on rotor blade aeroelastic behavior are investigated, and a probabilistic design method is proposed to control the impacts of uncertainty on blade structural performance. The uncertainty factors include dimensions, shapes, material properties, and service loads.

CHAPTER I

INTRODUCTION

In this chapter, the reader is first introduced to a brief background of rotor blade design and the motivation for this research work. Then, the previous research is summarized from composite blade modeling and analysis, composite fatigue, manufacturing uncertainty of composite structures, and optimization methods. This chapter ends with an overview of the present research and this thesis.

1.1 Motivation

The most critical parts of helicopters are main rotors, which provide thrust and lift as well as enable maneuvers. Rotor blade design is a complex coupling process, which involves several usually competing disciplines, including aerodynamics, structures, acoustics, and dynamics [86]. In fact, the blades of helicopter main rotors are slender, flexible beams. The deformation (twist and bending) of such blades changes the effective angles of attack along the blade span, resulting the change of aerodynamic forces acting on the blades. Therefore, the calculation of aerodynamic loads on the blades is a coupled process of structural deformations and air flow. Moreover, the main rotor of a helicopter in forward flight, may encounter transonic flow on the advancing blades, dynamic stall on the retreating blades, and radial flow on the front and back blades. Blade-vortex-interaction is the main source of helicopter noise. These competing disciplines are traded off by optimization techniques.

To deal with the complex rotor blade design problem, many researchers have relied on the hierarchical decomposition of the design process into global and local levels of optimization [17, 46, 53, 64, 98, 100, 107]. At the global level, the aerodynamic, acoustic, and aeroelastic behaviors of rotor blades are optimized so that the levels of

noise and vibration are reduced. On the other hand, at the local level, cross-section layouts and material distribution that provide specific sectional stiffnesses need to be determined. In addition to sectional stiffnesses, the cross-sections of rotor blades are required to satisfy other requirements. For example, the location of mass center (MC) and shear center (SC) are desired to be coincident with the aerodynamic center (AC). The blades should have sufficient fatigue life and have safe levels of stress during extreme flight conditions.

Advanced composite materials have been used in rotor blades mainly because of their high strength-to-weight ratio, but their superior damage tolerance and fatigue properties are also desirable. Another more promising aspect of composites is their anisotropy, which allows designers substantial freedom to tailor the stiffness properties of structures. Currently, rotor blade designs utilize the unique elastic tailoring of composites to improve aeroelastic response, to reduce vibratory loads, and to prolong fatigue life.

While composites provide many benefits to designers they also bring a host of new challenges to rotor blade design. One of the key problems is how to efficiently and accurately model composite blades. Fortunately, in the past decades, nonlinear anisotropic beam theory has greatly progressed. VABS (variational asymptotic beam section) [33, 15, 106], an composite beam analysis tool, has become mature. The accuracy and efficiency of VABS have proved by applications within academia and industry [96]. Another great challenge is composite fatigue analysis and fatigue life prediction. Extensive research has been conducted on various aspects from theoretical models to experimental techniques. Unfortunately, at this time, there are no systematic methods and general models available for composite fatigue analysis. In addition, composites also complicate the optimization process because they cause a large number of design variables to be introduced into design optimization, leading to increasing computational cost. The situation is further exacerbated by the fact that

many of the design variables will end up being discrete because of manufacturability constraints.

Except the challenges of analysis and design, manufactured composite structures exhibit various unique defects such as ply waviness in laminated materials, leading to the variability of sectional properties. Furthermore, the service loads of rotor blades are uncertain in reality. To compensate for the threat of uncertainty, a safety factor is set in the design process. The problem with the safety factor is that it cannot tell how safe the product will be in a specific loading condition.

This research attempts to develop an efficient and high-fidelity modular tool for composite rotor blade design. This tool optimizes the internal structure of a blade cross-section with a fixed airfoil. The blade structural properties are tailored using automated optimization techniques to reduce vibrations and stress/strain on rotor blades. Fatigue analysis are integrated into finite-element-based dynamic analysis and rotor blade structural optimization. Blade design optimization also includes manufacturability constraints so that the optimal design can be easily manufactured. Moreover, a probabilistic design based on the modular tool is proposed to improve the reliability of rotor blades. The impacts of manufacturing uncertainty, including dimensions, geometry, material properties, and service loads, are investigated in this work. This modular tool will assist with rotorcraft industry to shorten design cycle. By using the probabilistic design, designers can foresee the potential hazard of the design in the early stage and the quality of the products with given manufacturing condition.

1.2 Previous Work

1.2.1 Rotor Blade Design

Main rotor blades are slender, flexible beams. The rotating blades deform structurally and interact with unsteady air flow and control systems. To deal with this complex

multidisciplinary design, many researchers have employed optimization techniques to trade off among the disciplines of aerodynamics, dynamics, structure, acoustics, and control. Optimization methods were introduced to helicopter design from the early 1980s [62]. Friedmann [24] summarized the early research of vibration reduction on helicopters using structural optimization. Celi [14] and Ganguli [26] provided further reviews of rotorcraft design optimization. A more recent review of multidisciplinary design of rotor blades can be found in Ref. [49].

Yuan and Friedmann [107] and Ganguli and Chopra [25] focused on forward flight vibratory load reduction at the hub subject to frequency and aeroelastic stability constraints. Kim and Sarigul-Klijn [45, 46] developed a multidisciplinary optimization method that strived for minimum weight and vibration and maximum material strength of the blade with a constraint to avoid flutter. Soykasap [87] focused on aeroelastic optimization for composite tilt rotor blades. Ozbay [65] investigated the potential of the star cross-section to tailor extension-twist coupling for tilt-rotor blades.

To deal with the complex rotor blade design problem, many researchers have relied on the hierarchical decomposition of the design process into global and local levels of optimization [17, 46, 53, 64, 98, 100, 107]. Walsh et al. [100] integrated aerodynamics, dynamics and structural models into the rotor blade design optimization using a multilevel decomposition method. The objective of the global level is to satisfy the global performance requirements such as thrust, frequencies, and aeroelastic stability. These global objectives for the blades can be translated into specific requirements on their sectional properties, such as stiffnesses, moments of inertia, stress levels, and locations of shear and/or mass center. The cross-sections that satisfy these requirements are found at the local level. Moreover, the blade structures are required to meet the safety regulations enforced by FAA [1, 2] and ADS-27. The sectional properties

are a small set of parameters compared to the complete set of geometric and material parameters associated with the cross-section. They serve as interface parameters between the two levels, and thus simplify the whole design optimization, allowing for modularization of design process. An efficient and high-fidelity modular tool can significantly improve blade aeroelastic characteristics and reduce the computational effort for the entire design cycle.

The optimization model includes design objectives, constraints, assumptions, and variables. Currently, in rotor blade structural design, it is quite popular to assume a specific topology of structural components inside a given airfoil shape. This sort of assumption reduces the problem to a sizing optimization in which one varies dimensions, orientations, and locations of structural components to achieve the desired sectional properties. For example, Ganguli and Chopra [25] varied skin thickness and fiber orientations of a two-celled cross-section in order to obtain cross-sectional stiffnesses for aeroelastic optimization of helicopter rotor blades. In order to satisfy the cross-sectional stiffness requirements, Orr and Hajela [64] considered a multi-cellular cross-section with strengthened flanges in a multi-disciplinary tiltrotor design. Volovoi et al. [67, 98, 99] assumed a cross-section with a D-spar and varied thicknesses, fiber orientations, and D-spar locations to maintain the shear center and stiffness values within a target range. Lemanski et al. [54] made similar use of a “C” wall and a channel spar.

On the other hand, some researchers did not assume any specific connectivity and designed the cross-section layout from scratch. This design concept is called “topology optimization.” [81] Using this concept, Fanjoy and Crossley [22] minimized the distance between the shear center and point of load application for a given airfoil; but, as the authors pointed out, the computational load was significant. Arora and Wang [7] reviewed alternative formulations for optimization of structural and mechanical systems, including configuration and topology design, and discussed features of

various formulations. Compared to sizing optimization, topology optimization provides innovative cross-section layouts that can meet sophisticated requirements for sectional properties. However, the resulting layouts from topology optimization need to be refined by sizing or shape optimization [81]. As computing capability increases continuously, topology optimization is attracting more attention.

1.2.2 Modeling of Composite Blades

Modern rotorcraft utilize composite materials to optimize the aeroelastic performance of rotor blades. Composite rotor blades are generally modeled as initially curved and twisted anisotropic beams. One of the critical steps of blade analysis is to generate the equivalent 1D sectional properties from a blade 3D model. The flexible beams of rotor blades undergo elastic deformations in bending and torsion. In normal operating conditions, the deformations can be beyond the limits of linear beam theories. Thus, moderately large nonlinear deformations need to be taken into account. Numerous state-of-art composite blade modeling techniques have been proposed in the past two decades. Hodges [35] reviewed the early stage of modeling techniques of composite rotor blades. Yu [104] summarized more recent work on composite structure analysis. In this section, the analysis models that have been applied to design optimization are summarized.

Walsh et al. [100] used a thin-walled, box-beam model with isotropic materials in the local level optimization of helicopter blade design. Because isotropic, thin-walled, box-beams have simple closed-form formulations for cross-sectional properties, this choice reduces the iteration time of design optimization. Instead of isotropic materials, Lee and Hajela [53] used laminated composite materials with a box-beam model in multi-disciplinary rotor blade design. To improve the optimization efficiency, they applied a parallel implementation of the genetic algorithm (GA). The leading and trailing parts of the airfoil section were not accounted for, leading to a reduction in the

accuracy of the cross-sectional properties. Furthermore, when laminated composite (i.e. anisotropic) materials are used in design, the computational advantage of the box-beam model becomes marginal.

To improve the accuracy of section analysis, designers have tried more advanced theories and methods. Smith and Chopra [85] developed a Vlasov model, an analytical beam formulation, for predicting the effective elastic stiffness and load deformation behavior of composite box-beams. Deformation of the beam is described by extension, bending, torsion, transverse shearing, and torsion-related warping. Ganguli and Chopra [25] applied the Vlasov model to two-cell composite blades for aeroelastic optimization of a helicopter rotor. Orr and Hajela [64] adopted classical beam theory and thin-walled, multi-celled beam theory to bending and torsional stiffness analysis, respectively, for composite tiltrotor blade design.

Wörndle [101] formulated a two-dimensional (2D), finite-element-based procedure to determine shear center and warping functions. Lemanski et al. [54] used 3D FEM procedure to analyze sectional properties of composite blades with realistic cross-sections. Although 3D FEM is the most accurate approach to model realistic rotor blades, it is not appropriate for preliminary design because of the large computational overhead.

VABS is another section analysis tool. The concept of VABS was first proposed by Hodges and his co-workers [33], and VABS is continually updated by the recent research results of anisotropic beam theories [15, 95, 105, 106]. The mathematical basis of VABS is the variational-asymptotic method [10], through which the general 3D nonlinear elasticity problem of a beam-like structure is split into a 2D linear cross-sectional analysis and a 1D nonlinear beam analysis. VABS is capable of capturing the trapeze and Vlasov effects and calculating the 1D sectional properties with transverse shear refinement for any initially twisted and curved, inhomogeneous, anisotropic beam with arbitrary geometry and material properties. In addition, VABS

can provide 3D stress and strain fields so that one can study stress concentrations and interlaminar stresses. The accuracy of stresses recovered using VABS is comparable to that of standard 3D FEM for sections that are not close to discontinuities or to the ends of the beam, but with far smaller computing requirements [106]. The specific theory and formulation of VABS can be found in [34].

Paik et al. [67] first attempted to use VABS to design a cross-section layout for a composite blade. Volovoi et al. [98, 99] improved the methodology of cross-section design and utilized this methodology for frequency placement in the design of a four-bladed rotor. Li et al. [56] expanded the cross-section design to include manufacturing constraints. Cesnik et al. [16] proposed a design framework of active twist rotor blades using VABS. Patil and Johnson [68] developed closed-form formulations for cross-sectional analysis of thin-walled composite beams with embedded strain actuation. Volovoi et al. [96] compared recent composite beam theories for rotor blade application, and VABS achieved the best match with experimental results.

Once the sectional analysis model has been determined, another challenging task is to develop a parametric mesh generator that can rapidly generate a precise layout with appropriate mesh given values of the design variables. Generally, a flexible definition of geometry can be provided by CAD software, but a smooth transfer of the geometric definition from CAD to FEM is presently very cumbersome and prohibitively expensive from the computational standpoint. In recent years, many efforts have been made in an attempt to improve this communication. Those efforts include STEP project (ISO 10303) for a robust neutral file exchange, as well as proprietary products such as “Design Space” from ANSYS [4]. Another method of parametrically varying the geometry in FEM applications involves direct manipulation of the mesh. For example, in Hyperworks the mesh is altered by automatically moving the nodes in the existing mesh. In order to maintain fitness of the mesh, Hyperworks restricts changes in the geometric configuration [42].

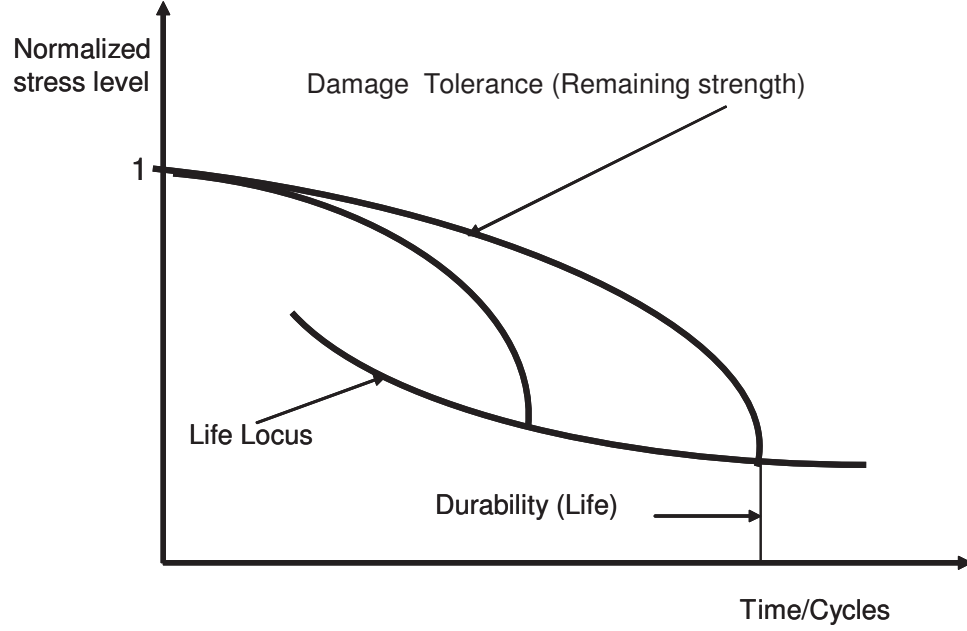


Figure 1: Concepts and relationship associated with durability and damage tolerance

1.2.3 Fatigue of Composite Blades

Another critical and complicated problem is a proper modeling of fatigue damage and durability of composite materials. Durability is relative to the life of a component or material, while damage tolerance is a discussion of how much strength is left after some periods of service and history of load application [79]. Figure 1 shows the relationship of durability and damage tolerance [79]. Because vibration is a key issue of rotor systems, the fatigue life of rotor blade under vibratory loads is mainly concerned for the durability analysis.

Fatigue behavior of laminated materials is governed by many parameters. These parameters include fiber and matrix type, fiber volume fraction, fiber orientation, layer thickness, the number of layers, and the stacking sequence. Rotor blades made of such materials exhibit various competing fatigue modes such as delamination, fiber matrix debonding, fiber breakage, fiber pull-out, and matrix cracking. In addition, fatigue life of laminated materials highly depends on fabrication methods and environmental factors. Currently, the existing fatigue models for fiber-reinforced composites

can generally be classified into fatigue life models (S-N curves), damage accumulation models, and phenomenological residual stiffness/strength models [19].

The damage accumulation models are usually associated with a specific failure mode, such as matrix cracking. Tan and Nuismer [89] studied progressive matrix cracking of composite laminates with a crack in 90° ply subject to uniaxial tensile or shear loading. They obtained closed-form solutions for laminate stiffnesses and Poisson's ratio as a function of crack density or load level using a fracture mechanics approach and elasticity theory. Flaggs and Laws [23] presented a simple mixed mode analysis model for prediction tensile matrix failure using a strain energy release rate fracture criteria and an approximate two-dimensional shear-lag model. Fatigue life prediction based on this model required an input from non-destructive inspection tests.

Phenomenological fatigue models generally define damage in terms of macroscopically measured properties such as strength or stiffness. These models utilize stress-life fatigue data traditionally generated for design. The multi-axial loading problem is often handled by introducing a static failure criterion (e.g. Tsai-Wu, Tsai-Hill) and replacing the static strengths with the residual strengths in the criterion [43]. Schaff [84] integrated a strength-based fatigue model with finite element analysis and applied to a helicopter tail rotor spar. The drawback of this approach is that the fatigue strengths must be determined experimentally for different stress amplitudes, stress ratios and bi-axial ratios [66]. Moreover, phenomenological models neither predict the initiation or growth nor indicate the mechanisms of fatigue damage.

Due to the lack of a systematic approach for composite fatigue analysis, relatively little research has been conducted to facilitate the integration of the fatigue analysis into design optimization.

1.2.4 Manufacturing Uncertainty of Composite Blades

Imperfections in structures are undesirable because such imperfections can substantially influence the response of aircraft structures [73, 58, 77]. Therefore, manufacturers spend immense effort in improving product quality and reliability, especially in the aerospace industry. Although the aerospace engineering production process is better controlled than other industries, small variations inevitably exist in structural dimensions, geometric shape, and material properties. Moreover, the application of composite materials to aircraft causes a host of new challenges because composite structures compared to metallic structures, exhibit different behavior, defects, and failure modes. Thomsen [90] discussed the potential advantages and challenges of using composite materials in wind turbine blades. Pettit [72] presented a comprehensive survey of uncertainty analysis in aeroelasticity. However, as known to the author, those efforts on uncertainty analysis in aeroelasticity are related to fixed-wing aircraft [47, 72, 77], little work is related to aircraft[63].

The manufacturing uncertainty associated with composite blades can be classified into three categories: structural dimension variations, geometric shape uncertainty, and material property variability. The nominal material properties of composites used in the structural design are uncertain because of manufacturing process and lack of precise experiments [88]. In fact, the manufacturing process can significantly influence the in-service performance of a composite structural component [28, 40, 58, 103]. In general, the normal and Weibull distribution [48] is used to study material strength in tension and fatigue [48]. Assuming that the material properties satisfy normal distributions, d’Ippolito et al. [20] studied the static performance of a composite wing, whereas Murugan et al. investigated aeroelastic response of composite helicopter rotor blade.

Structural dimension variations are generally perturbations around the given values of design variables in sizing problems. As a result, structural performance changes

due to variations in dimension can be explored mathematically derivative or by means of design of experiment (DOE) [102]. Using analytical sensitivity derivatives, Rais-Rohani and Xie [78] examined the influence of design variables on the reliability of wing-spar structures. Using DOE, Li et al. [56] explored the sectional properties of a rotor blade. For the convenience of quality control, the structural dimension is denoted as $Z_{-\Delta l}^{+\Delta u}$. Here, Z means the exact value, $\Delta u + \Delta l$ is manufacturing tolerance that measures the variability of the value. The dimension upper bound of the products is $Z + \Delta u$, and the lower bound is $Z - \Delta l$.

In probabilistic design (reliability-based design and/or robust design), structural dimensions are usually assumed to be random variables that follow normal distributions. In such a setting, the expectation usually corresponds to the designed value, and the variance is estimated by the standard deviation decided by manufacturing tolerance [32]. For a structural dimension specified as $Z_{-\Delta l}^{+\Delta u}$, the standard deviation can be estimated as

$$\tilde{\sigma} = \frac{\Delta u + \Delta l}{F} \quad (1)$$

where parameter F depends on sample size or the number of parts produced. For example, for the number of parts equal to 25, $F = 4$, whereas $F = 5$ for the number of parts equal to 100. Equation (1) provides a connection between manufacturing tolerance and structural reliability.

Using this approach as well as the assumption of independence, d'Ippolito et al. [20] assessed the fatigue performance of a steel slate track with four random variables. Meanwhile, they used Latin Hypercube sampling to shorten the computation time in their research. Rais-Rohani and Xie [78] explored the influence of different probability distribution assumptions for random variables on wing-spar reliability-based design, but they did not mention which assumption was closer to manufacturing reality.

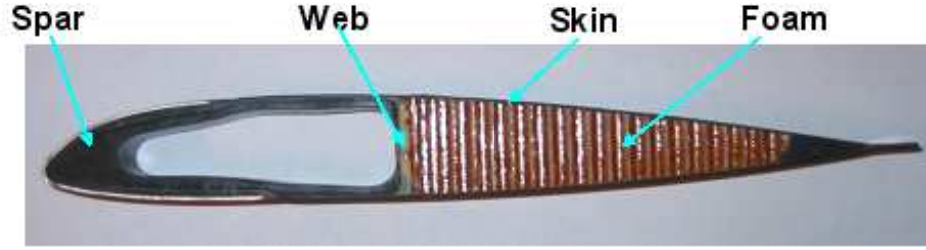


Figure 2: Cross-section of a composite rotor blade

As discussed above, structural dimension variations are relatively easy to deal with in that only design variables are perturbed. In addition to adding perturbation to design variables, the description of geometric shape uncertainty requires the introduction of new variables. For instance, the outer surface of a realistic composite rotor blade, shown in Figure 2 is very smooth, whereas the inner surface and the intersurface between the skin and the filled core are wavy instead. Indeed, this wavy structure is one of the most common phenomena in realistic composite structures. The waviness occurring to the inner surface of laminates is called “ply waviness”, which has been extensively studied [11, 76, 13, 55, 31, 27]. Ply waviness can be seriously harmful, for it can greatly reduce the stiffness and the strength of a composite structural component, especially the compressive performance [11, 76, 13].

Imperfections introduced in manufacturing processes as well as loading conditions during service lead to structural design uncertainty. To ensure efficient and reliable blade designs with low cost, uncertainty or randomness need to be accounted for in the optimization procedure for blade design.

1.2.5 Optimization Methods of Structural Design

In addition to complicating the modeling process, composite materials also provide many opportunities as well as challenges in the optimization of rotor blade design. Composite materials can have a wide range in the ratio of Young’s modulus to shear modulus. Furthermore, one can adjust the fiber orientations or stacking sequence

along with ply thicknesses to implement elastic tailoring. However, introducing a large number of variables associated with composite materials complicates the design optimization process and leads to increasing computational cost. The situation is further exacerbated by the fact that many of the design variables will end up being discrete because of manufacturing constraints such as those imposed on the minimum ply thickness (increments of 0.005 in.) [54] and fiber orientation (increments of, say, 5°). Because of the effects of fiber orientation or stacking sequence, the design space of cross-section optimization problems is highly nonconvex. Therefore, to develop the modular tool for cross-section design, it is necessary to require that the optimization algorithm converge rapidly and be able to handle problems with a mix of continuous and discrete variables.

The structural design of rotor blades is a nonlinear optimization problem. Available optimization algorithms for nonlinear problems can be categorized into gradient-based and nongradient methods. Arora and Wang [7] reviewed alternative optimization formulations and discussed gradient-based optimization techniques for structural and mechanical systems. Hajela [30] provided a general overview of nongradient methods in the optimal design of multidisciplinary systems, including the genetic algorithm (GA) and simulated annealing (SA). Coello [18] discussed application of GA in constrained optimization, and Trosset [91] explained application of SA in detail. Gradient-based methods such as sequential quadratic programming (SQP) converge to an optimal point much more rapidly than nongradient methods. Because gradient-based methods need derivative information to decide a next point from the current point, they can only be applied to continuous problems. Moreover, for an optimization problem with nonconvex spaces, gradient-based methods do not provide a direct means for finding the global optimum. Nongradient methods can handle design optimization problems with a mix of continuous, discrete, or integer design variables.

Volovoi et al. [99] compared the performance of SQP and GA when applied to cross-section design. However, the convergence speed of nongradient methods is extremely slow to obtain the sufficient precision of continuous variables. Furthermore, the resulting optimal solutions from non-gradient methods are not guarantee to be global optimum theoretically. Therefore, both of the two categories are not appropriate for the large-scale rotor blade design with mixed continuous and discrete variables.

Another algorithm that can deal with discrete optimization is branch and bound [51, 52]. The procedure of branch and bound is to solve a continuous variable problem first, and its solution is considered as upper or lower bound of the mixed problem dependent on concavity or convexity. Then, the mixed-variable problem is branched by raising or decreasing one of the discrete variable to its next discrete value. The bounding procedure is performed by recursively solving a sub-problem with the remaining variables. Such branching and bounding procedures keep continuing until the optimum is obtained. Theoretically, the method of branch and bound can find the global optimum, but the programming of this method is very complicate. Another disadvantage of this approach is that a multitude of nonlinear optimization sub-problem must be solved [94]. The efficiency of this method depends critically on the effectiveness of the branching and bounding algorithm. Bad choices could lead to repeated branching until the sub-region becomes very small.

1.3 Present Work

1.3.1 A Critique of Current Methods

While the application of composites provide many opportunities to improve aircraft flight performance, the application of composites introduces a host of new challenges to researchers. Although rotor blades are designed with the properties of composites in mind, their full potential is far from being explored. The primary reason is that

analysis methods for predicting the behavior of composite blade have not been validated to the point where the industry is comfortable to use them. Therefore, most rotor blade design optimization employs a simplified box-beam model. The results of such design is not accurate enough. Many necessary analyses and simulations have to be conducted after optimization. Once the detailed analysis denies a design resulting from the optimization, the design cycle has to start again. Therefore, the blade design requires a relatively long cycle.

Previous efforts focusing on composite blade design ignored manufacturability constraints so that the optimization was only dealt with continuous variables. As a result, the optimal designs are difficult to implement in reality. In order to manufacture such a blade, engineers will naturally round the ply angles and/or ply thicknesses from the optimal solution to the closest ones that can be manufactured. This intuitive rounding approach runs the risk of violating the structural requirements. To avoid such potential risks and facilitate the manufacturing, a better way is to improve the structural design optimization model by adding manufacturability constraints. Thus, the resulting design optimization become an optimization problem with mixed discrete continuous variables. However, the available single optimization algorithms can not handle such nonlinear and non-convex structural optimization efficiently. The algorithms that is feasible to mix-variable problems require a large number of function evaluation, leading to low convert speed.

The vibration and fatigue of main rotor blade has been a key issue in helicopter design for a long time. Numerous research work has focused on the reduction of vibratory loads for rotor blades through structural optimization methods. However, in traditional design practice, fatigue analysis is ignored during the structural optimization and only conducted at a later stage of the design cycle. The drawback is that the resulting blade may have short fatigue life and high life cycle cost. Life cycle cost is an important factor of customers' decision. If the life cycle cost is too high,

the blade is not competitive in the market. The blade structure has to be redesigned, leading to a long development cycle.

Imperfections are inevitably introduced in manufacturing processes. As a result, structural dimensions, shapes, and material properties deviate from their desired values. Such deviations can substantially influence the performance of the aircraft structure. In recent years, such potential hazard have been realized by many researchers. Much work has been conducted to investigate and quantify the effects of uncertainties on the global response of fixed-wing aircraft. However, little work has been done on composite helicopter rotor blades. The primary reason is short of an efficient and high-fidelity tool. The uncertainty of structures and materials are small in aerospace industry due to the strict quality control. The tool must be capable of capturing the small changes of blade structure performance resulting from the small perturbations. To investigate and quantify the uncertainty influence, stochastic methods have to be employed that generally require thousands and millions of simulations to obtain confident solutions. Therefore, an efficient and high-fidelity tool is vital for this task.

1.3.2 Overview

In the past two decades, composite blade modeling has substantially improved. Particularly, VABS has become mature and its accuracy and efficiency have been accepted in academic and industry. The objective of this thesis is to develop an efficient and high-fidelity modular method for composite rotor blade design. This method includes an efficient reliable cross-sectional analysis tool, VABS, and a parametric geometry generator. The geometry generator can generate a typical realistic cross-section for helicopter blades, and the VABS tool can best achieve the balance between the accuracy and efficiency for rotor blade analysis. Based on this design tool, three comprehensive design procedures for composite rotor blades are proposed. The first one is to

incorporate manufacturing constraints into the design optimization. The next is a design method that integrates fatigue analysis into current rotor blade structural design optimization. Finally, the manufacturing uncertainty influence on rotor blade design is explored and a probabilistic design method is proposed to manage the uncertainty of blade structural performance.

The principal reason for the success of the modular design method is the use of VABS. VABS is capable of handling composite beams with initial curvature and twist as well as with realistic cross-sections. In chapter 2, we summarize the rotor blade structural analysis, including the fundamental theory of VABS, the 3D stress recovery relationship, the parametric geometry generator, and the coupling procedure of the aeroelastic response and rotor trim. Next, a strength degradation fatigue model is discussed. This fatigue model does not require microscopic information of fatigue progress and is easily incorporated into the proposed structural design method. Finally, we summarize a general optimization model for rotor blade structural sizing problems.

In chapter 3, the blade structural sizing with manufacturing constraints is explored. Such sizing optimization requires an algorithm that can handle a mixed-variable problem and provide a balance between efficiency and quality. Thus, a hybrid optimization procedure is developed. This procedure combines the rapid convergence advantage of sequential quadratic programming and the capability of mixed-variable of generic algorithm. Although the optimal result may not be the global optimum, the solution improves a lot relative to the baseline. We also investigate the effects of design variables on sectional properties. The method of design of experiments is employed to find the main factors for structural sizing.

In chapter 4, a VABS-based design method is presented that integrate fatigue analysis in structural optimization. The method is demonstrated by a three-blade hingeless rotor blade design. In the design, the frequencies of the rotor blades are

separated from the excitation frequencies of harmonic aerodynamic loads. The blade is sized to provide required structural properties so that the aeroelastic performance is improved. The aerodynamic loads are predicted by DYMORE, a FEM-based multi-body dynamic analysis tool. Once the aerodynamic loads are obtained from the converged trim solution, fatigue analysis is conducted based on a strength degradation model.

In chapter 5, the VABS-based design approach is integrated with Monte Carlo Simulation. The effects of blade shape uncertainty on blade structural characteristics is investigated. The shape uncertainty is assumed to follow harmonic functions according to one of the defect natures of composite structure. After the statistical information has been collected from the simulation, a probabilistic design approach is developed to improve the reliability of the blades. The comprehensive effects, resulting from shape, dimension, material, and service loads uncertainties, are investigated as well.

Chapter 6 summarizes the conclusions of the thesis and future work.

CHAPTER II

ROTOR BLADE STRUCTURAL DESIGN

2.1 Rotor Blade Structural Analysis

2.1.1 Sectional Properties Analysis

Helicopter rotor blades are generally modeled as initially curved and twisted beams. The calculation of the equivalent 1D beam properties is one critical aspect of rotor dynamic analysis. For this purpose, the sectional analysis of composite blades is conducted by VABS [33, 15, 106]. VABS, as an alternative to 3D FEM and with substantial reduction in computational cost for a given level of accuracy, is capable of modeling initially curved and twisted, non-homogeneous anisotropic beams with arbitrary cross-sectional configurations.

The mathematical basis of VABS is the variational-asymptotic method (VAM) [10], through which a complex 3D model is replaced by a reduced-order model in terms of asymptotic series of certain small parameters inherent to the structure. The methodology is demonstrated in Figure 3. For rotor blades, one can use the VAM to split the original nonlinear 3D formulation into a 2D, linear, cross-sectional analysis and a 1D nonlinear beam analysis for the reference line with the help of small geometrical parameters a/l and a/R (where a is the characteristic size of the section, l the characteristic wavelength of deformation along the beam axial coordinate and R the characteristic radius of initial curvatures and twist of the beam.). Figure 4 demonstrates the idea of blade decomposition. A 1D constitutive law represented by the stiffness matrix S can be obtained from the cross-sectional analysis. The original 3D results can be recovered knowing the global deformation from the 1D beam analysis and the warping field from the 2D cross-sectional analysis [104].

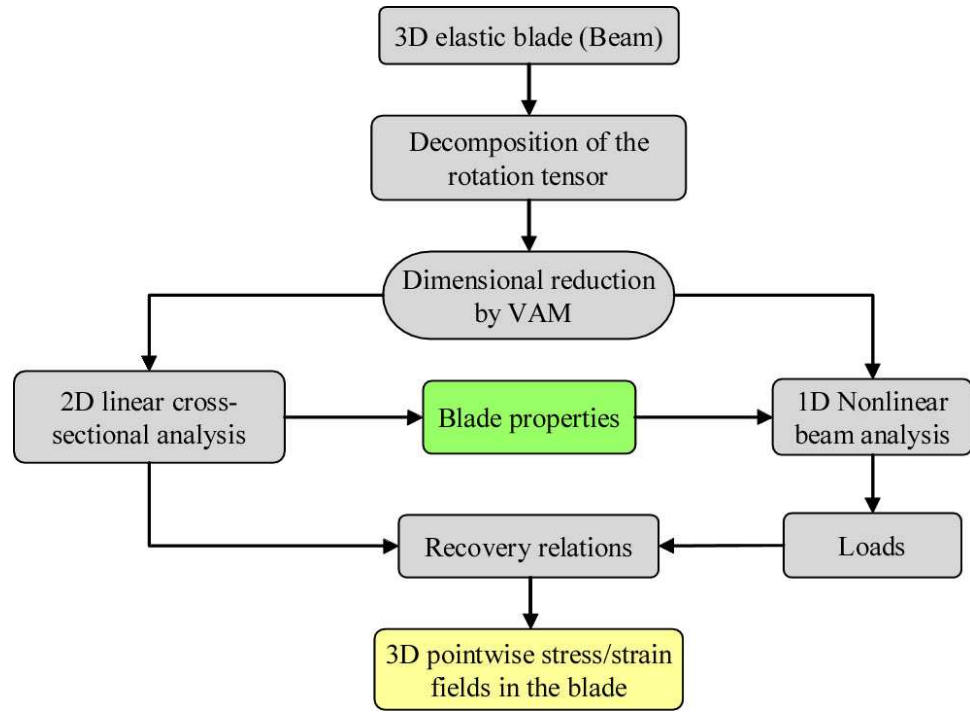


Figure 3: Overview of variational asymptotic beam modeling procedure

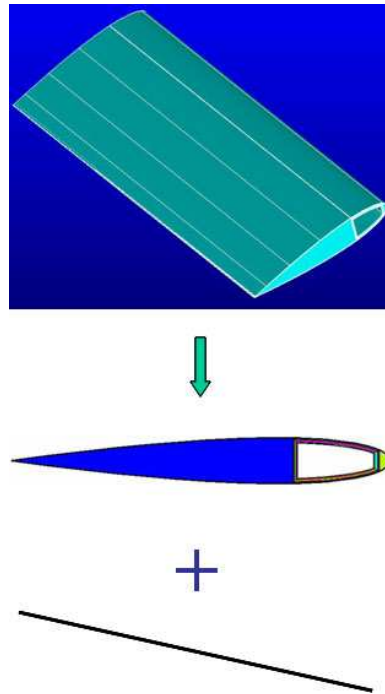


Figure 4: The decomposition of a three dimensional blade

VABS analysis formulations are derived by energy methods. The strain energy of the cross-section, or the strain energy per unit length of a beam, can be written as

$$U = \frac{1}{2} \int_A \Gamma^T D \Gamma \sqrt{g} dydz \quad (2)$$

where D is the 6×6 symmetric material matrix in a local Cartesian system of an undeformed beam, and g is the determinant of the metric tensor for the undeformed state. The 3D strain components are represented by the matrix

$$\Gamma = [\Gamma_{11} \ 2\Gamma_{12} \ 2\Gamma_{13} \ \Gamma_{22} \ 2\Gamma_{23} \ \Gamma_{33}]^T \quad (3)$$

The static 3D elastic beam problem is to minimize the strain energy of the cross-section given in Equation (2) by varying the warping displacements. The warping displacements w_i ($i = 1, 2, 3$) must satisfy the following constraints:

$$\int_A w_i dydz = 0, \quad i = 1, 2, 3 \quad (4)$$

$$\int_A (y w_3 - z w_2) dydz = 0 \quad (5)$$

where y and z are coordinates of points at the cross-section. Equations (4) and (5) imply that the warping does not contribute to the rigid-body motions of the cross-section. By using the VAM, the strain energy can be expressed by a series of asymptotically correct energy terms that correspond to different orders of the small parameter inherent in a beam.

$$U = U_0 + U_1 + U_2 + \cdots \quad (6)$$

where U_0 , U_1 , and U_2 are zeroth-order, first-order, and second-order approximations of the strain energy.

The second-order asymptotically correct energy accounts for the effects of initial twist and curvature. Once the first-order approximation of warping function is obtained, the strain energy is asymptotically correct through second-order approximation and can be expressed in terms of the generalized Timoshenko beam strain measures. By differentiating with respect to the generalized Timoshenko 1D strain measures, one can obtain the 1D constitutive law and the cross-sectional stiffness matrix, shown in Equation (7).

$$\begin{pmatrix} F_1 \\ F_2 \\ F_3 \\ M_1 \\ M_2 \\ M_3 \end{pmatrix} = \begin{bmatrix} S_{11} & S_{12} & S_{13} & S_{14} & S_{15} & S_{16} \\ S_{12} & S_{22} & S_{23} & S_{24} & S_{25} & S_{26} \\ S_{13} & S_{23} & S_{33} & S_{34} & S_{35} & S_{36} \\ S_{14} & S_{24} & S_{34} & S_{44} & S_{45} & S_{46} \\ S_{15} & S_{25} & S_{35} & S_{45} & S_{55} & S_{56} \\ S_{16} & S_{26} & S_{36} & S_{46} & S_{56} & S_{66} \end{bmatrix} \begin{pmatrix} \gamma_{11} \\ 2\gamma_{12} \\ 2\gamma_{13} \\ \kappa_1 \\ \kappa_2 \\ \kappa_3 \end{pmatrix} \quad (7)$$

where F_i and M_i ($i = 1, 2, 3$) are three forces and three and moments, respectively; and γ_{1i} and κ_i are the 1D strains and the curvature and twist measures of a beam, respectively. The matrix S is called the generalized Timoshenko stiffness matrix.

To obtain the generalized shear center location, we need to find a point with coordinates (ξ_2, ξ_3) through which any arbitrary transverse force results in zero twist.

$$\xi_2 = -\frac{\Phi_{34}}{\Phi_{44}} + \frac{\Phi_{45}}{\Phi_{44}}(L - x) \quad (8a)$$

$$\xi_3 = -\frac{\Phi_{24}}{\Phi_{44}} + \frac{\Phi_{46}}{\Phi_{44}}(L - x) \quad (8b)$$

where L and x are the length of a beam and the coordinate of the beam along the axis. Φ_{ij} are components of the flexibility matrix Φ , the inverse matrix of the generalized

Timoshenko matrix S in Equation (7).

For beams in which the bending-twist couplings vanish ($\Phi_{45} = \Phi_{46} = 0$), the shear center is a cross-sectional property independent of x . In such a case, choosing the locus of the shear centers as the beam reference line decouple not only shear and twist but bending and twist as well. For composite beams, generally, Φ_{45} and Φ_{46} are not equal to zero. One can generalize the definition of shear center by considering only the twist caused by the shear forces and excluding the twist produced by the bending-twist coupling. In such a case, the second terms of Equations (8) are drop out. Further detail formulation used by VABS to compute the generalized Timoshenko stiffness matrix and the location of shear center are available in [34].

After the sectional stiffness matrix and inertia matrix are obtained, the equivalent beam model is built for the aeroelastic analysis and rotor trim. Before continuing to discuss aeroelastic analysis, we need to discuss the cross-section geometry and mesh generation. For one reason, this rotor blade structural design employs an automatic optimization scheme that requires a parametric geometry generator to generate the cross-section layout corresponding to the given values of design variables. Furthermore, VABS uses a finite element method to discretize 2D cross-section and calculate sectional properties. The use of VABS cross-sectional analysis requires an appropriate mesh necessitate.

2.1.2 Parametric Geometry Generator with a Realistic Cross-Section

The composite rotor blade cross-sectional optimization in this work is based on the template illustrated in figure 5. Using this template, the structural design of rotor blades reduces the errors resulting from geometrical discrepancies and increases the fidelity of the preliminary design in the comparison with the simplistic box-beam models often used in the literature [53, 100, 25, 87, 46, 47, 63]. Based on this cross-sectional geometry, a stand-alone, fully parameterized geometry generator is constructed for

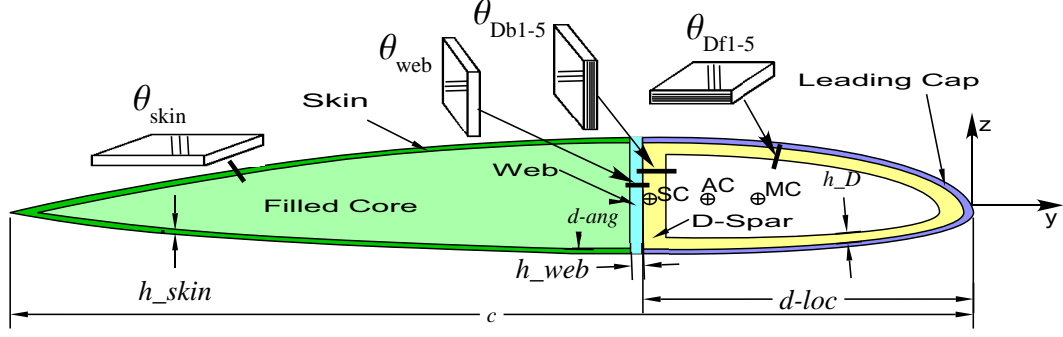


Figure 5: The structural template for the blade cross-sectional “geometry generator”

cross-section design optimization.

The geometry generator automatically produces a layout of the cross-section given the coordinates of control points on an airfoil and the values of design variables. In the process of creating such a parametric model, the curves are produced by NURBS (Non-Uniform Rational B-Splines) [75] because NURBS can accurately describe any shape from a simple 2D line, arc, or curve to the most complex 3-D organic free-form surface or solid. The amount of information required for a NURBS representation of a piece of geometry is much smaller than the amount of information required by common faceted approximations. A NURBS curve is defined by four things: degree, control points, knots, and an evaluation rule. Figure 6 shows a NURBS defined by control points. The NURBS curves are mathematically represented by the following general form:

$$C(u) = \sum_{i=1}^k R_{i,n} P_i \quad (9)$$

$$R_{i,n} = \frac{N_{i,n}(u)}{\sum_{j=1}^k N_{j,n} w_j} \quad (10)$$

where k is the number of control points P_i and w_j is the corresponding weights. $R_{i,n}$

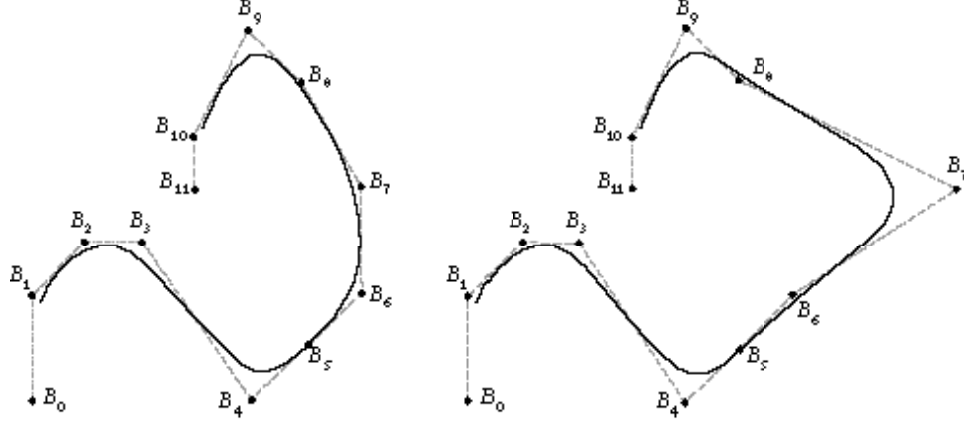


Figure 6: Defining a curve with control points

is the rational basis function. The denominator in Equation (10) is a normalizing factor that evaluates to one if all weights are one. $N_{i,n}(u)$ is the basis functions, in which i corresponds to the i th control point, n corresponds with the degree of the basis function, and u denotes the parameter dependence.

The basis function $N_{i,n}(u)$ is computed as

$$N_{i,n} = f_{i,n}N_{i,n-1} + g_{i+1,n}N_{i+1,n-1} \quad (11)$$

where the function f_i rises linearly from zero to one on the interval where $N_{i,n-1}$ is non-zero; the function g_{i+1} falls from one to zero on the interval where $N_{i+1,n-1}$ is non-zero.

A series of NURBS curves is also produced to define the interfaces between the layers (i.e. the lamina) of a laminated material. The intersection of each lamina with the cross-sectional plane is a planar surface bounded by two curves, referred to as the inner and outer curves. The inward directed normal from the outer curve will intersect the inner curve, and the lamina thickness can be defined as the distance between these two intersections along the normal. When the curvature of a bounding curve is small, the lamina thickness can be considered approximately constant along the outer curve. In such a case the inner curve can be obtained by simply translating the outer

curve. However, shifts of curved lines parallel to themselves can create difficulties for the regions of high curvature, such as at the leading edge. The thickness must be adjusted to compensate for the increasing curvature. This is done by holding the local area of the ply constant, implying that the local density of the material is preserved. In mathematical terms this translates into a requirement for the local thickness $h(s)$ of the lamina to be a function of the local radius of curvature $\rho(s)$ along the contour dimension s , so that

$$h(s) = \rho(s) - \sqrt{\rho(s)^2 - 2h_\infty\rho(s)} \quad (12)$$

where h_∞ is the thickness of flat lamina.

While the template is producing the section layout, consistency with the geometric constraints of the problem must be maintained. For example, the fixed outer shell of the blade implies that while the D-spar is moved horizontally as a design variable during the optimization process, its vertical dimension must be adjusted accordingly. This and other such consistencies are maintained automatically.

Another feature of this geometry generator is fillet creation at the intersection of two NURBS curves (or NURBS and a straight line). In addition, the geometry generator is compatible with VABS. The geometry generator generates an appropriate 2D finite element mesh for VABS and laminated material information. Figure 7 and 8 show VABS layup and element conventions. The geometry generator with these characteristics provides realistic layouts and suitable meshes for cross-sectional design optimization.

2.1.3 Aeroelastic Analysis and Load Calculation

This section describes the formulation of blade aeroelastic response equations, vehicle trim equations, and the calculations for the coupled trim procedure. Wind tunnel trim is used in this work. The wind tunnel trim procedure involves adjusting the controls

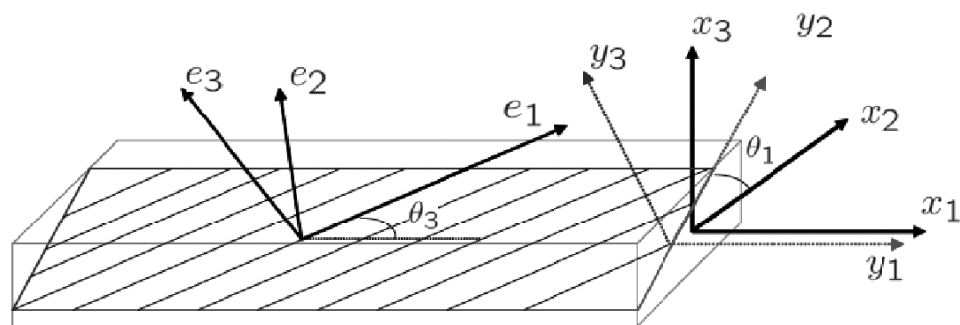


Figure 7: VABS layup convention

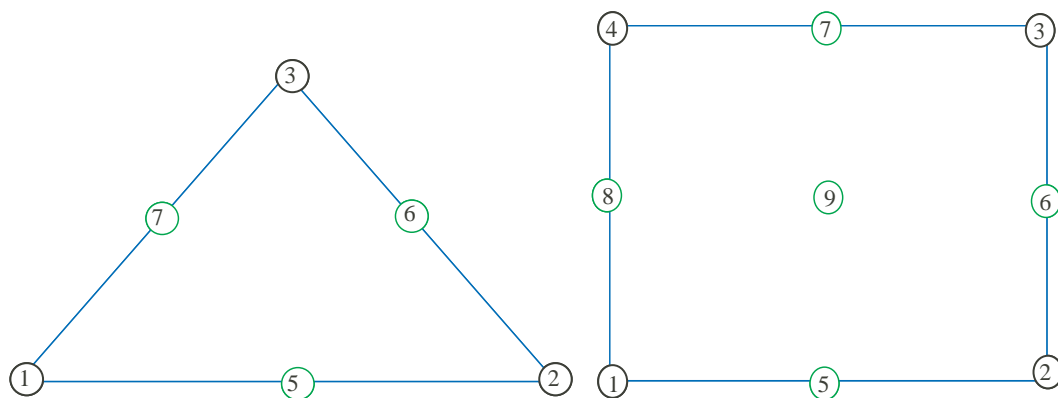


Figure 8: VABS elements

to achieve zero first harmonic blade flapping and lag moments with a prescribed thrust level. The rotor system loads depend on the blade response, so the determination of vehicle trim and blade response is coupled together. A coupled trim iterative procedure simultaneously solves for the blade responses and the trim equations until the blade responses converge [69].

To carry out the dynamic analysis, the governing equations of the rotor system are derived from the extended Hamilton's principle, given by

$$\int_{t_0}^{t_1} \int_0^l (\delta U - \delta K - \overline{\delta W}) dx dt = 0 \quad (13)$$

where δK and $\overline{\delta W}$ are the kinetic energy per unit length and the virtual work of the external forces acting on the blade. The aerodynamic forces are calculated by the finite-state dynamic inflow theory [70, 71], and 28 finite states are used in the dynamic inflow model.

For the convenience of numerical computation, the blade is discretized into a number of beam elements. Each element has four nodes (2 boundary nodes and 2 interior nodes), and each node has six degrees of freedom that correspond to three displacements and rotations. After the spatial discretization, the finite element equations are transformed into the normal mode space by using the blade natural rotating vibration modes. As a result, the equations of motion can be written in the form

$$\mathbf{M}\ddot{\mathbf{q}} + \mathbf{C}\dot{\mathbf{q}} + \mathbf{K}\mathbf{q} = \mathbf{F}(\mathbf{q}, \dot{\mathbf{q}}, t) \quad (14)$$

where \mathbf{M} , \mathbf{C} , \mathbf{K} , \mathbf{F} , and \mathbf{q} represent the mass matrix, gyroscopic/damping matrix, stiffness matrix, the column matrix of generalized force, and the column matrix of the generalized coordinates, respectively.

The solutions of the preceding equations are used to calculate the sectional loads of the rotor blades. The blade loads are integrated over the blade span and transformed from rotating frame to inertial frame to obtain the hub loads. The steady-state

components of hub loads are used for wind tunnel trim in which only rotor thrust is trimmed and the blade flapping is trimmed such that the 1/rev flapping is eliminated. The control variables are collective pitch and cyclic pitch. The auto-pilot control law [69] is used in the trim. The following discrete equations are introduced to compute the control outputs at each time step

$$\mathbf{u}_f = \mathbf{u}_i + \Delta t \mathbf{J}^{-1} \mathbf{G}(\hat{\mathbf{y}} - \mathbf{y}_f) \quad (15)$$

where \mathbf{u}_i and \mathbf{u}_f are the initial and final values of the state vector, respectively. Δt , \mathbf{J} , \mathbf{G} , $\hat{\mathbf{y}}$, and \mathbf{y}_f are the time step size, the Jacobian matrix, the diagonal gain matrix, the specified target values and the present input values, respectively. The controls are then individually perturbed to form the Jacobian matrix that is evaluated numerically using a finite differencing process [9].

The blade aeroelastic responses (14) and the trim control settings (15) were solved simultaneously to calculate the wind tunnel trim solutions. The trim solution and blade responses are updated iteratively until the convergence criteria are reached [9]. Once the convergence trim solution is obtained, the steady-state loads history at the specified position of the blade can be extracted for local stress analysis and fatigue design.

2.1.4 Stress Analysis

Stress analysis is carried out by using VABS recovery theory [39]. The recover relations express the 3D displacements, strain, and stresses in terms of local cross-sectional coordinates (y, z) and 1D beam quantities, including sectional stress resultants that have been obtained in last section. In addition, the calculation of the 3D strain/stress requires the warping functions, the generalized Timoshenko flexibility matrix, and stress resultants that have been obtained in sectional analysis. Because of the weak nonlinear relationship between the 1D stress resultants and 3D

strain/stress, superposition method is used for stress analysis to improve computation efficiency. The stress history at point P is obtained by

$$\sigma_P(t) = F_1(t)\sigma_P^1 + F_2(t)\sigma_P^2 + F_3(t)\sigma_P^3 + M_1(t)\sigma_P^4 + M_2(t)\sigma_P^5 + M_3(t)\sigma_P^6 \quad (16)$$

where σ_P^i ($i = 1, \dots, 6$) are the 3D stresses associated with a unit load at point P. The recovery relations are only calculated six times for each of the six unit loads with the superposition method used to recover the stresses at each moment in time.

2.2 Strength-Based Fatigue Analysis

Since composite laminates exhibit very complex failure processes, a general systematic fatigue analysis methods have not been established at this time. In this work, fatigue and durability analysis employs a strength degradation model [82, 83] for several reasons. First, in this model, fatigue damage is defined in terms of macroscopically measured properties, typically strength or stiffness, instead of microscopic properties such as crack length. Recent experiments have shown that matrix cracking in transverse plies normally starts first and results in a gradual loss of stiffness and strength [23, 50, 21, 93]. Laminated composite fatigue failure is characterized by a multitude of matrix cracks and fiber breaks rather than the growth of a single dominant crack. Furthermore, this model can be easily incorporated into existing design practices. This model is compatible with the standard stress-life fatigue experiments so that these data can be directly used for design. In this section, the strength degradation model is described. More detail discuss can be found in [92].

The initial residual strength of a composite is assumed to be equal to the static strength and to decrease monotonically as a function of load cycles. If the material age is related with stress level σ and the number of cycles n , the residual strength can be expressed as follows:

$$R^\lambda(n) = R_0^\lambda - f(\sigma)n \quad (17)$$

where R_0 is the static strength of the composite. λ is a constant, and it is determined by experimental data.

In general, material age also depends on frequency and stress ratio. For simplicity, these two parameters are fixed in Equation (17). From the S-N curve relationship, an expression for $f(\sigma)$ is obtained as

$$N = \frac{1}{K\sigma^b} = \frac{\beta_0^\lambda}{f(\sigma)} \quad (18)$$

$$f(\sigma) = \beta_0^\lambda K \sigma^b \quad (19)$$

where N , b , and K are composite fatigue life and the two parameters of the classical power law of the S-N curve, respectively. The static strength of composite samples is assumed to have a two-parameter Weibull distribution [48]. β_0 in Equation (19) is the scale parameter of such a Weibull distribution.

The distribution of the static strength is written as

$$f_X(x) = \begin{cases} \frac{\alpha_0}{\beta_0} \left(\frac{x}{\beta_0}\right)^{\alpha_0-1} \exp\left[-\left(\frac{x}{\beta_0}\right)^{\alpha_0}\right], & \text{if } x > 0, \\ 0, & \text{otherwise.} \end{cases} \quad (20)$$

where α_0 and β_0 are the shape and the scale parameters, respectively.

The shape and scale parameters are estimated by a maximum likelihood method [37]. Assuming the experimental static strength data x_i ($i = 1, 2, \dots, n$) from the same distribution, α_0 and β_0 are solved from the following maximum likelihood equations:

$$\frac{\sum_{i=1}^n x_i^{\alpha_0} \ln x_i}{\sum_{i=1}^n x_i^{\alpha_0}} - \frac{1}{\alpha_0} - \frac{\sum_{i=1}^n \ln x_i}{n} = 0 \quad (21)$$

$$\beta_0 = \left[\frac{1}{n} \sum_{i=1}^n x_i^{\alpha_0} \right]^{\frac{1}{\alpha_0}} \quad (22)$$

The fatigue strength is assumed to satisfy a Weibull distribution as well. The shape parameters of fatigue strength distribution is assumed to be the same for all different stress levels. With these assumptions, the shape parameter of fatigue strength, denoted as α_f , can be estimated from the pooled fatigue data under the i th level of stress $x_{i1}, x_{i2}, \dots, x_{in}$:

$$y_{ij} = \frac{x_{ij}}{\beta_i} \quad (23)$$

$$\frac{\sum_{i=1}^m \sum_{j=1}^n y_{ij}^{\alpha_f} \ln y_{ij}}{\sum_{i=1}^m \sum_{j=1}^n y_{ij}^{\alpha_f}} - \frac{1}{\alpha_f} - \frac{\sum_{i=1}^m \sum_{j=1}^n \ln y_{ij}}{nm} = 0 \quad (24)$$

$$\beta_i = \left[\frac{1}{n} \sum_{j=1}^n x_{ij}^{\alpha_f} \right]^{\frac{1}{\alpha_f}}, \quad i = 1, 2, \dots, m \quad (25)$$

Once the parameters α_0 and α_f are obtained, the constant λ is defined by

$$\lambda = \frac{\alpha_0}{\alpha_f} \quad (26)$$

By substituting Equation (19) into Equation (17), one finds the residual strength given by

$$R^\lambda(n) = R_0^\lambda - \beta_0^\lambda K \sigma^b n \quad (27)$$

The equations above are valid for the composites with the same stacking sequence. Liu and Lessard [59] extended this idea and provided an approximate analytical formulation for composite laminates with different stacking sequence. The unidirectional properties can be computed from the coupon properties, shown in Equation (27), by using the following approximate equations:

$$b_0 = b \quad (28a)$$

$$K_0 = K \left(\frac{\sigma}{\sigma_0} \right)^{b_0} \quad (28b)$$

where b_0 and K_0 are the two S-N curve constants of a unidirectional zero-degree-ply laminate, respectively. The deriving details can be found in [59]. The data used for computation are from [92, 59].

Once we obtain the unidirectional properties, the strength-based fatigue analysis can be conducted layer by layer for laminates. When the applied stress equals or exceeds the residual strength, failure occurs in terms of the Tsai-Wu failure criteria. The Tsai-Wu failure criteria [29] is used for the multi-axial stress states in laminates. The coupling fatigue strength analysis is conducted once per cycle until the fatigue strength is equal to the applied stress.

2.3 General Optimization Model for Blade Structural Design

When a helicopter flies, the deformed blades of main rotor interact with unsteady air flow and control systems. In general, aerodynamic design focuses on optimizing external shape, including airfoil shape, twist rate, taper ratio, and span. By contrast, structural design focuses on the internal structure of the blade and material distribution, or the detail cross-section layout.

The cross-section design problem is posed as follows: Determine values of all design variables including cross-sectional stiffness and inertia constants so as to satisfy chosen constraints and minimize a chosen objective function. Ingredients for the constraints and objective function may include such things as the local weight per unit length, specific stiffness coefficients such as torsional or bending stiffness and locations of the shear center (SC) or mass center (MC), all of which follow from a cross-sectional analysis such as VABS. In order to improve the payload of aircraft, the

mass is generally expected to minimum. To avoid resonance conditions, the cross-section design must guarantee bending and torsional stiffnesses to be in a desired range. Another concern in helicopter rotor design is the dynamic coupling of bending and torsional loads since this coupling is responsible for flutter and other dynamic instabilities in rotor blades. The coupling depends on the lift (a transverse load) and the distance between the SC and the aerodynamic center (AC). Hence, the cross-section design attempts to minimize the distance between the SC and AC as well as the distance between the mass center (MC) and the AC for similar reasons. Moreover, the structure must perform without failure under specified service loads. Whether or not failure occurs is measured by the Von Mises criterion for isotropic materials and the Tsai-Wu criterion for anisotropic materials.

Figure 5 shows a template of blade cross-sections. The cross-sectional template consists of four components: a leading-edge cap, a skin, a D-spar, and a web. These components contribute to the sectional properties and carry forces. The thickness of the leading cap is the same as that of the skin. The leading cap and the web are always adjacent to the D-spar. As the D-spar and the web move along the y direction or rotate, the length of D-spar and web automatically adjust to fit inside the airfoil. A core material is filled in the back part of the cross-section, while no material is filled in the D-spar. With all these assumption, the cross-section design presented here is a sizing problem. That is, the outer configuration and the topology remain fixed during the whole optimization process. Design variables include thicknesses of the four components, the location and the orientation of the D-spar, and material properties. If the components are made of laminated composites, the design variables also include fiber orientations or stacking sequence.

The objective of the design is to minimize the following function:

$$\begin{aligned}
z(\mathbf{x}) &= w_1 \frac{|e(\mathbf{x})|}{c} \times 100\% + w_2 \frac{m(\mathbf{x})}{m_b} + w_3 \frac{1}{g_{min}(\mathbf{x})} + w_4 \frac{|d(\mathbf{x})|}{c} \times 100\% \quad (29) \\
\mathbf{x} &= \{x_1, x_2, \dots, x_n\}^T
\end{aligned}$$

where \mathbf{x} is a design vector, the components of which are the design variables; N is the number of variables; e and d are the offset of SC from AC and the offset of MC from AC, respectively; m and g_{min} are the mass per unit length and the minimum safety factor over the cross-section, respectively. The location of AC is assumed at a quarter of chord, denoted c , in this research. If $e > 0$, SC is in front of AC; $e < 0$, SC is behind AC, and d follows the same rule. The above objective function combines several design requirements through cost ratios or weight factors, denoted w_1, w_2, w_3, w_4 .

The optimization is subject to the following constraints:

- Torsion stiffness and bending stiffness constraints

$$GJ^L \leq GJ(\mathbf{x}) \leq GJ^U \quad (30a)$$

$$EI_{jj}^L \leq EI_{jj}(\mathbf{x}) \leq EI_{jj}^U, \quad j = 2, 3 \quad (30b)$$

where $()^L$ and $()^U$ denote the lower and upper bounds of the variables, respectively.

- Mass constraints

$$m^L \leq m(\mathbf{x}) \leq m^U \quad (31)$$

- Constraints for the coupling terms in stiffness matrix

$$g(S_{kl}) \leq g^U, \quad k, l = 1, \dots, 6 \quad (32)$$

where S_{kl} are components of the generalized Timoshenko stiffness matrix from the 1D constitutive law, shown in Equation (7).

- Structural integrity constraints

$$SF^L \leq g_{min}(\mathbf{x}) \quad (33)$$

$$g_{min}(\mathbf{x}) = \min_{\Xi}(g(\mathbf{x})) \quad (34)$$

where Ξ denotes the area occupied by the same materials. Safety factor g is defined by Tsai-Wu failure criterion for composite materials and Von Mises criterion for isotropic materials.

The Von Mises criterion [29] is written as

$$\sigma_{eq} = \frac{1}{g} = \frac{1}{\sqrt{2}\sigma^a} \sqrt{(\sigma_1 - \sigma_2)^2 + (\sigma_2 - \sigma_3)^2 + (\sigma_3 - \sigma_1)^2} \quad (35)$$

where σ_1 , σ_2 , and σ_3 are the principal stresses at the point of interest, σ^a is the ultimate stress of the material. The physical meaning of $1/g$ is the equivalent mono-axial stress normalized by material strength. When the safety factor g is greater than one, or the equivalent stress smaller than material strength, failure is assumed not to occur. Generally, the given safety factor of structures is greater than unity, such as 1.5 used in the aerospace industry.

For composite materials, g is computed using the Tsai-Wu criteria [29].

$$\begin{aligned} \sigma_{eq} = \frac{1}{g} = & \left(-\frac{1}{X_c} + \frac{1}{X_t} \right) \sigma_1 + \frac{\sigma_1^2}{X_c X_t} + \left(-\frac{1}{Y_c} + \frac{1}{Y_t} \right) \sigma_2 \\ & + \frac{\sigma_2^2}{Y_c Y_t} - \frac{\sigma_1 \sigma_2}{\sqrt{X_c X_t Y_c Y_t}} + \frac{\tau_{12}^2}{S^2} \end{aligned} \quad (36)$$

where X_t , Y_t , X_c , Y_c and S are the ultimate tension, the compression stresses, and shear stress of unidirectional laminated materials, respectively. σ_1 , σ_2 , and τ_{12} are stresses along the two material directions and the shear stress, respectively. The inverse safety factor $1/g$ with the Tsai-Wu failure criteria, similar to Von Mises stress normalized by the ultimate strength, indicates a dangerous level locally.

The nominal material properties of composites in Equation (36) and metals in Equations (35) are uncertain because of the manufacturing process, environmental conditions, and experimental error [11, 76, 88]. The applied stresses are also uncertain because they depend on random design variables and uncertain service loads.

- Manufacturability constraints

$$x_i \in \begin{cases} [x_i^L, x_i^U], & \text{for continuous variables;} \\ \{\text{feasible discrete values}\}, & \text{for discrete variables;} \end{cases}$$

CHAPTER III

STRUCTURAL SIZING WITH MANUFACTURABILITY CONSTRAINTS

This chapter demonstrates the design methodology developed in chapter 2 for the rotor blade design. The goal of design is to improve the baseline model by reducing the weight of the blade, locating the shear center to the aerodynamic center, and decreasing the stress level of the blade structure while the difference of the sectional stiffnesses between the optimal blade and baseline is in the range of $\pm 5\%$ of the baseline. In the first section of this chapter, we build the baseline of the blade. The cross-section of the baseline is an objective of template, shown in 5. The specific design variables are also discussed in this section. In the second and third sections, two optimization examples are presented. The first example focuses on adjusting the shear center; the second focuses on adjusting both shear and mass centers. In both designs, manufacturability constraints are added so the fiber orientations are treated as discrete variables. To search for the optimum design, a hybrid optimization method is developed that is capable of rapidly obtaining the optimal solution for problems having both continuous and discrete design variables. Finally, we explore the design space around optimal design by the design of experiments and find the variables that have most significant effects on sectional properties.

3.1 Baseline Model

The baseline is modeled using the NASA preliminary design report for a composite blade retrofit for the XV-15 rotor [5]. The leading-edge cap was assumed to be made of Titanium; and the D-spar, web and back part of the skin are made of the composite

material T300/5208. The back part of the section is filled with honeycomb. Design variables are ply angles, thicknesses of the D-spar (h_D), skin (h_{skin}) and web (d_{web}), as well as the web location (d_{loc}) and orientation d_{ang} . Note that the trailing edge part of the D-spar is connected with the web. The trailing edge part of the skin is considered to have two balanced layers. Thus, there is only one design variable, θ_{skin} , corresponding to the skin ply angle. The web is considered as a single layer θ_{web} . Finally, we assume that the D-spar has five plies of equal thicknesses. As a result, the D-spar has a total of ten independent ply angle variables: five angles θ_{D_f} that correspond to the leading edge portion of the D-spar, and five other angles θ_{D_b} that correspond to the trailing edge part of the D-spar. Tables 1 and 2 summarize the material properties [3, 74] and the baseline values of the design variables, respectively. Figure 9 shows the geometry and mesh of the baseline layout.

A hingeless rotor in the hovering flight condition is assumed. The chord and the length of the blade is 20.2 and 150 inches, respectively. Other parameters are air density, 1.2 kg/m³; rotor angular speed, 25 rad/s; blade angle of attack, 10; blade airfoil lift curve slope, $a = 5.7$; and blade airfoil drag coefficient, 0.01. Because this chapter is to demonstrate the cross-section design, the representative values of blade aerodynamic loads are estimated from blade-element/momentum theory [44] for simplicity. The axial force at the blade root is calculated to be $T = 11000$ lb. Under aerodynamic loads, the cross-section at the root of the blade suffers the most severe state of stress; at the root of the blade these are $Q_2 = 8$ lb and $Q_3 = 400$ lb for shear forces, and $M_2 = 45000$ lb-in and $M_3 = 1000$ lb-in for bending moments. Since Q_2 is too small to have any noticeable influence, it is ignored in the optimization. The sectional properties are given in Table 3.

Table 1: Material Properties

Property	Titanium	T300/5208	Honeycomb
ρ (lb·s ² /in ⁴)	4.220×10^{-4}	1.497×10^{-4}	6.00×10^{-6}
E_{11} (lb/in ²)	1.495×10^7	2.625×10^7	2.8×10^4
E_{22} (lb/in ²)	1.495×10^7	1.494×10^6	2.8×10^4
E_{33} (lb/in ²)	1.495×10^7	1.494×10^6	2.8×10^4
G_{12} (lb/in ²)	5.578×10^6	1.040×10^6	4.7×10^4
G_{13} (lb/in ²)	5.578×10^6	1.040×10^6	4.7×10^4
G_{23} (lb/in ²)	5.578×10^6	1.040×10^5	4.7×10^4
ν_{12}	0.34	0.28	0.3
ν_{13}	0.34	0.28	0.3
ν_{23}	0.34	0.33	0.3
Failure criteria	Von-Mises	Tsai-Wu	Tsai-Wu

Table 2: Geometric parameters of the baseline layout

Component	Variable	No.	Value	Feasible Range	Units
skin	h_{skin}	1	0.04	[0.01, 0.05]	inch
	θ_{skin}	2	+45	$\theta = \pm 10i, i = 0, 1, \dots, 9$	degree
web	h_{web}	3	0.04	[0.01, 0.05]	inch
	θ_{web}	4	0	$\theta = \pm 10i, i = 0, 1, \dots, 9$	degree
D-spar	h_D	5	0.35	[0.1, 0.4]	inch
	d_{loc}	6	-8.4025	[-8.6, -6.2]	inch
	d_{ang}	7	90	[60, 120]	degree
	$\theta_{D_{f1-5}}$	8-12	[+45, -45, 0, 0, 0]	$\theta = \pm 10i, i = 0, 1, \dots, 9$	degree
	$\theta_{D_{b1-5}}$	13-17	[+45, -45, 0, 0, 0]	$\theta = \pm 10i, i = 0, 1, \dots, 9$	degree

Table 3: The sectional properties of the baseline layout

$(GJ)_b$	3.4539×10^7	(lb-in ²)
$(EI_{22})_b$	8.3964×10^7	(lb-in ²)
$(EI_{33})_b$	1.2731×10^9	(lb-in ²)
$(m)_b$	0.001546	(lb-s ² /in ²)
$(e/c)_b$	-4.15%	
$(d/c)_b$	-4.17%	
$(\sigma_{eqmax})_b$	0.5765	

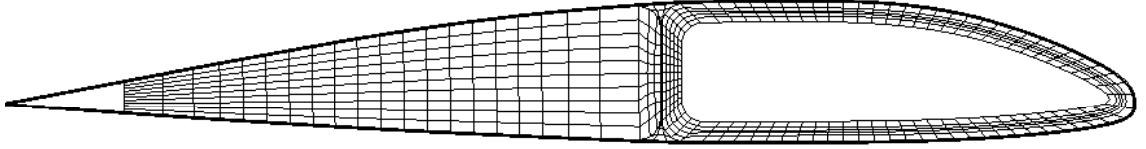


Figure 9: The geometry layout and the mesh of the baseline cross-section

3.2 *Minimizing the Distance from Shear Center to Aerodynamic Center*

In this example the goal is to improve the baseline model by minimizing the distance from shear center to aerodynamic center. The mass per unit length and the maximum equivalent stress over the cross-section is minimized as well by using different weight factor. The extension-torsion and bending-torsion coupling terms are restricted to be small compared with the diagonal terms of the stiffness matrix. The fiber orientations are discrete variables, the values of which assume multiples of 10° ranging from -90° to 90° due to manufacturing limitations. The objective function is shown in Equation (30). The constraints are specified below.

- Mass per unit length of optimal cross-section is no more than that of the baseline:

$$\frac{m(\mathbf{x})}{m_b} \leq 1.0 \quad (37)$$

where $(\)_b$ denotes the value of the baseline.

- The stress level of optimal cross-section is less than that of the baseline:

$$\frac{\sigma_{eqmax}(\mathbf{x})}{(\sigma_{eqmax})_b} \leq 1.0 \quad (38)$$

- The sectional stiffnesses of optimal cross-section is in the range of $\pm 5\%$ of baseline values:

$$0.95 \leq \frac{GJ(\mathbf{x})}{(GJ)_b} \leq 1.05 \quad (39a)$$

$$0.95 \leq \frac{EI_{22}(\mathbf{x})}{(EI_{22})_b} \leq 1.05 \quad (39b)$$

$$0.95 \leq \frac{EI_{33}(\mathbf{x})}{(EI_{33})_b} \leq 1.05 \quad (39c)$$

- The coupling stiffnesses of extension-twist and bending-twist are far smaller than the stiffnesses they couple:

$$\frac{S_{14}(\mathbf{x})^2}{S_{11}(\mathbf{x})S_{44}(\mathbf{x})} \leq 0.01 \quad (40a)$$

$$\frac{S_{45}(\mathbf{x})^2}{S_{44}(\mathbf{x})S_{55}(\mathbf{x})} \leq 0.01 \quad (40b)$$

$$\frac{S_{46}(\mathbf{x})^2}{S_{44}(\mathbf{x})S_{66}(\mathbf{x})} \leq 0.01 \quad (40c)$$

The reason of adding the coupling term constraints are that the effects of coupling terms on rotor blade aeroelastic response have not been fully investigated. Designers are not confident to use the coupling effects in design application.

- The feasible values of each design variables due to manufacturability constraints are summarized in Table 2.

3.2.1 The Hybrid Optimization Method

Current cross-section design optimization is nonlinear optimization problem with mixed continuous and discrete variables. Introducing fiber orientation leads to the non-convexity of the cross-section design space. To solve the non-convex and nonlinear optimization problem with mixed variables, a hybrid optimization method is developed. In the first stage, a continuous optimization problem is solved by using SQP [12]. To increase the probability of achieving a global optimum, a population of initial points is randomly selected in the design space before running SQP. The optimal solution for the continuous model is the best one among all the local optima resulting from SQP. After the optimal solution for continuous model is obtained, one can find out between which two nearest discrete points the optimal solution is located for each discrete variable. In the second stage, the GA [38] is used to determine which combination has the best objective function and satisfies the constraints among all combinations of these upper and lower bounds. Figure 10 shows the optimization flow chart.

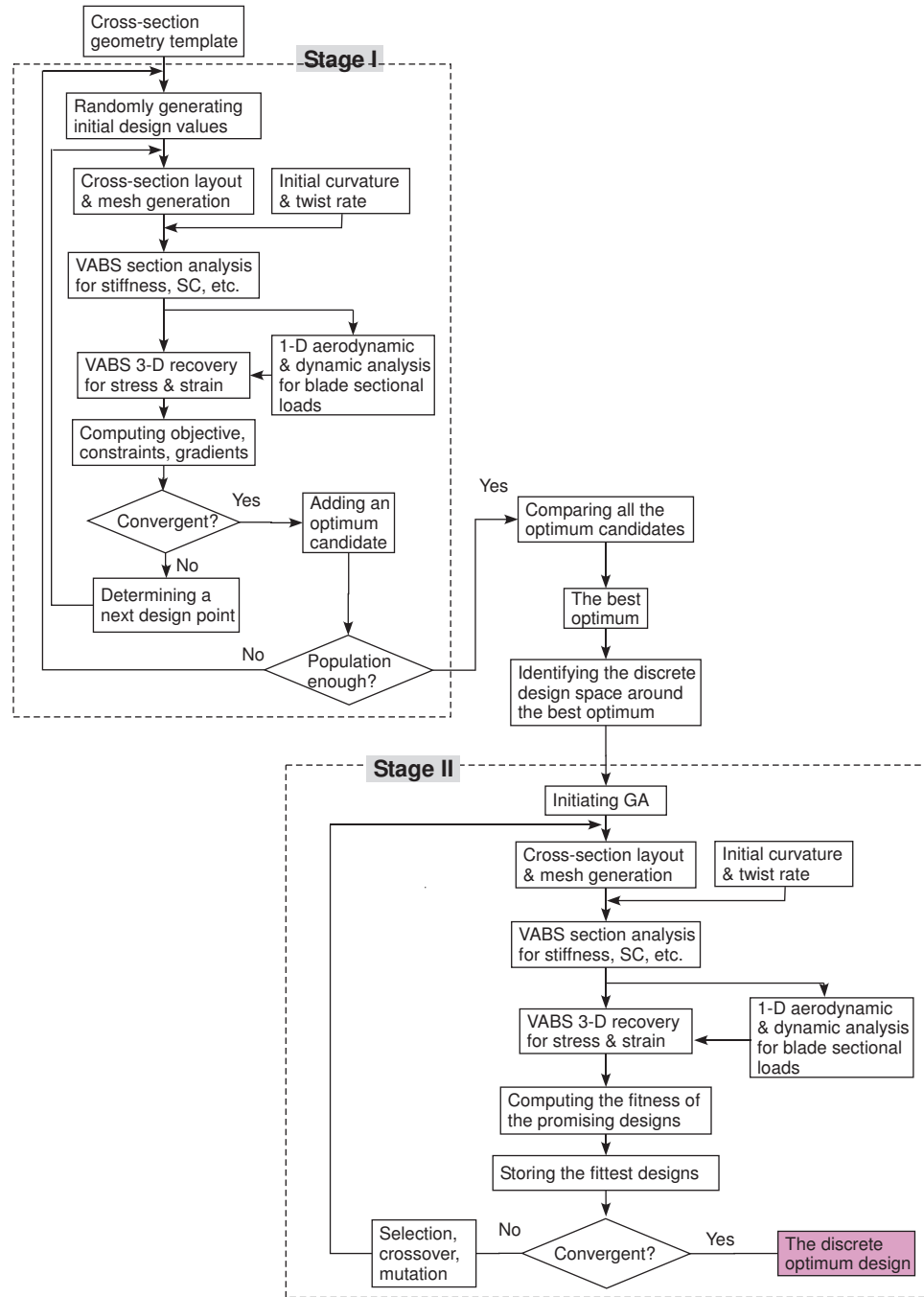


Figure 10: The optimization flow chart for composite blade design with mixed continuous and discrete variables due to manufacturability constraints

This hybrid method combines the advantages of SQP and GA. It utilizes the rapid convergence of SQP and avoids slow convergence of GA for obtaining the optimal continuous solution. Once the optimal continuous solution is found, the GA is restricted to search the optimal discrete solutions around the optimal continuous one. Since the searching space of GA is much smaller than the entire design space, the efficiency of optimization is improved significantly compared with a one-step GA, albeit at the expense of less confidence in finding the global optimum. Accounting for the computational load of SQP in the first stage, the total computational load of this hybrid optimization scheme is smaller than that for a one-step GA. Instead of using the GA, if one rounds the solution of SQP to the closest discrete values in the second stage, one runs the risk of constraint violations and a suboptimal solution. These two disadvantages are illustrated in the optimization example below. Therefore, by using this hybrid scheme, one can efficiently and robustly solve cross-sectional optimization problems with mixed continuous and discrete variables.

Some researchers have used a similar hybrid optimization technique but in the reverse order of the present scheme. That is, the GA is used to search the global optimum in the whole solution region to obtain a quasi-optimal solution, and then resulting solutions are refined by SQP [60, 41, 97]. Although the reverse order has a higher probability of achieving the global optimum, it cannot handle the optimization problem with both continuous and discrete design variables.

3.2.2 Design Results

A cost ratio describes the relative importance of the factor it multiplies in the objective function. The larger the cost ratio, the more important the factor it multiplies participates in the objective function calculation. Three sets of cost ratios are selected for use in illustrating their effect on the optimization. The set of cost ratios $w = (1, 0, 0, , 0)$ is an extreme case, where only the offset between SC and AC is

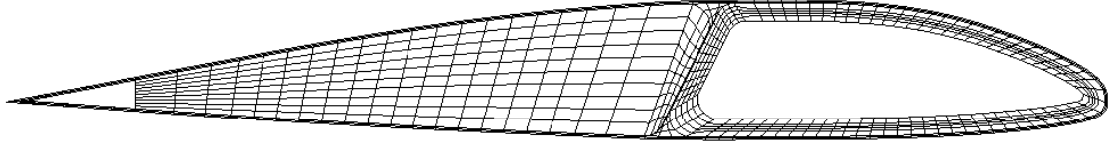


Figure 11: The cross-sectional layout and the mesh of the optimal solution with weight factors $w=(1, 0, 0, 0)$

minimized in the optimization process. Because stresses and inertia are ignored in objective function, we turn them into hard constraints, as shown in Equations (38) and (37). The other two sets of cost ratios mean that the weighted sum of the offset, the mass and the maximum equivalent stress, is minimized, so these two constraints are omitted. For the set of cost ratio $w = (1/2, 1/4, 1/4, 0)$, the distance is more important than the mass and the stress constraints, while the set of $w = (1/3, 1/3, 1/3, 0)$ implies the three factors are equally important.

In the first set of cost ratios, which can be denoted as $w=(1, 0, 0, 0, 0)$, the continuous solution not only satisfies all the stress, mass and stiffness constraints, but the non-dimensional offset e is as small as 0.0155% chord. It is worth noting that the maximum equivalent stress over the root cross-section is only 67.4% of the value of baseline. The optimal cross-section layout is shown in Figure 11. Another interesting observation is that the mass per unit length of the discrete solution is equal to that of the continuous solution. The reason is that ply angles do not affect the mass per unit length. This can also be concluded from the design space exploration in the last section of this chapter.

The best discrete solution that GA found near the continuous one and the solution rounded to the nearest discrete values are also summarized in Table 4. The omitted values are unchanged compared to the continuous solution. The hybrid solution is better overall than the one obtained by simple rounding. All the constraints are satisfied for both discrete solutions in the case of cost ratio $(1, 0, 0, 0)$. The value of the objective function resulting from the hybrid approach is smaller than the one

Table 4: The optimization results of locating shear center to aerodynamic center

Design	$w=(1, 0, 0, 0)$			$w=(1/2, 1/4, 1/4, 0)$			$w=(1/3, 1/3, 1/3, 0)$		
variables	cont.	round	2-step	cont.	round	2-step	cont.	round	2-step
$\frac{d}{c}$ (%)	-4.12	-4.12	-4.12	-5.55	-5.55	-5.55	-2.87	-2.87	-2.87
$\frac{e}{c}$ (%)	-0.015	-0.098	-0.024	-0.077	-0.096	0.025	-0.496	0.445	-0.491
$\frac{m}{m_b}$	0.988	0.988	0.988	0.921	0.921	0.921	1.067	1.067	1.067
$\frac{\sigma_{eqmax}}{(\sigma_{eqmax})_b}$	0.674	0.670	0.673	0.831	0.786	0.798	0.762	0.753	0.910
$\frac{GJ}{(GJ)_b}$	0.955	0.958	0.951	0.959	0.960	0.962	0.950	0.948	0.953
$\frac{EI_{22}}{(EI_{22})_b}$	1.041	1.047	1.044	1.033	1.076	0.998	1.046	1.059	1.032
$\frac{EI_{33}}{(EI_{33})_b}$	0.984	0.959	0.959	0.967	1.016	0.984	0.951	0.964	0.951
h_{skin}	0.050			0.050			0.050		
θ_{skin}	38.2	40	40	43.69	40	40	40.58	40	40
h_{web}	0.016	0.016			0.014		0.030		
θ_{web}	0.0	0	0	-1.03	0	0	0.37	0	10
d_{loc}	-7.67			-8.396			-7.267		
d_{ang}	63.4			100.86			72.47		
h_D	0.329			0.270			0.399		
θ_{Df1}	64.1	60	70	84.0	80	90	58.33	60	60
θ_{Df2}	-10.7	-10	-10	-12.42	-10	-10	-31.60	-30	-30
θ_{Df3}	0.0	0	0	1.83	0	0	1.22	0	0
θ_{Df4}	0.0	0	0	-0.41	0	0	1.69	0	0
θ_{Df5}	9.9	10	10	0.30	0	0	1.69	0	0
θ_{Db1}	87.5	90	90	85.83	90	90	90.00	90	90
θ_{Db2}	-19.9	-20	-20	-2.69	0	0	-32.00	-30	-30
θ_{Db3}	-5.7	-10	0	-0.19	0	0	0.00	0	0
θ_{Db4}	0.0	0	0	-0.20	0	0	0.00	0	0
θ_{Db5}	-1.8	0	-10	-0.14	0	0	0.00	0	0

Table 5: The comparison of approximate computation costs between the general GA and the proposed hybrid optimization scheme

	General GA	Proposed hybrid	
		First stage (SQP)	Second stage (GA)
Design space size	7.4×10^{22}		4096
Population size	80	30	8
iteration	> 100	15	30
Function calls	> 16000	7650	480
Total function calls	> 16000	8130	

from rounding, but slightly larger than the one from SQP. For the cost ratios $(1/2, 1/4, 1/4, 0)$ and $(1/3, 1/3, 1/3, 0)$, no constraints are violated for hybrid solution, but one or two constraints are violated for the rounded solution. Sometimes the solution rounded to the nearest discrete values does not violate the constraints, but sometimes it does. Actually, one has 2^{12} , or 4096, options to round 12 discrete variables. Most of them violate the constraints. The hybrid method, SQP followed by GA, always chooses a discrete solution that does not violate the constraints. Although this “smart rounding” adds some computational time, it is worth running the GA to get the best discrete solution.

Table 5 compares the computation costs for the GA alone and for the present hybrid method. The hybrid method has less computational cost. In this comparison, each continuous variable is represented with a five-bit string. Thus, the precisions of skin thickness, web thickness, D-spar thickness, and D-spar orientation are 0.00063, 0.00063, 0.0094 and 0.075, respectively, in the general GA. In the hybrid method, to avoid local optima, SQP was initiated randomly; and the best result from the 30 resulting optima was selected for the second-stage optimization.

Table 6: The optimization results of locating both mass and shear centers to aerodynamic center

$\frac{e}{c}$	-0.006%	h_{skin}	0.048	θ_{Df3}	22.550
$\frac{d}{c}$	-2.443%	θ_{skin}	25.076	θ_{Df4}	-0.320
$\frac{m}{(m)_b}$	1.000	h_{web}	0.018	θ_{Df5}	-18.285
$\frac{\sigma_{eqmax}}{(\sigma_{eqmax})_b}$	1.024	θ_{web}	36.206	θ_{Db1}	31.693
$\frac{GJ}{(GJ)_b}$	0.950	d_{loc}	-6.959	θ_{Db2}	-0.060
$\frac{EI_{22}}{(EI_{22})_b}$	0.990	d_{ang}	86.595	θ_{Db3}	34.629
$\frac{EI_{33}}{(EI_{33})_b}$	1.041	h_D	0.389	θ_{Db4}	4.829
θ_{Df2}	1.371	θ_{Df1}	19.166	θ_{Db5}	-11.166

3.3 Locating Both Mass and Shear Centers to Aerodynamic Center

In this example the objective is to improve the baseline model further, based on example 1, so that the distance between the mass center (MC) and AC is also minimized. The constraints remain the same as those of the example in the last section.

Table 6 summarized the optimization results of locating both MC and SC to AC. Moving both MC and SC is more difficult than moving only the SC. Actually, it is not possible to make the distance between MC and AC as small as the distance between SC and AC while the stiffnesses are constrained to remain in the range specified. This can be explained by the fact that both the torsional stiffness and the offset between MC and AC and are sensitive to web location; see the sensitivity analysis below. Changing the web location has counteracting effects on these two response variables. To decrease the distance further, the web location must be moved forward ($d_{loc} > -7.0$ in); to satisfy the torsional stiffness, the web location has to be moved backward (at least $d_{loc} < -7.0$ in). One way to resolve this conundrum is add one or more design variables, such as the chordwise location and mass of a non-structural point mass near the leading edge.

3.4 Parametric Study and Sensitivity Analysis

Sensitivity analysis is an essential part of structural optimization. Sensitivity analysis facilitates the understanding of the robustness of the design. One can know how the change of constraints would affect the values of design variables. One can also understand how each design variable affects the response variables. In industry, due to manufacturing techniques and cost limitations, the optimal value of each design variable might not be exactly attained. This could lead to some of the constraints being violated and a failure to attain some of the design goals. In addition, one can focus on some important design parameters based on the knowledge of how those design variables would change the objective function and constraints. For example, if the objective function is sensitive to a design parameter, one attempt to improve the manufacturing precision of that parameter; otherwise, one may expend a lot of effort and/or cost and wind up not improving the design. The design of experiments (DOE) tool is used to find the main effects on the response variables in the whole design space. The Eighth Fractional Factorial (16,384 function calls) and Box-Behnken (561 function calls) experiment methods are used. Results from these two methods are shown in Figures 12–17. The length of the bars in those figures represents the contribution of the design variable to the response variables. Among the 17 design variables, some of them contribute only slightly to all the response variables such as the fiber orientations in the web. The web location, the skin thickness, the fiber orientations in the skin and the D-spar thickness play important roles in determining cross-sectional properties. Mass per unit length is affected by skin thickness, D-spar thickness, web location, web thickness and web orientation. The first three factors contribute more than 95% of the mass change, meaning that mass quite sensitive to skin thickness, D-spar thickness and web location. The ply angles do not change the blade mass because the fiber orientation neither increases nor decreases the amount of material in the blade. The MC location is affected by design variables in a manner

quite similar to the mass per unit length. However, SC, equivalent stresses and stiffnesses exhibit a quite different character, being sensitive to more factors. Some of the ply angles play an important role in changing SC, stress and stiffnesses. For example, fiber orientation in the skin has the largest contributions to SC and chord-wise stiffness. Figures 18–21 show how the two most important variables affect the mass per unit length, location of SC, torsional stiffness, and location of MC.

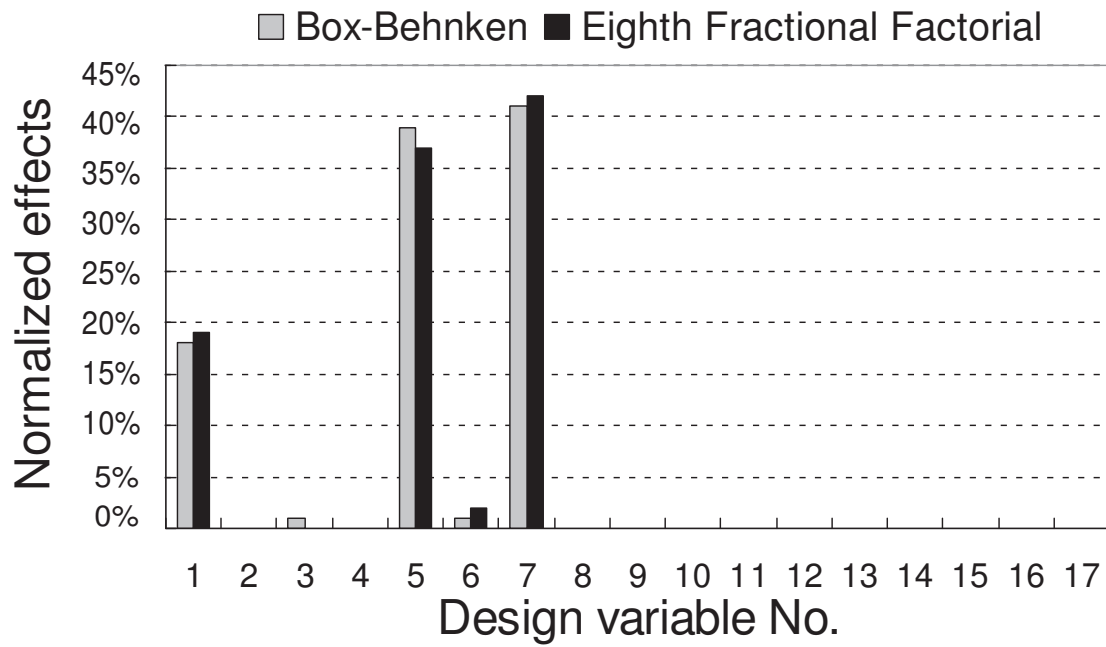


Figure 12: The contribution of each design variable to mass per unit length

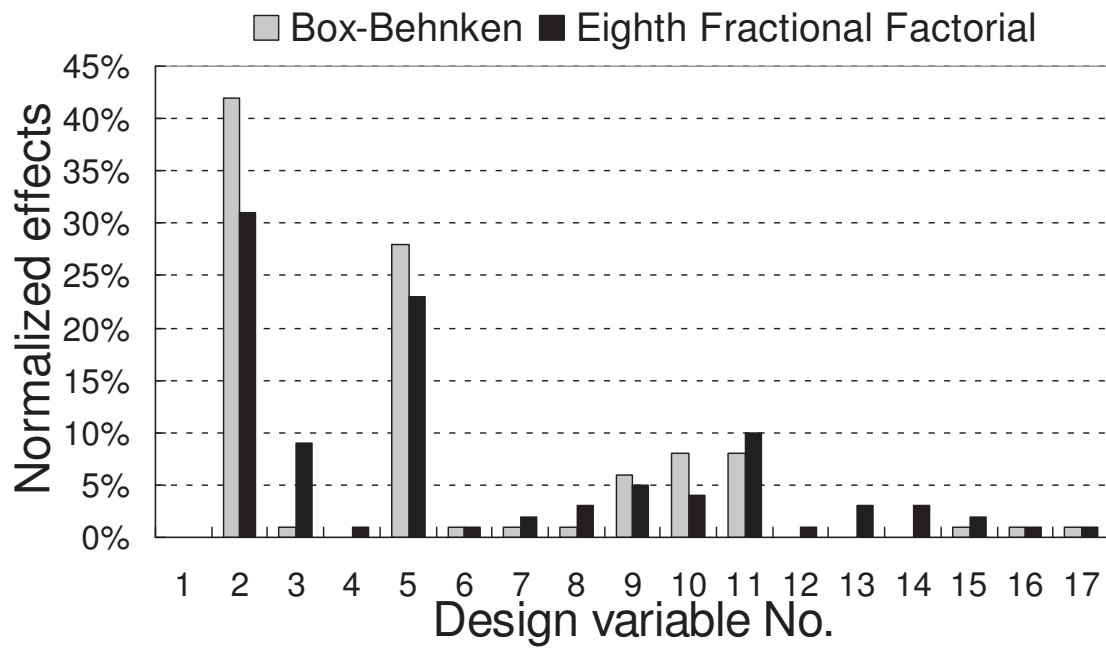


Figure 13: The contribution of each design variable to shear center

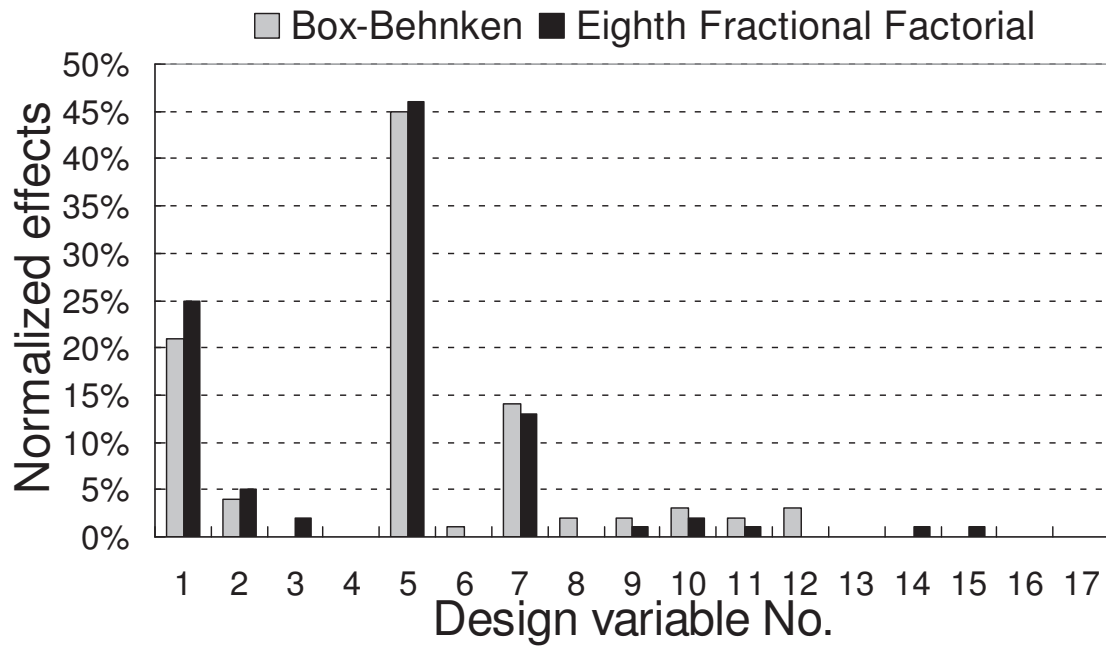


Figure 14: The contribution of each design variable to torsional stiffness

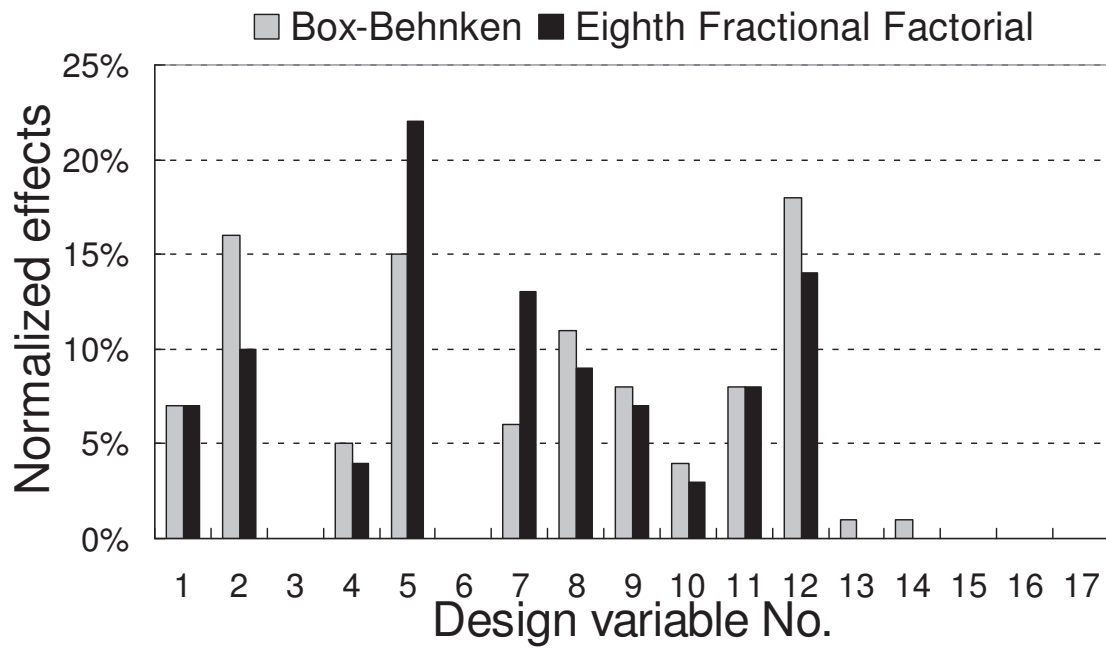


Figure 15: The contribution of each design variable to flapwise stiffness

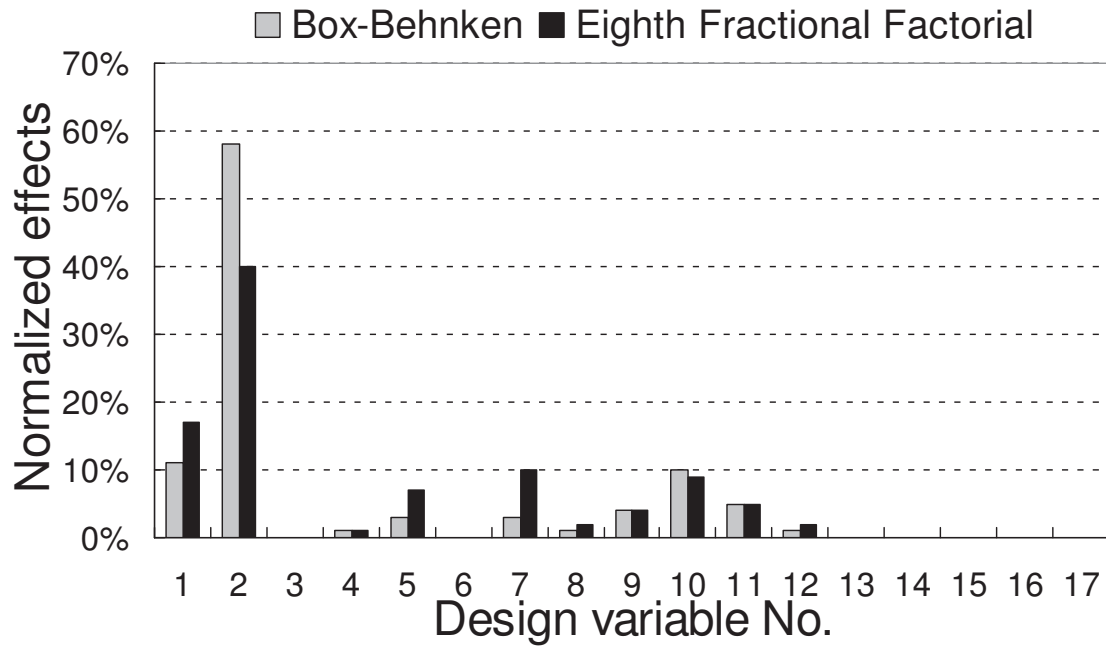


Figure 16: The contribution of each design variable to chordwise stiffness

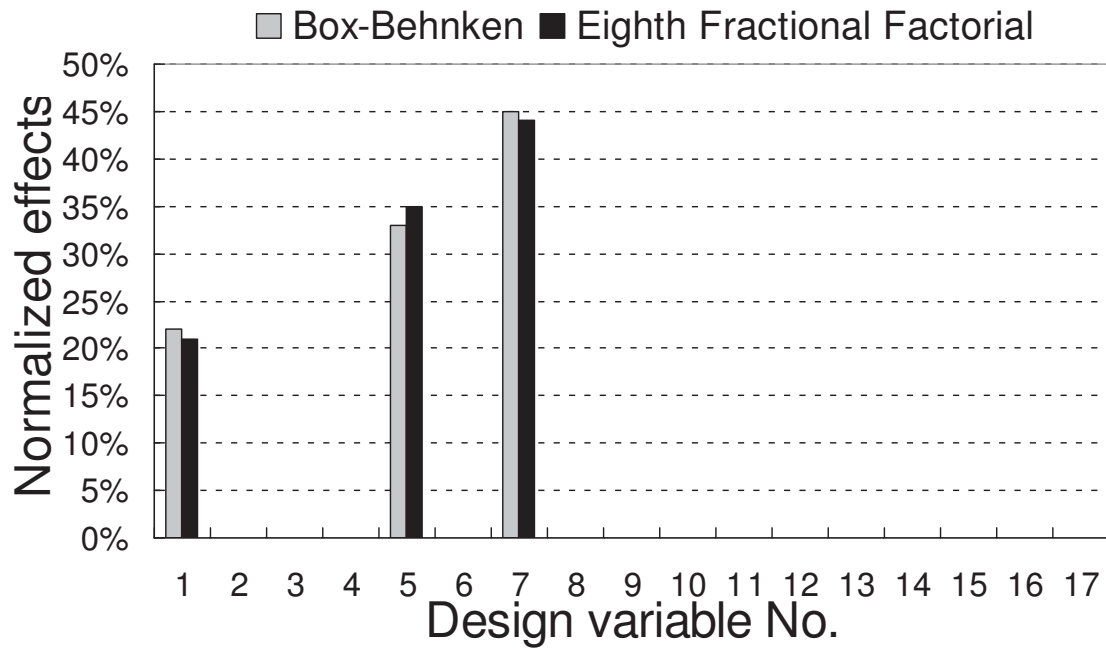


Figure 17: The contribution of each design variable to mass center

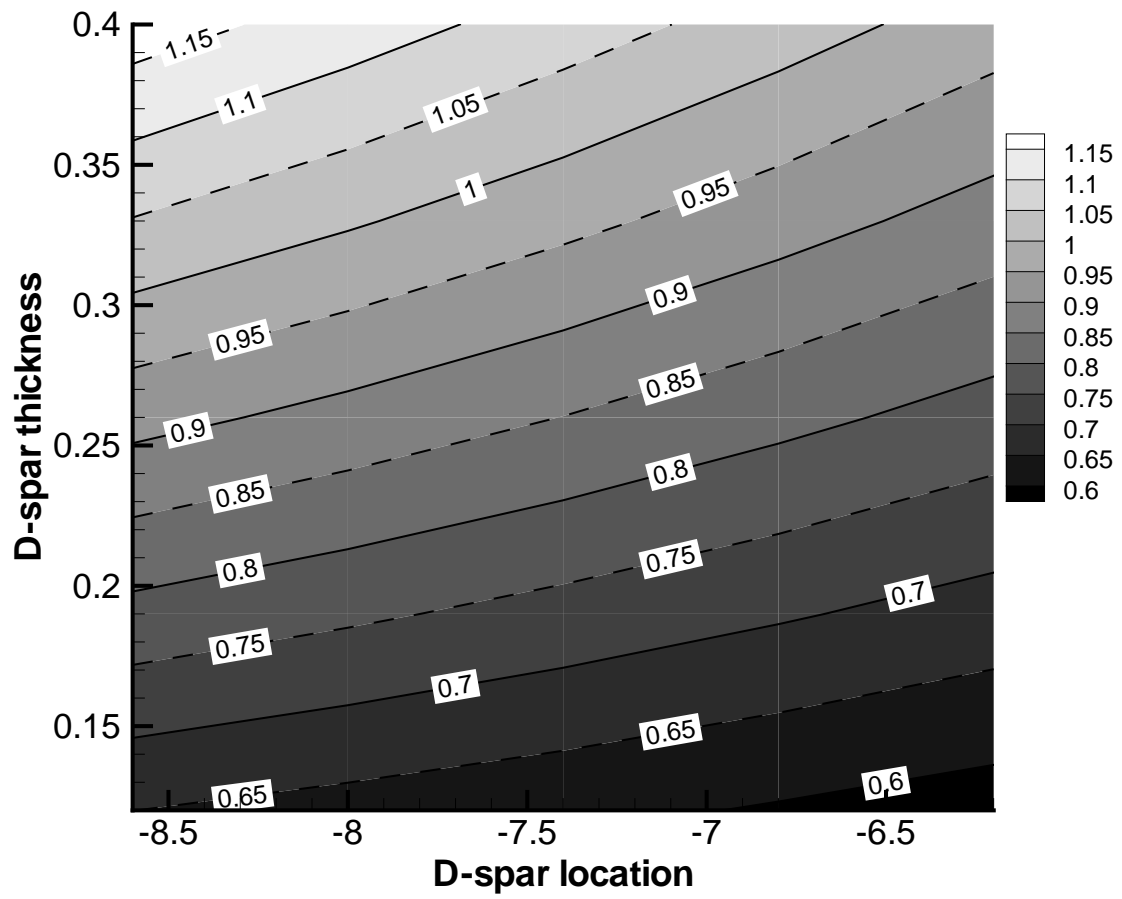


Figure 18: Mass per unit length vs. D-spar thickness and web location

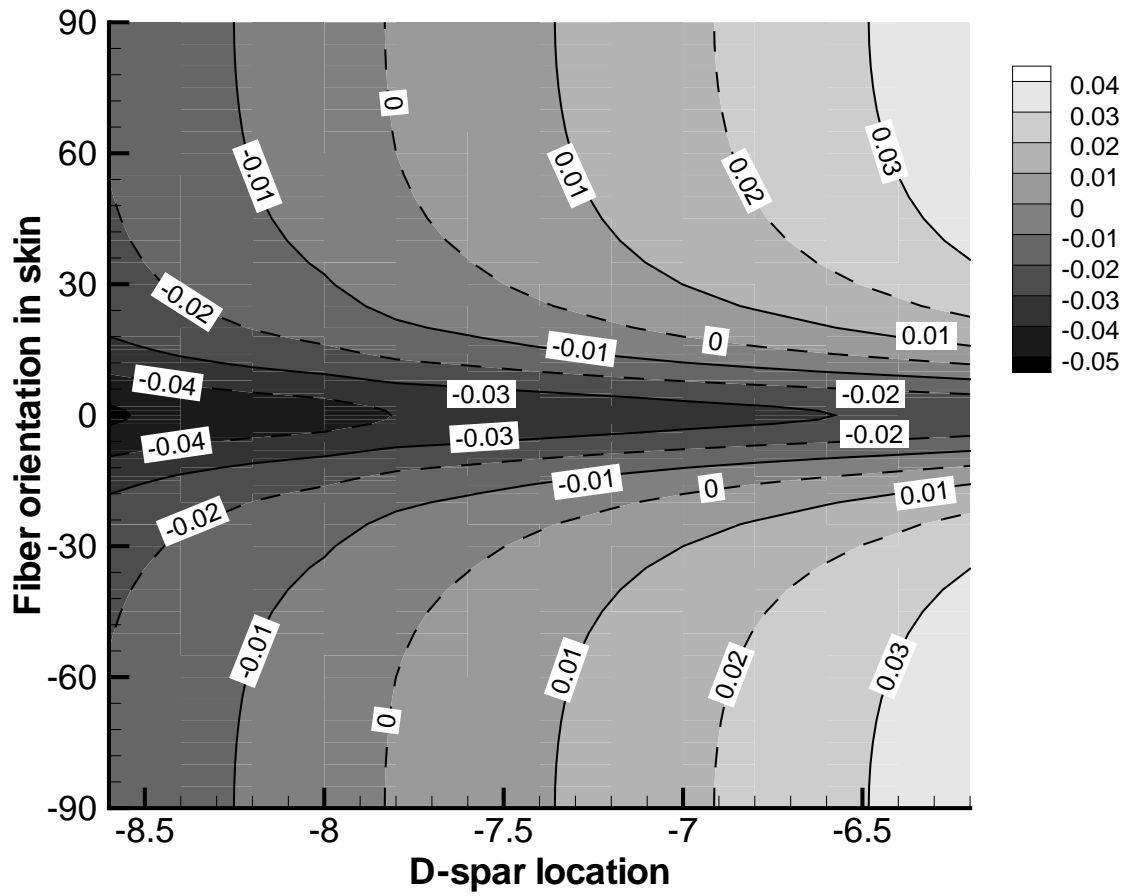


Figure 19: Non-dimensional SC offset from AC vs. fiber orientation in the skin and the D-spar location

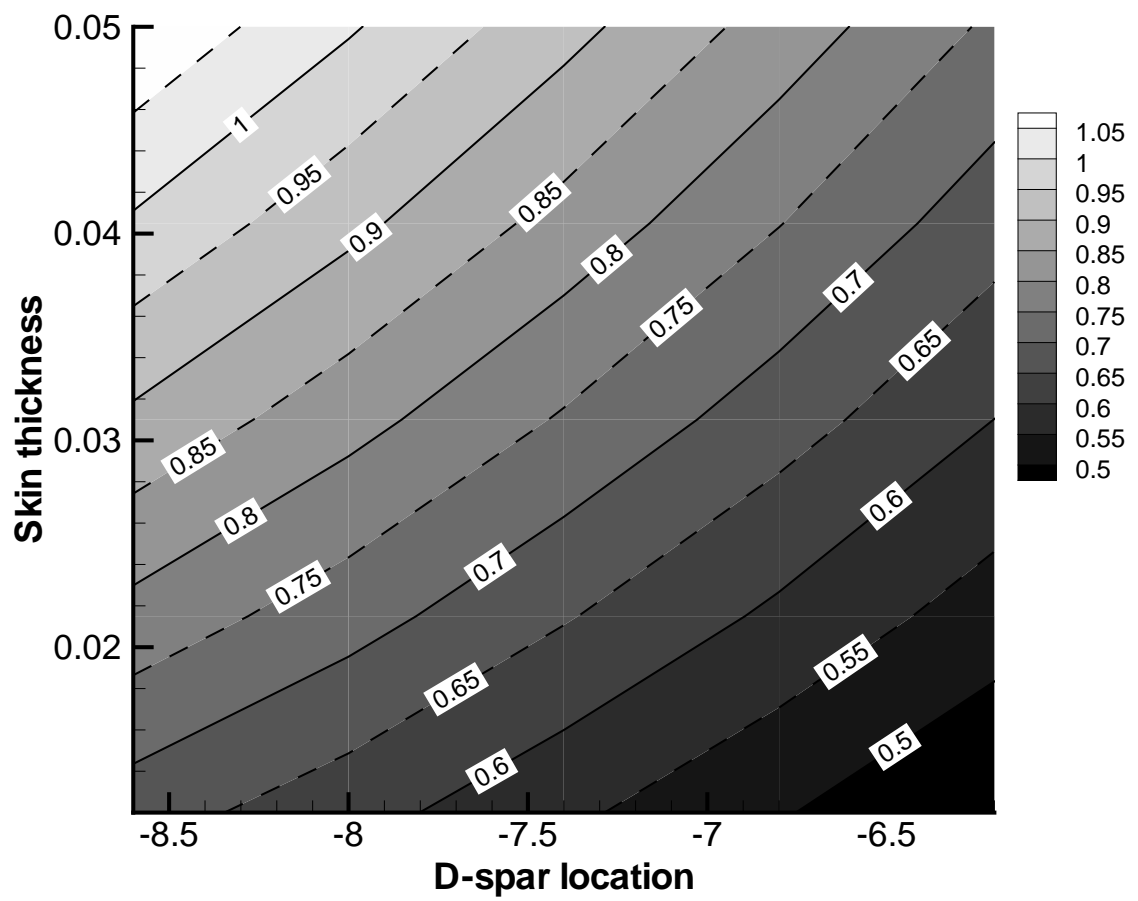


Figure 20: Torsional stiffness vs. skin thickness and D-spar location

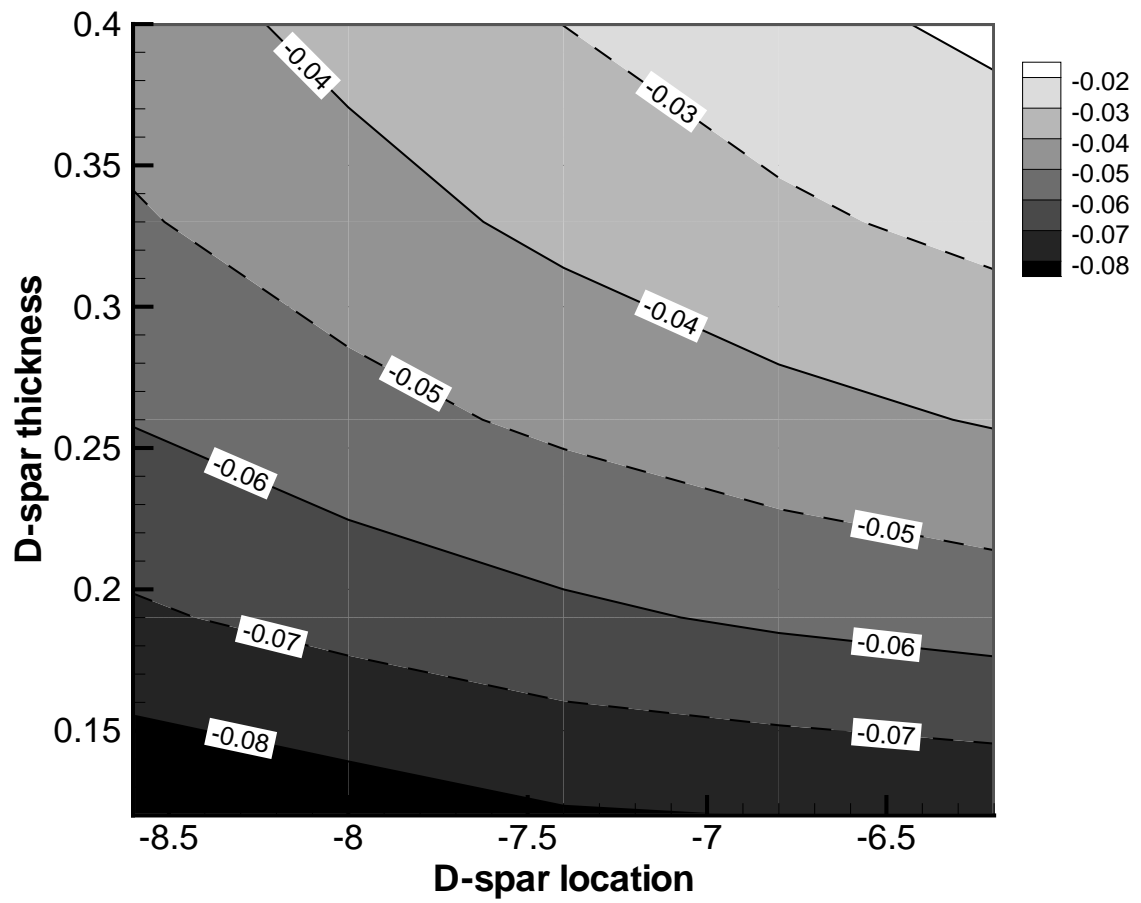


Figure 21: Non-dimensional MC offset from AC vs. D-spar thickness and D-spar location

CHAPTER IV

STRUCTURAL DESIGN AGAINST FATIGUE FAILURE

In this chapter, we attempt to incorporate fatigue and durability analysis into rotor blade design optimization. The optimization also includes the stiffness, weight, and frequency constraints. A new optimization implementation procedure is developed for blade structural design and applied to a three-blade hingeless-rotor case [36]. Fatigue life prediction employs VABS 3-D stress recovery relation and a strength-based fatigue model, in which fatigue failure occurs when the residual strength is equal to the applied stress. Failure is defined by the Tsai-Wu failure criterion, which accounts for the interaction of all stress components. The relations of residual strength characterizes in terms of unidirectional S-N data and laminate static strength.

4.1 Design Methodology

4.1.1 Cross-Section with Nonstructural Mass

In chapter 3, parametric study and design results have shown that based on the cross-section template in Figure 5 it is difficult to locate both shear and mass center at aerodynamic center. A nonstructural mass is added at the leading edge in the new cross-section, shown in Figure 22, so that the mass center of the cross-section is coincident with the aerodynamic center. The inertia effect of the mass is counted in sectional inertia. However, the stiffness and strength effects of the mass are ignored in the calculation of sectional stiffnesses. The sectional stiffness are mainly contributed by four structural components: the skin, web, D-spar, and leading-edge cap. Moreover, these four components carry most the loads and significantly contribute to other sectional properties. The skin, web, and D-spar have two, one, and four layers, respectively, each with an independent ply angle. The vertical wall of the D-spar are

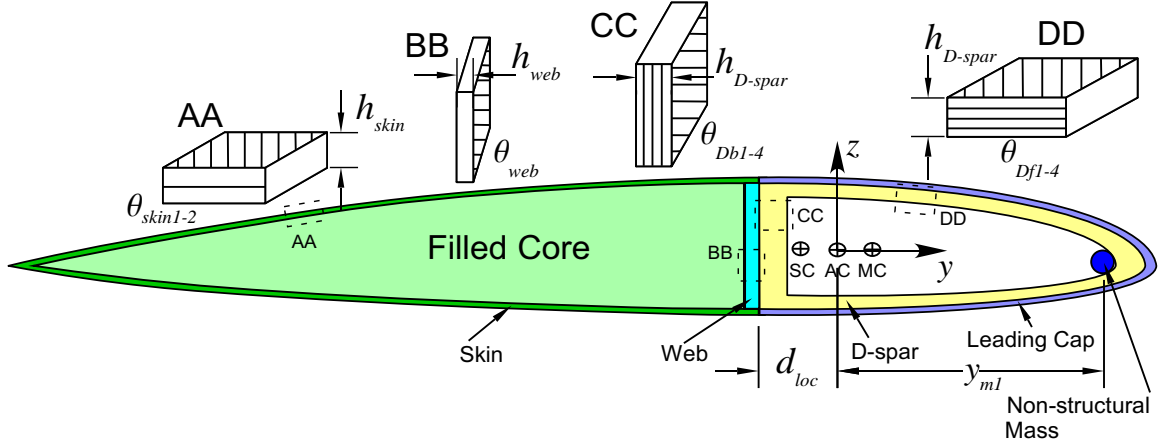


Figure 22: The structural template of a typical blade cross-section with a non-structural mass

independent on the curve wall of the D-spar. AA, BB, CC, and DD of Figure 22 show the detail sequence of composite layers in each components. The skin, the D-spar, and the web are designed by T300/5208 laminated composite materials. The leading cap is made of titanium for erosion protection.

4.1.2 Design Objectives and Constraints

The cross-section layout is designed to satisfy the requirements of stiffness, natural frequencies, fatigue life, and strength. In order to improve the payload of aircraft, the mass is generally expected to be minimized. To avoid resonance conditions, the natural frequencies of the blade are selected to be spaced away from the rotation speed and the integer times of rotation speed. Another concern of in helicopter rotor design is the dynamic coupling of bending and torsional loads since this coupling is responsible for flutter and other dynamic instabilities in rotor blades. The coupling depends on the lift (a transverse load) and the distance between the shear center (SC) and the aerodynamic center (AC). Hence, the cross-section design attempts to minimize the distance between the SC and AC. Moreover, the structure must perform without failure under specified service loads and have enough fatigue life. Design variables include thicknesses of the four structural components, the location

and the orientation of the D-spar, and fiber orientations. The design variables and material properties [74] are summarized in Tables 7 and 1, respectively.

Table 7: Design variables and feasible ranges

Component	Variable	Feasible range	Units
skin	h_{skin}	[0.0075, 0.035]	inch
	$\theta_{\text{skin1-2}}$	[-90, 90]	degree
web	h_{web}	[0.0075, 0.035]	inch
	θ_{web}	[-90, 90]	degree
D-spar	h_D	[0.04, 0.16]	inch
	d_{loc}	[-1.65, -0.2]	inch
	d_{ang}	[80, 100]	degree
	θ_{Df1-4}	[-90, 90]	degree
	θ_{Db1-4}	[-90, 90]	degree

The objective is to minimize the blade weight and locate shear center to aerodynamic center. Weight factors are used to convert the multi-objective function into a single objective function.

$$\min: 10m(\mathbf{X}) + 100 \frac{|e(\mathbf{X})|}{c} \quad (41)$$

$$\mathbf{X} = \{X_1, X_2, \dots, X_n\}^T$$

where \mathbf{x} is a column matrix, and the components x_1, x_2, \dots, x_n are the design variables, summarized in Table 7.

The design constraints are summarized below.

- The first six natural frequencies of the blade are placed away from the rotor rotation speed and its integer times. The frequency constraints are written as

$$0.2 < \frac{f_1(\mathbf{X})}{\Omega} < 0.8 \quad (42a)$$

$$1.08 < \frac{f_2(\mathbf{X})}{\Omega} < 1.7 \quad (42b)$$

$$0.15 < \frac{f_i(\mathbf{X})}{\Omega} - \left\lfloor \frac{f_i(\mathbf{X})}{\Omega} \right\rfloor < 0.85, \quad i = 3, 4, 5, 6 \quad (42c)$$

where f_i is the i th frequency of the blade, and $\lfloor \cdot \rfloor$ implies the integer part of the value.

- To reduce the dynamic coupling of bending and torsional loads, the distance between SC and AC is restricted to be smaller than 0.1% chord, which is

$$\frac{|e(\mathbf{X})|}{c} < 0.1\% \quad (43)$$

where e is the offset from aerodynamic center to shear center, and c is the chord.

- The coupling terms of tension-twist and bending-twist are required to very small in comparison with the diagonal terms in stiffness matrix shown in equation (40).
- The structure must be safe under the service loads in terms of strength failure criteria. For isotropic material, Von Mises criteria Equation (35) used, and Tsai-Wu Equation (36) for laminated materials. The blade is designed for infinite life using 10,000 hours as the cycle criteria.
- The manufacturing constraints are

$$X_i^L \leq X_i \leq X_i^U, \quad i = 1, \dots, n \quad (44)$$

where the superscript $(\cdot)^L$ and $(\cdot)^U$ indicate the lower and upper bounds of the design variables.

4.1.3 Sectional Properties Analysis

In chapter 2, we have discussed the sectional properties analysis associated with the cross-section without nonstructural mass. Since the nonstructural mass is assumed not contribute to sectional stiffness, the generalized Timoshenko stiffness matrix is the same as the case without nonstructural mass. Furthermore, the shear center that computed based on the flexibility matrix is the same as the case without nonstructural mass, too. Stress/strain analysis is also the same. However, the sectional mass is altered by the non-structural mass, resulting in the change of the natural frequencies and aeroelastic behavior of the blade.

The sectional inertia of the cross-section with nonstructural mass has two parts: the inertia of non-structural mass and non-structural cross-section. The total sectional mass is computed as

$$m = m_0 + m_1 \quad (45)$$

$$y_{m0} = \frac{1}{m_0} \int_A \rho y dydz \quad (46)$$

where m_0 , m_1 , ρ , and y_{m0} are sectional mass without non-structural mass, non-structural mass, material density, and y-coordinate of the mass center without non-structural mass. m_0 and y_{m0} have been determined in cross-sectional analysis without nonstructural mass. $y_{m0} < 0$ implies that MC is behind aerodynamic center, which is unstable. In this situation, a non-structural mass is added so that MC is coincidence with AC. m_1 is computed as

$$m_1 = \frac{m_0 y_{m0}}{y_{m1}} \quad (47)$$

where y_{m1} , y-coordinate of the non-structural mass, is known.

The total mass moment of inertia is

$$I_{yy} = I_{yy0} + m_0 y_{m0}^2 + m_1 y_{m1}^2 \quad (48)$$

where I_{yy0} is the mass moment of inertia without the non-structural mass.

4.1.4 Aeroelastic Analysis and Rotor Trim

A three-bladed hingeless rotor [36], shown in Figure 23, is considered here. The blade is assumed to be an elastic beam undergoing axial extension, flap bending, lag bending, and elastic twist, with a rotation speed of Ω . The blade connects with a flexural beam. The revolute joint provides the pitch control of the blade. Figure 24 shows the DYMORE topology model of the rotor system.

A comprehensive multi-body dynamic analysis code DYMORE developed by Bauchau [9] is used to simulate the helicopter blade dynamic aeroelastic response. The aeroelastic response equations developed in chapter 2 include centrifugal forces, gravity, and aerodynamic forces. The aerodynamic forces are calculated by the unsteady aerodynamic theory [70], and 28 finite states are used in the dynamic inflow model.

For the convenience of numerical computation, the blade is discretized into a number of beam elements. Each element has four nodes (2 boundary nodes and 2 interior nodes), and each node has six degrees of freedom that correspond to three displacements and rotations. After the spatial discretization, an eigenvalue problem is solved for natural vibration modes of the rotor system. Then, the aeroelastic response equations are solved. The blade loads are integrated over the blade span and transformed from rotating frame to inertial frame to obtain the hub loads. The steady-state components of hub loads are used for wind tunnel trim. Auto-pilot control law [69] is used in the trim with a forward level flight speed 123 ft/sec and the total lift 1500lb.

4.1.5 Stress and Fatigue Analysis

Once the converged trim solution is obtained, stress analysis is carried out by using VABS recovery theory [34]. The calculation of the 3D strain/stress requires the

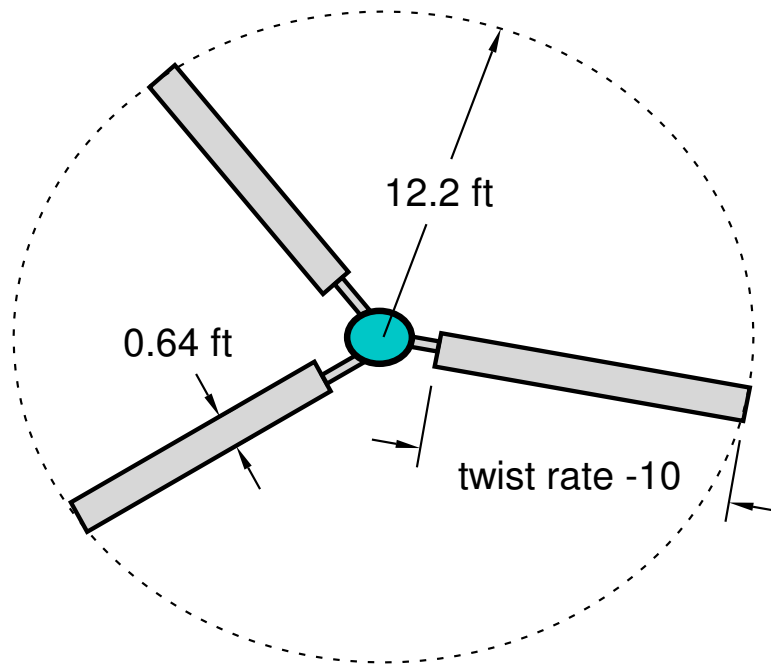


Figure 23: A three-bladed hingeless rotor

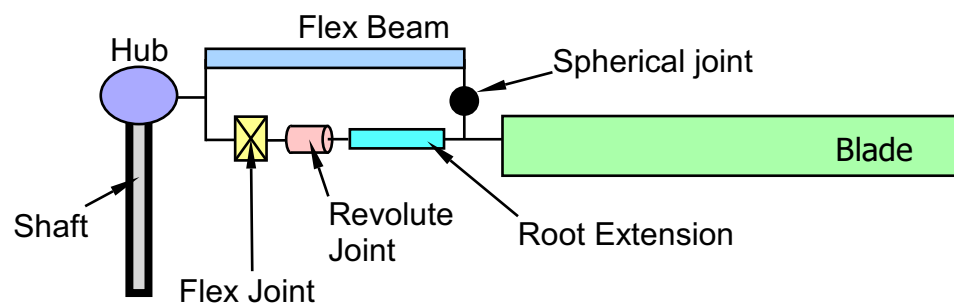


Figure 24: The DYMORE topology model of the hingeless rotor

Table 8: Parameters for Fatigue Analysis

K_0	b_0	λ	β_0
2.38×10^{-58}	17.3	9.231	598.4 MPa

warping function, the generalized Timoshenko compliance matrix, and curvature information that have been obtained in sectional analysis. To improve computation efficiency, superposition method is employed in stress analysis.

Fatigue analysis is conducted layer by layer for laminates using a strength-based fatigue model that have been discussed in chapter 2. The unidirectional parameters are summarized in table 8 calculating based on the data from [92, 59]. When the applied stress equals or exceeds the residual strength, failure occurs in terms of the Tsai-Wu failure criteria [29]. Tsai-Wu failure criterion is used for the multi-axial stress states in laminates. The coupling fatigue strength analysis is conducted once a cycle until fatigue strength is equal to the applied stress.

4.1.6 Optimization Procedure

The optimal design, or the solution of the above equations, are searched using sequential quadratic programming optimization algorithm [80, 6]. During the design optimization, the outer configuration and the connectivity of the structural components remain fixed. Figure 25 shows the design procedure. In each iteration, the values of design variables and material properties are passed to the geometry generator that generates the required cross-section layout and an appropriate mesh. The geometry, mesh and initial twist information are used by VABS to compute the sectional properties. The results of VABS are used to model the blade as one dimensional rotating beam with a multy-body dynamics code DYMORE [9] being used to compute the natural frequencies. If the frequencies satisfy the constraints, the rotor is trimmed for a forward level flight condition. Otherwise, the optimizer determines the next design point by perturbing the last point that satisfies all the constraints, and

new iteration begins. Once a convergent trim solution is obtained, VABS recovery relation is used to compute the stress over the cross-section. By using the stress history, fatigue life is predicted by strength degradation model. If fatigue life satisfies the requirement, a candidate design is stored, then another iteration begins.

4.2 *Design Results*

As an example, the blade structural design is based on a three-bladed hingeless rotor. The service rotation speed is 50.0 rad/sec. Loading condition is obtained using the trim results for a forward level flight with a speed of 123 ft/sec and total lift 1500 lb. Because the coupling procedure of trim and aeroelastic response analysis takes a long time, this procedure is conducted only when the basic design constraints are satisfied during the optimization. To reduce the probability of the local optimum, the optimization starts from a population of randomly initialized designs. There were 16 initial designs that resulted in five local optimums that satisfy the basic constraints.

The following figures and tables shows the results of the best local optimum in terms of the sectional mass, stiffnesses, natural frequencies, and fatigue life. Figure 26 shows the optimization history of the objective function. Figures 27 to 31 show the steady-state loads history at the root of section and stress history at the critical point over the root section. Table 9 shows the comparisons between the initial design and optimal design. In the initial design, the frequency of the second flap (the third mode) is 3.056 times the rotor angular speed. The design does not satisfy the frequency constraints, so the aeroelastic response and fatigue analysis are not conducted. Obviously, the amplitudes of dynamic responses are quite significant resulting in a shorter fatigue life. The fatigue life for the optimal design is 4.531×10^8 cycles or 1.58×10^4 hours, satisfying the infinite life criterion. The accuracy of this model should be tested by experimental data.

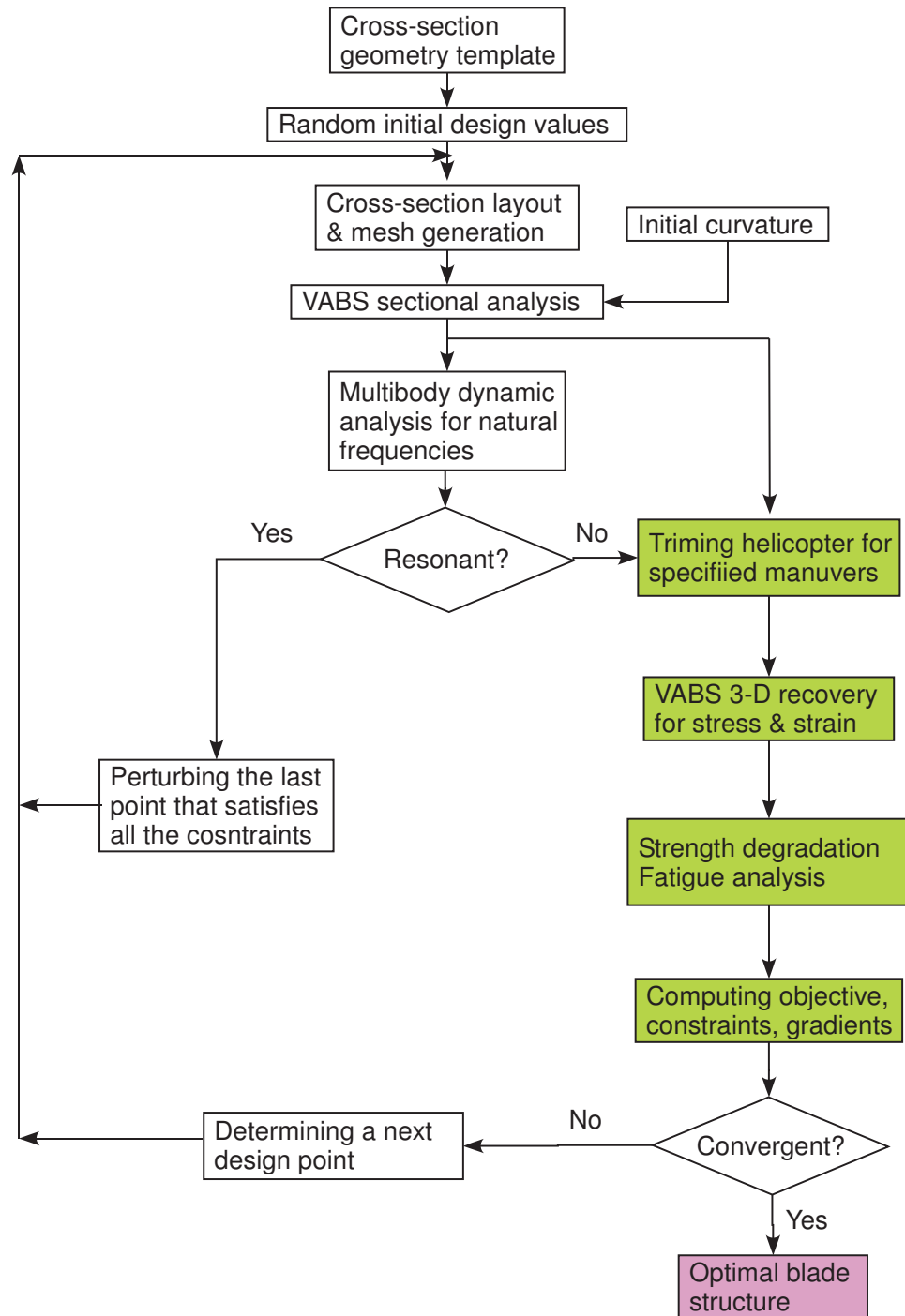


Figure 25: The optimization flow chart for composite blade design with durability analysis

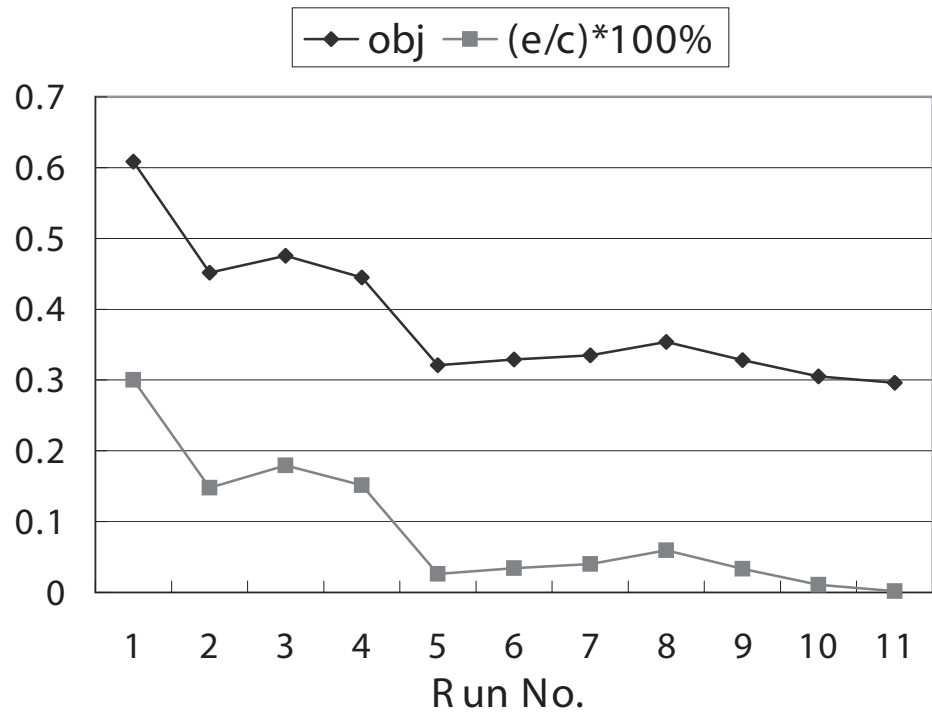


Figure 26: Optimization history of the objective function

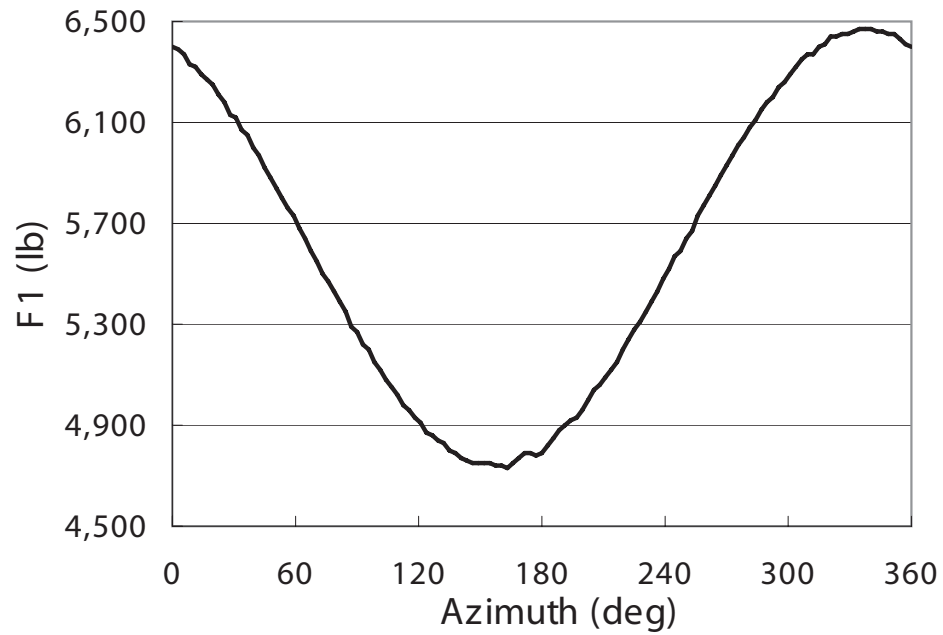


Figure 27: Steady-state axial loads history at the root of the blade

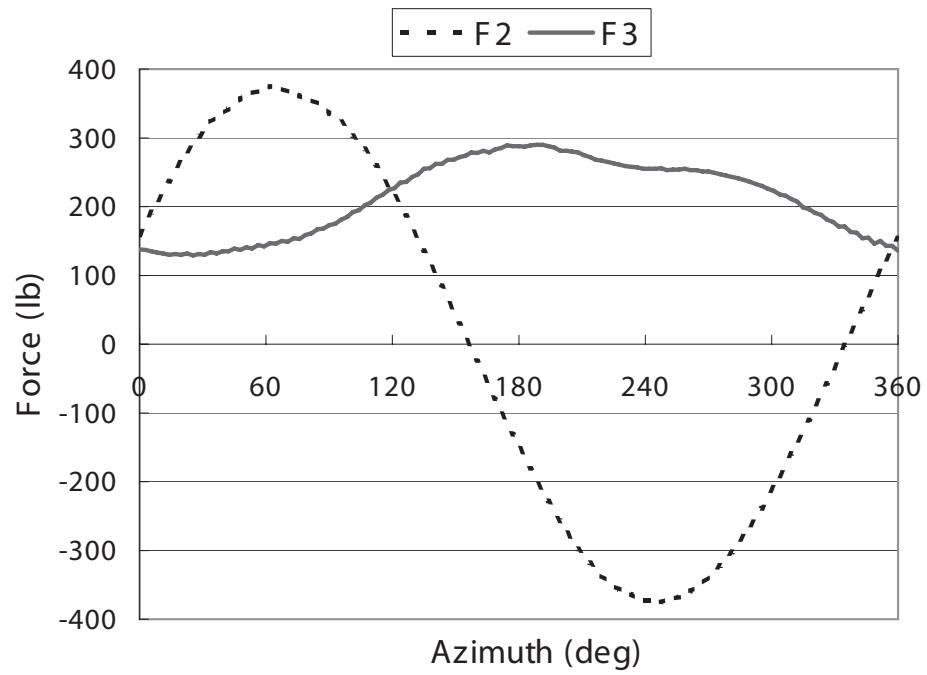


Figure 28: Steady-state shear forces history at the root of the blade

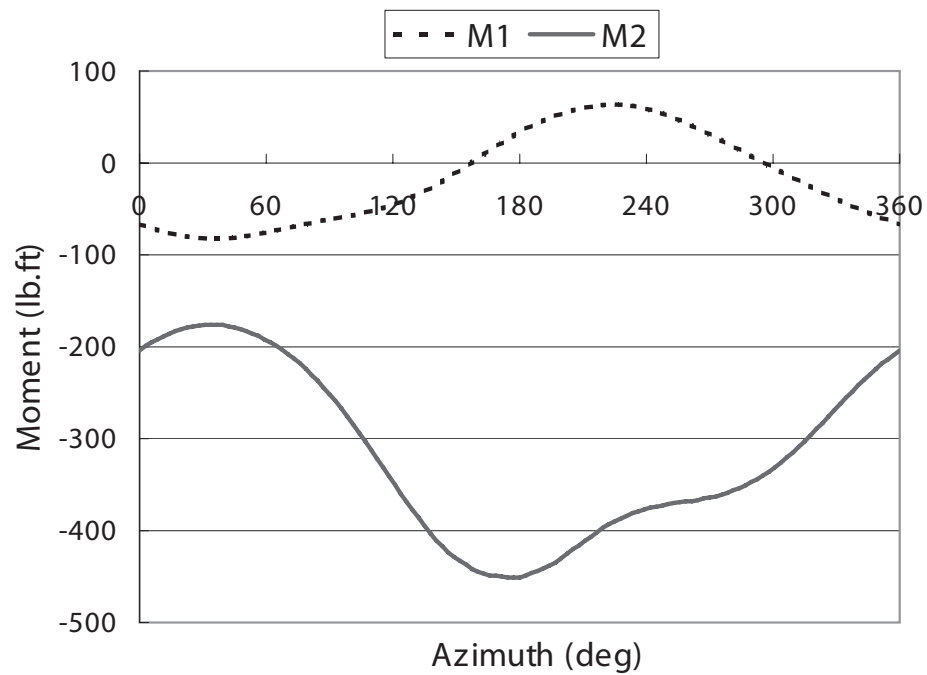


Figure 29: Steady-state torsion and lag moments history at the root of the blade

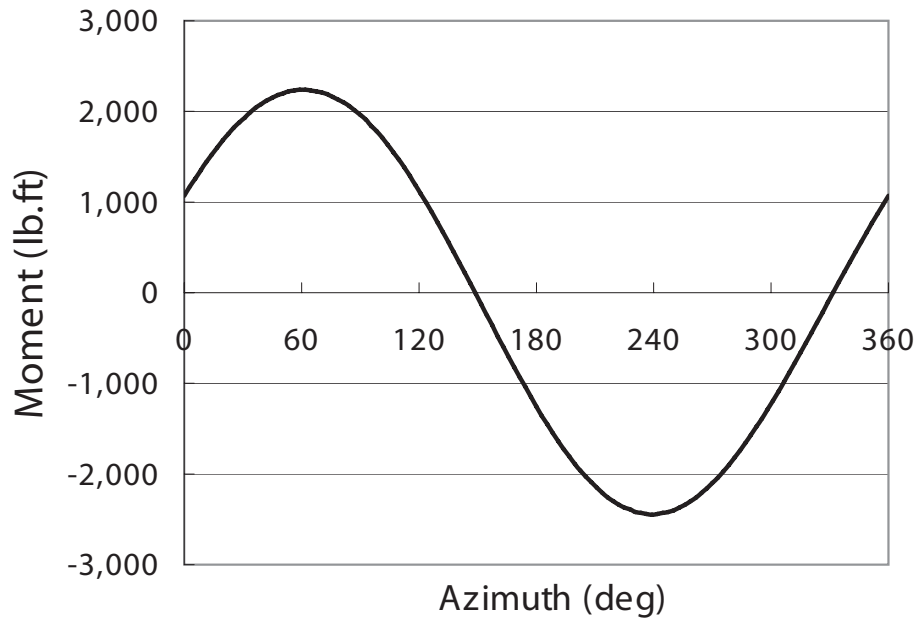


Figure 30: Steady-state flap moments history at the root of the blade

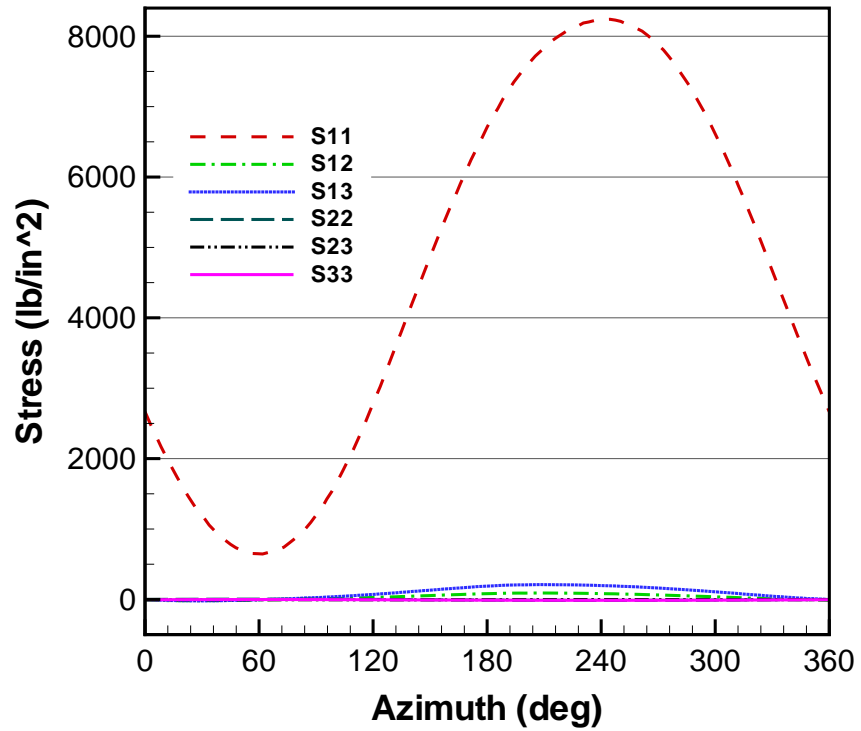


Figure 31: Steady-state stress history of the critical point over the root section

Table 9: The comparison between the initial design and the optimal design

Design variables			Response variables		
Name	Initial	Optimal	Name	Initial	Optimal
h_{skin} (in)	0.011	0.012	m (slug/ft)	0.031	0.029
θ_{skin1}	45.00	-0.342	$m_1 \times 10^{-3}$ (slug/ft)	4.431	1.122
θ_{skin2}	-45.00	-22.879	$\frac{e}{c} \times 100\%$	0.3	0.002
h_{web} (in)	0.011	0.008	EA (lb)	1.345	1.948
θ_{web}	0.00	0.665	$EI_{yy} \times 10^3$ (lb-ft ²)	8.875	1.265
h_D (in)	0.114	0.150	$EI_{zz} \times 10^5$ (lb-ft ²)	1.322	3.551
d_{loc} (in)	-1.141	-0.519	$GJ \times 10^3$ (lb-ft ²)	3.860	3.538
d_{ang}	90.00	103.028	$\frac{f_1}{\Omega}$	0.690	0.752
θ_{Df1}	45.00	17.599	$\frac{f_2}{\Omega}$	1.072	1.080
θ_{Df2}	0.00	0.03	$\frac{f_3}{\Omega}$	3.056	3.217
θ_{Df3}	0.00	-0.237	$\frac{f_4}{\Omega}$	5.133	6.619
θ_{Df4}	-45.00	14.138	$\frac{f_5}{\Omega}$	6.188	6.849
θ_{Db1}	45.00	87.812	$\frac{f_6}{\Omega}$	7.072	7.150
θ_{Db2}	0.00	1.277	$N_f \times 10^8$ (cycles)	N/A	4.531
θ_{Db3}	0.00	0.451			
θ_{Db4}	-45.00	-88.026			

CHAPTER V

PROBABILISTIC DESIGN

The uncertainty or randomness associated with the imperfections exists in all real-life products. Although the aerospace engineering production processes are better controlled than those of other industries, small variations inevitably exist in structural dimensions, geometric shape, and material properties. These imperfections can substantially influence a rotor blade's performance, stability margin and fatigue life. The principal objective of this chapter is to find a probabilistic model for the sectional properties of rotor blades due to geometric uncertainty and material property variability. After that, we incorporate statistical information obtained from manufacturing and simulation into the design optimization to improve the reliability of the blades. As a result of this study, engineers will better understand the actual effect of manufacturing tolerances and material property variability. This study may assist manufacturers in setting quality control standards for composite rotor blades.

5.1 Probabilistic Design Approach

To manage the manufacturing and environmental uncertainty, we employ a probabilistic design approach in a composite rotor blade design. To conduct the probabilistic design, one must clearly identify the inputs to the system and their consequent responses. In the structural design of composite blades, this implies the specification of which design variables should be treated as random. For example, manufacturing process and the choice of measurement device could lead to inaccuracy of shape and size. The temperature and the moisture at which blades work could result in material properties deviating from their designated values. The resulting uncertainty of design variables could be characterized by statistical parameters. Given the statistical

characteristics of the design variables, the probabilistic design optimizes the mean performance of blades and minimizes performance changes subject to the reliability constraints. The reliability constraints ensure that blades perform their intended function or maintain safety under normal conditions during the designed life time. The following section will define the measure of mean performance, performance changes, reliability constraints and Monte Carlo simulation methods.

5.1.1 Mean performance and performance variation

The structural performance of blades, including cross-sectional mass, stiffnesses, frequencies, and safety, is determined by the geometry shape, component size, component location, and materials that are chosen as design variables in blade design. Mathematically, the performance is a function of these design variables. Since some of the design variables are random variables, the values of performance function also randomly change. Therefore, to represent the general significance of these unequal values, given a performance function f , the mean performance is defined as

$$\begin{aligned}\overline{f(\mathbf{x})} &= E[f(\mathbf{x} + \delta, a)|\mathbf{x}] \\ &= \int \int f(\mathbf{x} + \delta, a)p(\delta, a|\mathbf{x}) d\delta da\end{aligned}\tag{49}$$

where \mathbf{x} is the vector of design variables; δ and a are random variables, representing perturbations of the design variables and the variation of the working environment, respectively; and function $p(\delta, a|\mathbf{x})$ is a joint conditioning PDF of the random variables. The performance change is measured through its variation, given by

$$\begin{aligned}\text{Var}(f(\mathbf{x})) &= E\left[\left(f(\mathbf{x} + \delta, a) - \overline{f(\mathbf{x})}\right)^2|\mathbf{x}\right] \\ &= \int \int \left(f(\mathbf{x} + \delta, a) - \overline{f(\mathbf{x})}\right)^2 p(\delta, a|\mathbf{x}) d\delta da\end{aligned}\tag{50}$$

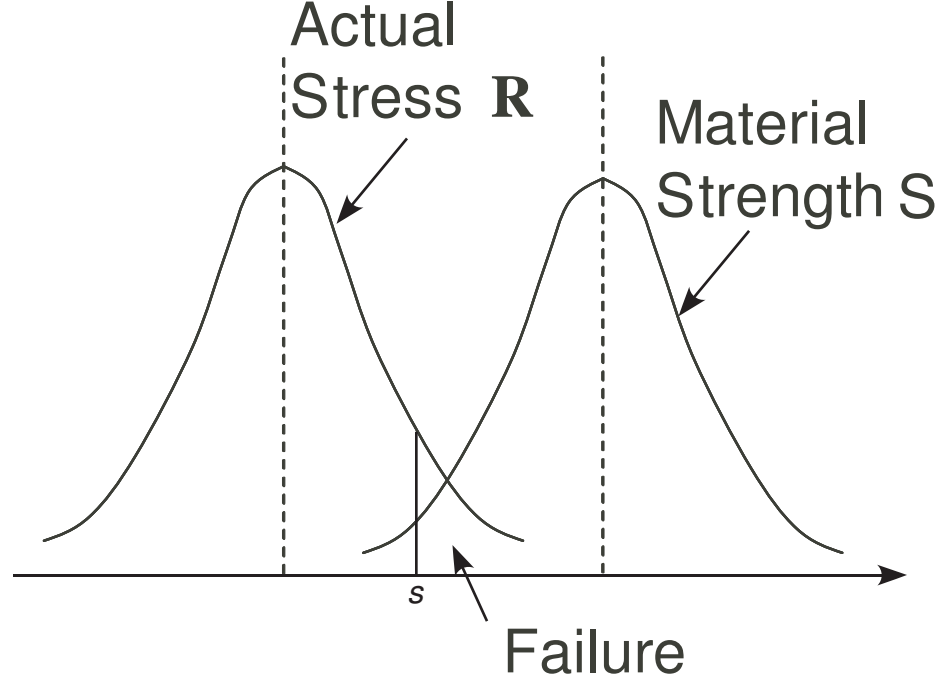


Figure 32: The concept of reliability and the event region of failure

5.1.2 Reliability constraints

As defined in the beginning of this section, reliability is associated with the safety factor of the blade structure. The reliability can be evaluated through the probability of failure. Typically, safety rules require the maximum response of a structure less than its capacity such as material strength. Therefore, safety factor can be defined by a normalized function. When the value of a safety factor function is less than unity, failure occurs, which can be expressed as

$$g(\mathbf{R}(\mathbf{x} + \delta, a), \mathbf{S}) \leq q \quad (51)$$

where \mathbf{R} and \mathbf{S} , which are randomly varying in general, are stress or strain at a critical point and material ultimate strength, respectively. The factor of safety g is a random variable, associated with a certain failure criteria. The selection of failure criteria for composite materials will be explained later. A constant q is the design safety factor. It can be one, but usually it is greater than one and given by design regulations [1, 2].

Because of the uncertainty in manufacturing process and environmental conditions, both the applied loads and material strength are random variables that follow a certain probability distribution. Figure 32 shows the concept of reliability and the event region of failure. A reliability constraint is formulated as a probabilistic requirement for safety ratio, which is

$$P_f(\mathbf{x}) \leq P_T \quad (52)$$

$$\begin{aligned} P_f(\mathbf{x}) &= \text{Prob}(g(\mathbf{R}, \mathbf{S}) \leq q|\mathbf{x}) \\ &= \underbrace{\int \int \int_A p(\delta, a, S|\mathbf{x}) d\delta da dS} \end{aligned} \quad (53)$$

where A , P_T and P_f are a failure region prescribed by g , the target failure probability and the failure probability of the specified design, respectively. Mathematically, P_f is the cumulative distribution function (CDF) of the safety factor g . In general, because it is very difficult to perform the integration in Equation (49), (50), and (53), we have to use numerical integration schemes such as Monte Carlo simulation.

5.1.3 Monte Carlo Simulation

Monte Carlo simulation (MCS) and direct sampling technique are used to calculate the probability of failure in this design. MCS is most suitable to calculate the integration shown in Equation (53), in which the failure region is an implicit function [57]. MCS is also capable to calculate high-dimensional integration resulting from a system affected by a large number of uncertain factors. In addition, MCS is a special stochastic method that simulates the system behavior without further modification of the existing deterministic model and analysis program. Therefore, MCS is the most feasible uncertainty analysis technique for helicopter blade design, which involves strong non-linearities and multiple disciplines [63].

The drawback of MCS is extensive computation. In order to improve the MCS

efficiency, different sampling strategies have been used in different structural problems [57, 78]. Reference [61] discussed the selection of sampling strategies and their restrictions in detail. Because the design space of composite blade design is highly nonlinear and non-convex, the advanced sampling strategies complicate the design. Therefore, direct sampling technique is employed in this research.

If the number of simulation times is N and the number of failure times is N_f , then the failure probability resulting from MCS is

$$P_f = \frac{N_f}{N} \quad (54)$$

Obviously, the accuracy of the probability estimation is governed by the number of simulation times. Given a confidence level C , the number of simulation times can be estimated by

$$N \geq \frac{-\ln(1 - C)}{P_f} \quad (55)$$

For details on the implementation of MCS, please refer to [61].

5.2 *Design Objectives and Constraints with Uncertainty*

Compared with the deterministic design model, the probabilistic design model has probabilistic constraints such as reliability and performance variation. The objective of the probabilistic design is to minimize the mean performance:

$$\min: 10 \overline{m(\mathbf{x})} + 100 \frac{\overline{|e(\mathbf{x})|}}{c} + \frac{1}{\overline{g_{min}(\mathbf{x})}} \quad (56)$$

where \mathbf{x} is a design vector; $\overline{(\cdot)}$ denotes mean value; m , e , and g_{min} are sectional mass, the offset from SC to AC, and the minimum safety factor over the cross-section, respectively.

Because MCS is computationally expensive, we do not set a very high reliability level – only 0.85 – to improve the optimization efficiency. One reason is that we use a

conservative extreme load assumption so that the maximum values of all six sectional load components are reached simultaneously. For preliminary design, efficiency is more important. The objective of preliminary design is to filter out some very bad designs and to find the best candidate for further analysis. In the reliability constraint, the safety factor is defined by Tsai-Wu failure criteria that represents the interaction of different stress components in composite failure mechanisms [29].

The safety factor g with Tsai-Wu criteria has been defined in equation (36). In this equation, the values of X_t , Y_t , X_c , Y_c and S are uncertain because of the manufacturing process, environmental conditions, and experimental error [11, 76, 88]. Stresses denoted with σ_1 , σ_2 , and τ_{12} are also uncertain because they depend on random design variables and uncertain service loads.

Another sets of probabilistic constraints include the variation of sectional mass and the stiffness of flap, lag, and torsional are less than five percent of the mean values.

To ensure the blade have sufficient sectional stiffness, we constrain the first non-rotating flapping frequency, torsional stiffness ratio, and lag stiffness ratio:

$$\frac{1.875^2}{\Omega} \left(\sqrt{\frac{EI_{22}}{mL^4}} \right) \leq 0.35 \quad (57)$$

$$5 \leq \left(\frac{EI_{33}}{EI_{22}} \right) \leq 80 \quad (58)$$

$$0.1 \leq \left(\frac{GJ}{EI_{22}} \right) \leq 5 \quad (59)$$

The frequency constraints are expressed in terms of average values:

In addition, the constraints of the frequencies Equations (42) and the coupling terms Equations (40) are expressed in terms of averages values instead of the deterministic value. The manufacturability constraints is the same as Equations (44).

5.3 Geometrical Uncertainty Effects

The inner surface of a realistic blade cross-section generally is not smooth, but it typically has a wavy structure. To describe such a wavy structure, we introduce a curvilinear coordinate. The wavy structure is modeled by harmonic functions with some random parameters, such that

$$r(s) = r_0 + A_1 \sin(f_1 s + \phi_1) + A_2 \sin(f_2 s + \phi_2) \quad (60)$$

where amplitudes A_1 , A_2 , frequencies f_1 , f_2 , and phase angles ϕ_1 , ϕ_2 are random numbers, and s is a natural curvilinear coordinate.

Preliminary results presented herein are based on only hollow laminated blades made from graphite/epoxy with stacking sequence $[0^\circ, 45^\circ, -45^\circ, 0^\circ]$ from the inner surface to the outer surface of the blade skin. In this preliminary investigation, the material property variation resulting from ply waviness is ignored. Monte Carlo simulation is carried out with the assumption that the amplitude follows a uniform distribution between 0% and 0.35% chord, and the frequency follows a uniform distribution between 0 and 100 rad/s.

Simulation results show that the geometry uncertainty has little effects on the stiffness and mass per unit length of blade cross-sections. However, the geometry uncertainty can affect the stress distribution, the shear center, and the mass center substantially. Figures 33 and 34 compare the stress level of a perfect symmetric cross-section and a cross-section with geometry uncertainty. The stress level of a cross-section with geometry uncertainty could be 25% higher than that of the perfect section. Figures 5.3 and 36 compare the stress level of unsymmetric cross-sections with geometry uncertainty and without uncertainty. The stress level of the cross-section with geometry uncertainty could be 30% higher than that of the perfect one.

In Figure 37, compared to the perfect section, the safety factor of the critical point

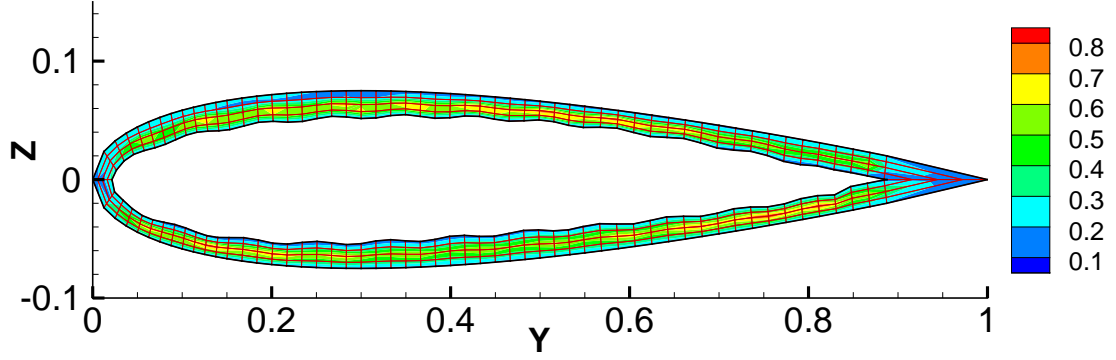


Figure 33: The normalized equivalent stress σ_{eq} distribution over a perturbed hollow cross-sections with NACA0015 airfoil. Perturbation amplitude parameters A_1 and A_2 are 3% and 7% skin thickness, respectively. Frequency parameters f_1 and f_2 are 78.8 and 7.88, respectively. Phase angle ϕ is zero.

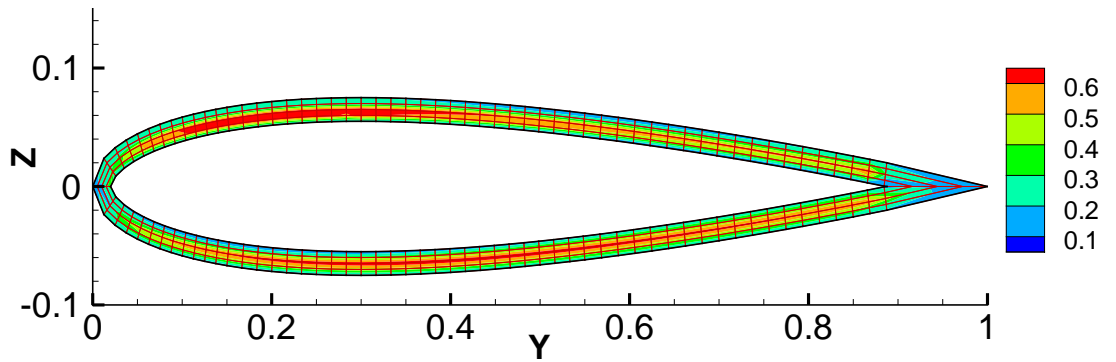


Figure 34: The normalized equivalent stress σ_{eq} distribution over the perfect section with NACA0015 airfoil

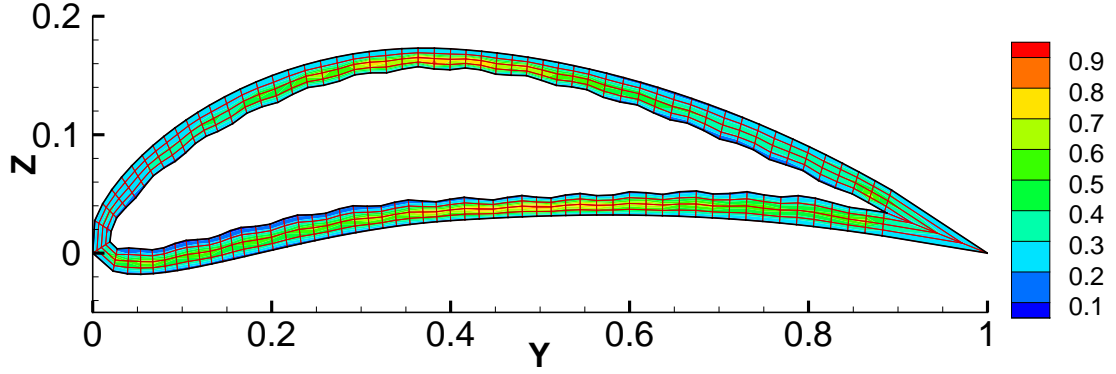


Figure 35: The normalized equivalent stress σ_{eq} distribution over a perturbed hollow cross-sections with NACA1415 airfoil. Perturbation amplitude parameters A_1 and A_2 are 3% and 7% skin thickness, respectively. Frequency parameters f_1 and f_2 are 78.8 and 7.88, respectively. Phase angle ϕ is zero.

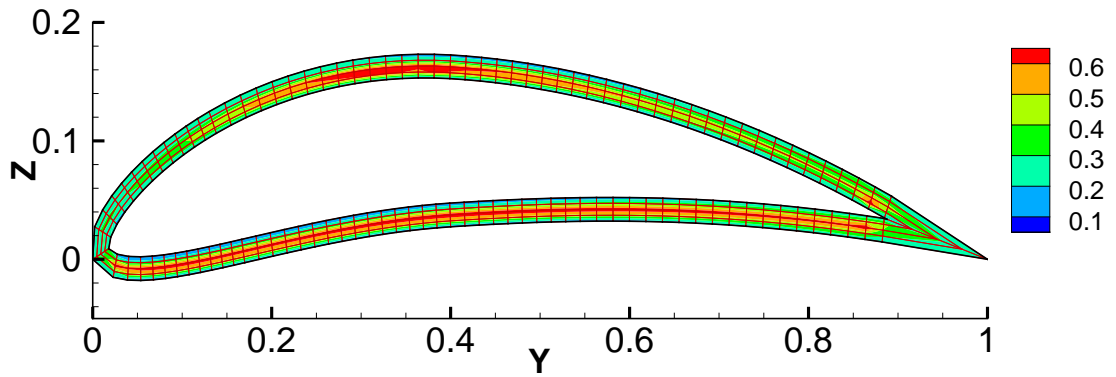


Figure 36: The normalized equivalent stress σ_{eq} distribution over a perfect section with NACA1415 airfoil

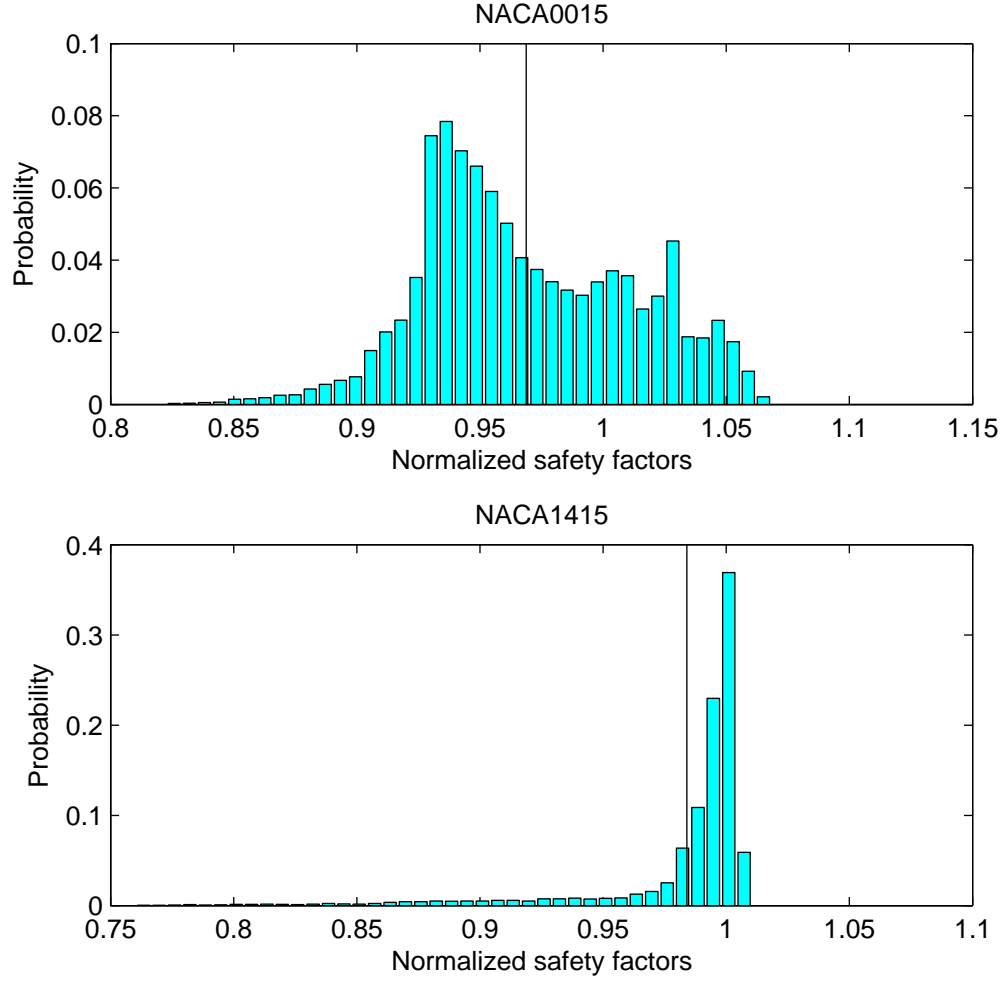


Figure 37: The histogram of the minimum safety factors g_{min} of perturbed cross-sections normalized with respect to that of the perfect section (vertical thin lines are mean values 0.969 and 0.984 for sections with NACA0015 and NACA1415 airfoils, respectively.)

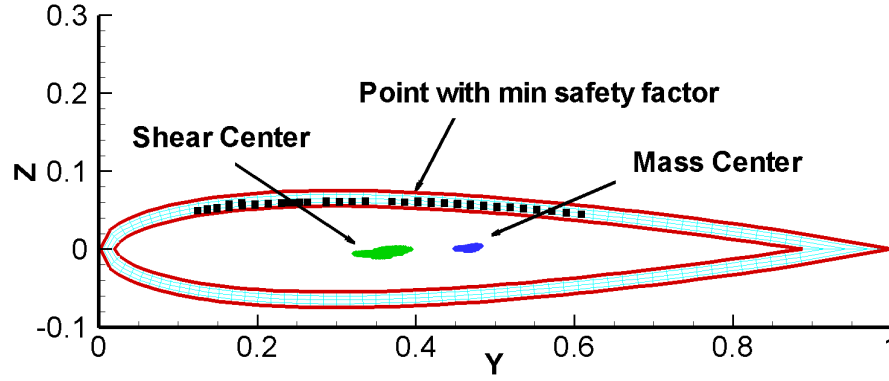


Figure 38: Possible locations of point with minimum safety factor g , mass center, and shear center for perturbed hollow cross-sections with NACA0015 airfoil

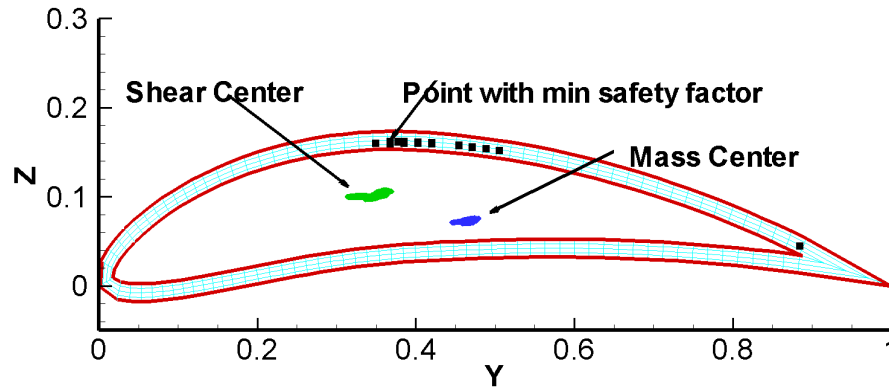


Figure 39: Possible locations of point with minimum safety factor g , mass center, and shear center for perturbed hollow cross-sections with NACA1415 airfoil

in a perturbed section can reduce by up to 15% and 10% for sections with airfoils NACA0015 and NACA1415, respectively, with the mentioned geometry uncertainty. The average safety factors for the perturbed sections are 96.9% and 98.4% that of the perfect section for sections with airfoils NACA0015 and NACA1415, respectively. The impact of the geometrical uncertainty greatly depends on the section shapes.

Figures 38 and 39 shows the possible locations of point with minimum safety factor, mass center, and shear center of the hollow cross-sections with geometry uncertainty. The shear center is more sensitive to geometry uncertainty than the mass center. Because the coupling of torsion and bending depends on the location of the shear center, geometry uncertainty have substantial effects on the aeroelastic response of the blade.

5.4 Design Results

Sequential quadratic programming is used in the proposed probabilistic design for rotor blades. Figure 40 shows the optimization flow chart. During each iteration, the sectional analysis and aeroelastic analysis of the composite blades without uncertainty are conducted first. If the natural rotating frequencies are too close to the integer times of rotation speed, resonance is assumed to happen and this iteration stops without rotor trim. A refined design point is decided by perturbing the last design point that satisfies all the constraints. If resonance does not occur, rotor trim is conducted. After rotor trim, Monte Carlo simulation begins. Manufacturing uncertainties are introduced to the perfect geometry layout, while service load uncertainties are introduced to the rotor trim results. Then, the average, the variation, and the reliability of blade performance are calculated to obtain the objective and constraints. This optimization iteration is updated until the objective function is converged to the minimal value. This implementation procedure assumes that the small perturbation will not severely alter the blade sectional properties and natural frequencies. Figure

41 shows the optimization history of objective function value. Table 10 compare the optimization results with uncertainty and without uncertainty.

The results show that the amount of uncertainty present in the design variables and service loads significantly affect the design. When uncertainty is introduced, moving the shear center close to the aerodynamic center in the range of 0.2% chord cannot be achieved. Without uncertainty, the distance of SC and AC can be optimized to only 0.01% chord. In contrast, in the case with uncertainty, the mean value of probablistic design is 0.23% chord, and the coefficient of variance is 0.85. The mass per unit length of the resulting optimal designs from deterministic methods and the proposed probablisitic method do not differ significantly.

After the optimum design is obtained, a more accurate MCS simulation (6400) is conduced to investigate the reliability of the resulting design. The failure probability of the optimal design with the given uncertainty is 0.83%. The confidence level is 99.9%. The histogram of stiffnesses and frequencies is shown in Figures 42, 43, and 44, respectively. The statistical results are shown in Table 10.

The coefficient of variation of the extension, torsion, flap, and lag stiffnesses are all less than the smallest coefficient of variation of the introduced uncertainties 5%. The greatest coefficient of variation among the stiffnesses is lag stiffness 4.1%, the smallest one is flap stiffness 3.0%.

Table 11 summarizes the frequencies of the optimal design resulting from probabilistic approach. The coefficients of variation of the natural rotating frequencies are less than those of nonrotating frequencies, which implies that the natural rotating frequencies are not so sensitive to the manufacturing uncertainties as those of non-rotating frequencies. The explanation is that the centrifugal forces increase the stiffnesse. The coefficient of variation of the first flap, torsion, and lag rotating modes are 0.3%, 1.4%, and 1.1%, respectively. The flap modes are less sensitive to manufacturing uncertainties because the centrifugal stiffness has a large portion of the total

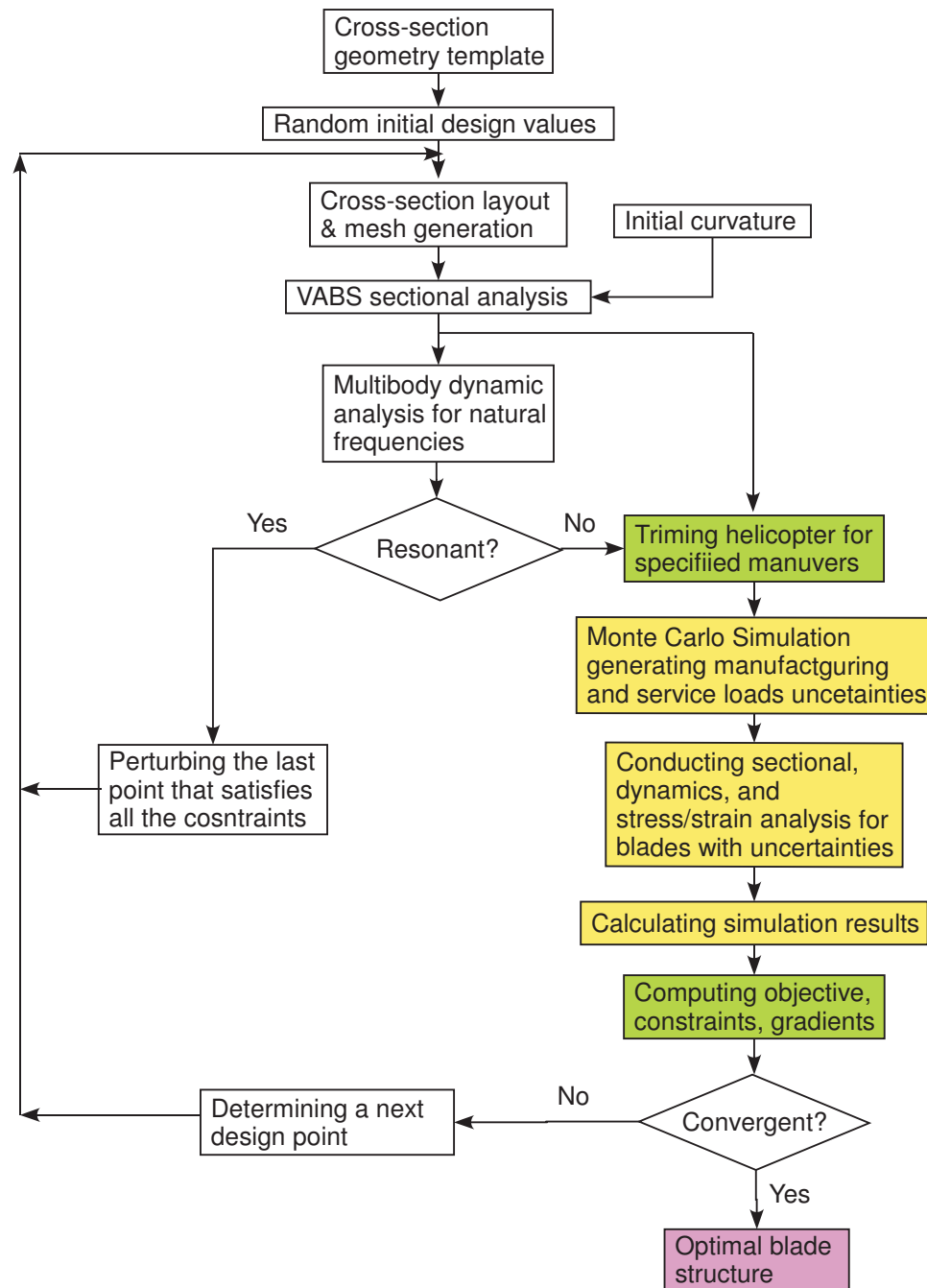


Figure 40: The flow chart of probabilistic approach for composite blade structural design

Table 10: The comparison of optimization results between the design with and without uncertainties

Design variables			Response variables			
Name	Determin.	Prob.	Name	Deterministic	Probabilistic	
					Mean	Coef. Var.
h_{skin} (in)	0.030	0.027	m (slug/ft)	0.03	0.03	0.026
θ_{skin1}	-1.37	-0.54	g_{min}	12.01	12.11	0.18
θ_{skin2}	-37.76	-36.66	$\frac{e}{c} \times 100\%$	0.01	0.23	0.85
h_{web} (in)	0.020	0.020	EA (lb)	2.01×10^7	1.88×10^7	0.031
θ_{web}	0.21	0.65	GJ (lb-ft ²)	2.50×10^3	2.55×10^3	0.035
h_D (in)	0.398	0.400	EI_{yy} (lb-ft ²)	1.32×10^4	1.23×10^4	0.030
d_{loc} (in)	-1.29	-1.49	EI_{zz} (lb-ft ²)	3.21×10^5	2.92×10^5	0.041
d_{ang}	80.00	84.81	$\frac{f_1}{\Omega}$ 1L	0.80	0.80	0.011
θ_{Df1}	14.34	16.88	$\frac{f_2}{\Omega}$ 1F	1.12	1.12	0.003
θ_{Df2}	-0.42	0.08	$\frac{f_3}{\Omega}$ 2F	3.44	3.41	0.007
θ_{Df3}	-0.05	0.39	$\frac{f_4}{\Omega}$ 1T	6.36	6.54	0.014
θ_{Df4}	9.10	11.68	$\frac{f_5}{\Omega}$ 2L	6.78	6.73	0.012
θ_{Db1}	89.61	89.70	$\frac{f_6}{\Omega}$ 3F	7.25	7.17	0.010
θ_{Db2}	0.81	1.11				
θ_{Db3}	0.19	0.50				
θ_{Db4}	-89.76	-89.93				

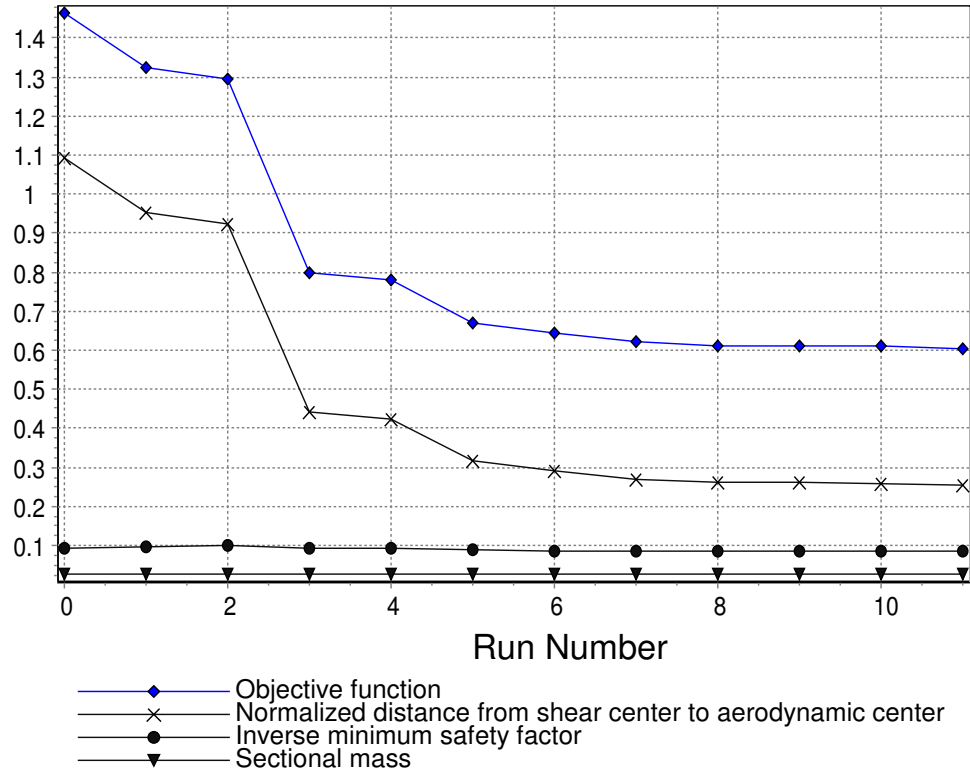


Figure 41: Optimization history of the objective function

Table 11: The frequencies of the optimal design

	Nonrotating frequency		Rotating frequency	
	Mean	Coef. Var.	Mean	Coef. Var.
1L	0.78	0.013	0.8	0.011
1F	0.36	0.017	1.12	0.003
2F	2.21	0.017	3.41	0.007
1T	6.50	0.015	6.54	0.014
2L	6.35	0.013	6.73	0.012
3F	5.91	0.016	7.17	0.01

stiffness for flap modes. As the mode number increase, the portion for structural flap stiffness is increase, so the effects of manufacturing uncertainties are increase, too. Thus, the coefficient of variation of the first, second, and third flap modes are 0.3%, 0.7%, and 1.0%, respectively.

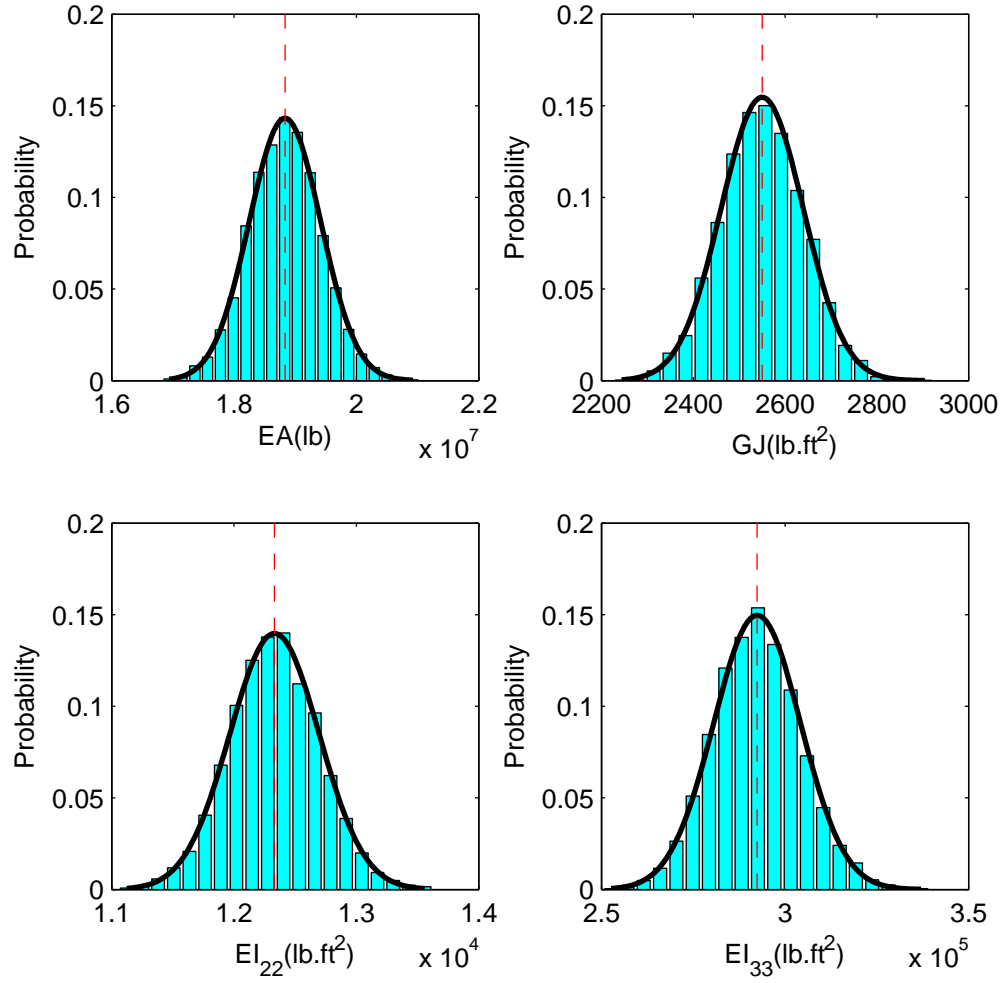


Figure 42: Probability histogram of sectional stiffness(thick black solid line is fitted normal distribution; vertical thin dash line is mean value of the design with introduced uncertainties)

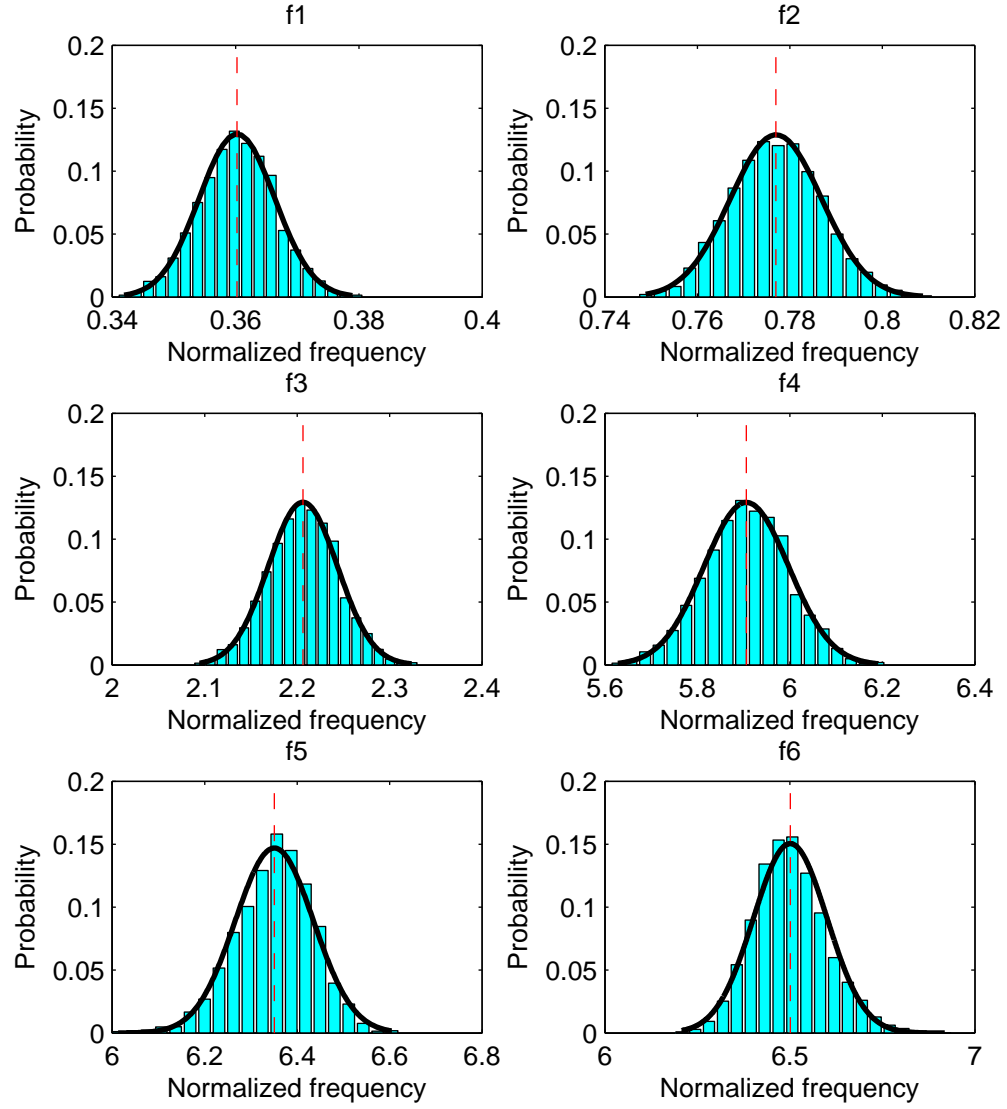


Figure 43: Probability histogram of the first six nonrotating natural frequencies (thick black solid line is fitted normal distribution; vertical thin dash line is mean value of the design with introduced uncertainties)

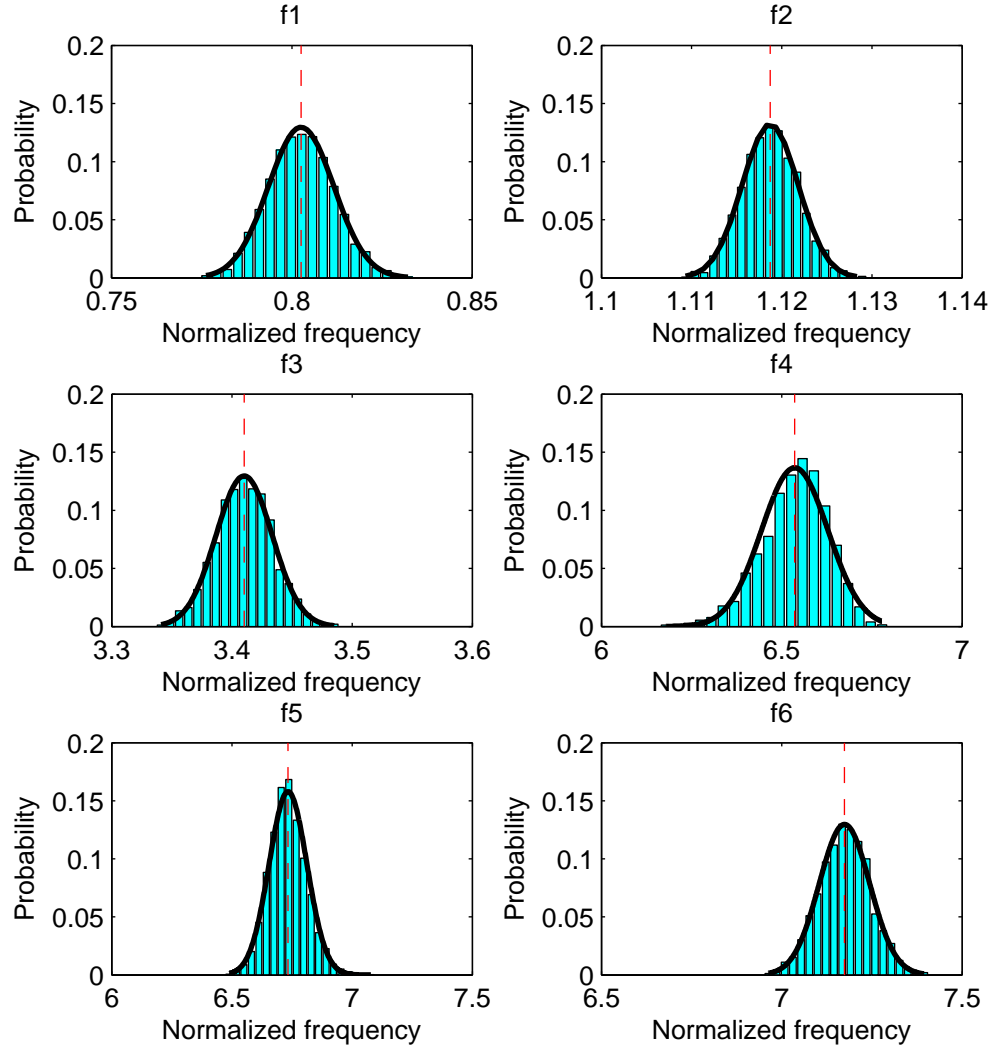


Figure 44: Probability histogram of the first six rotating natural frequencies (thick black solid line is fitted normal distribution; vertical thin dash line is mean value of the design with introduced uncertainties)

CHAPTER VI

CONCLUSION AND FUTURE WORK

6.1 Conclusion

This research proposes a modular methodology for composite rotor blade structural design. The method is applied to study three new aspects of the structural design. The following conclusions are reached:

1. The proposed method is demonstrated by local cross-section optimization of rotor blades. Compared with other the traditional design methods, this design method is more efficient and accurate, and it can be easily plugged into other multidisciplinary design.
2. The proposed method is applied to solve the structural optimization problem with manufacturability constraints. This optimization problem is a mixed-variable problem. To solve such a mixed-variable problem, a hybrid optimization procedure is proposed that utilizes the advantages of both sequential quadratic programming and genetic algorithm. The test example shows that the optimal solution improves significantly with 1% less mass per unit length and 32% less stress level in comparison with the baseline model. The offset from shear center to aerodynamic center reduced from 4.17% chord of baseline model to -0.0015% chord of optimal solution. All the stiffnesses are in the target ranges. The computation cost is about half of the general genetic algorithm.
3. The sensitivity analysis show that shear center and stress level are very sensitive to the variation of design variables. Moreover, using the cross-section template without nonstructural mass, both the shear center and the mass center can be

moved close to the aerodynamic center without violating current stiffness constraints, but the mass center cannot be moved as close as the shear center. The distance between mass center and aerodynamic center can be further reduced if another design variable (e.g. a non-structural point mass near the leading edge) is added.

4. A new design method is proposed for design against fatigue that combined the above structural design method. The proposed method integrates with sectional analysis, aeroelastic analysis, rotor trim, and durability analysis. Fatigue life prediction employs the 3D stress recovery from VABS in conjunction with a strength-based fatigue model. The proposed method is demonstrated by a three-bladed hingeless-rotor structural design. The optimization minimizes the sectional weight subject to constraints on stiffness, weight, frequency and fatigue life. The resulting optimal solution meets the durability requirement that traditional design method requires multitude design optimization to satisfy. Preliminary results indicate that this approach is promising for blade structural design against fatigue failure.
5. The impacts of manufacturing uncertainties, especially the geometry perturbation (the wavy ply and inner surface), are investigated by VABS sectional properties analysis tool and Monte Carlo simulation. Harmonic functions are used to model the wavy perturbation. Based on the preliminary results, the effects of such geometry perturbations depend on the cross-section shape. The effects on shear center are worse than mass center. The geometry perturbations have few impacts on stiffness.
6. The combinatorial impacts of manufacturing uncertainties, including dimension, geometry, and material properties, are investigated by Monte Carlo simulation.

Manufacturing uncertainties have significant impacts on the stiffness and aeroelastic behavior of rotor blades. The rotating frequencies are less affected than the non-rotating frequencies, especially for the flap modes because of centrifugal forces. As the mode the number increases, the impacts of manufacturing uncertainties become more serious as well.

7. Probabilistic approach is proposed to control the uncertainties. The uncertainties introduced to the design include geometry, material properties, and service loads. In this approach, the object is to minimize the average the structural performance subject the constraints of stiffness, frequencies, performance variation, and reliability. The Monte Carlo simulation and the above structural design method are combined. The probabilistic approach is also demonstrated by a three-bladed hingeless-rotor design. The optimal design resulting from probabilistic approach improves significantly, but not as good as the design from deterministic approach. In the test example, the coefficient of variation of stiffness, frequencies, mass per unit length are less than that of the introduced uncertainties. The shear center is significantly affected by manufacturing uncertainties. In the test example, the coefficient of variation is 85%. With uncertainties, the shear center can be optimized to 0.01% chord; without uncertainties, it can only be 0.23% chord.

6.2 *Future Work*

1. In the current design, the number of layers of composites is fixed, and each layer has the same layer thickness. That is, the layer thickness is equal to the total thickness divides by the number of layers. However, because the feasible values of layer thickness are certain discrete numbers, this assumption possibly results in the infeasible layer thickness. A better way is to choose layer thickness and the number of layers as design variables. If the fiber orientations of all layers are

dependent design variables, the number of variables of the optimization problem is changeable. The applicable algorithm for such problem is very difficult to find in literature.

2. The fatigue life prediction is based on a strength-degradation fatigue model. This model is easy to incorporate into the proposed structural optimization procedure. However, the accuracy of this model requires a large number of fatigue experimental data for various laminates layups. To simplify the fatigue analysis, the material Young's modulus is assumed to be constant with only the strength decreasing. In fact, both the material Young's modulus and strength decrease. The former affects the blade sectional properties, and consequently the blade aeroelastic response. As a result, the sectional, aeroelastic response, trim and fatigue analysis become fully coupled and extremely challenging from the computational standpoint. Further research needs to be conducted in order to justify the validity and relative impact of time-dependent material properties, and the appropriate corrections need to be made to the model.
3. The investigation of geometry uncertainty impacts ignores the material property variability around the ply waviness. The geometry uncertainty model need be calibrated by the realistic manufacturing data. The proposed method need to be applied to the calibrated model and compared with the measured structural performance data.
4. In this research, the impacts of manufacturing uncertainties of stiffnesses and frequencies are investigated. The thorough investigation on aeroelastic response such as stability needs to be conducted in the future.
5. Fatigue behavior is another important problem of rotor blades. Fatigue behaviors are governed by many factors including manufacturing process and imperfection. The proposed method of VABS in conjunction with strength-based

fatigue model can be used to study the impacts of manufacturing uncertainties on fatigue behaviors.

REFERENCES

- [1] “Damage tolerance and fatigue evaluation of structure,” Tech. Rep. No. 25.571-1C, FAA Advisory Circular.
- [2] “Fatigue of rotorcraft structure,” Tech. Rep. 20-95, FAA Advisory Circular, 1995.
- [3] “The material properties of commercial pure titanium,” 2004. http://www.ife.no/media/446_FactsTiAlloy.pdf.
- [4] “Design space report,” 2005. <http://www.ansys.com/products/downloads/report1/report.htm>.
- [5] ALEXANDER, H. R., SMITH, K. E., McVEIGH, M. A., DIXON, P. G., and McMANUS, B. L., “Preliminary design study of advanced composite blade and hub and nonmechanical control system for the tilt-rotor aircraft,” Tech. Rep. CR-152336-1, NASA, November, 1979.
- [6] ARORA, J. S., “Computational design optimization: A review of future directions,” *Structural Safety*, vol. 7, pp. 131–148, 1990.
- [7] ARORA, J. S. and WANG, Q., “Review of formulations for structural and mechanical system optimization,” *Structural and Multidisciplinary Optimization*, vol. 30, no. 4, pp. 251–272, 2005.
- [8] BAUCHAU, O., BOTTASSO, C., and NIKISHKOV, Y., “Modeling rotorcraft dynamics with finite element multibody procedures,” *Mathematical and Computer Modeling*, vol. 33, pp. 1113–1137, 2001.
- [9] BAUCHAU, O. A., “DYMORE user’s manual,” 2007. <http://www.ae.gatech.edu/people/obauchau/>.
- [10] BERDICHEVSKY, V. L., “Variational-asymptotic method of constructing a theory of shells,” *Journal of Applied Mathematics and Mechanics (English translation of Prikladnaya Matematika i Mekhanika)*, vol. 43, no. 4, pp. 664–687, 1979.
- [11] BOGETTI, T. A., GILLESPIE, JR., J. W., and LAMONTIA, M. A., “Influence of ply waviness on the stiffness and strength reduction on composite laminates,” *Journal of Thermoplastic Composite Materials*, vol. 5, no. 4, pp. 344 – 369, 1992.
- [12] BOGGS, P. T. and TOLLE, J. W., “Sequential quadratic programming,” *Acta Numerica*, vol. 4, pp. 1–15, 1996.

- [13] BRADLEY, D. J., ADAMS, D. O., and GASCOIGNE, H. E., "Interlaminar strains and compressive strength reductions due to nested layer waviness in composite laminates," *Journal of Reinforced Plastics and Composites*, vol. 17, no. 11, pp. 989–1011, 1998.
- [14] CELI, R., "Recent applications of design optimization to rotorcrafta survey," *Journal of Aircraft*, vol. 36, no. 1, pp. 176–189, 1999.
- [15] CESNIK, C. E. S. and HODGES, D. H., "VABS: A new concept for composite rotor blade cross-sectional modeling," *Journal of the American Helicopter Society*, vol. 42, no. 1, pp. 27–38, 1997.
- [16] CESNIK, C. E. S., MOK, J., PARIKH, A. S., and SHIN, S., "Optimization design framework for integrally twisted helicopter blades," in *Proceedings of the 45th AIAA/ASME/ASCE/AHS/ASC Structures, Structural Dynamics and Materials Conference*, vol. 4, (Palm Springs, CA.), pp. 2736–2750, 2004.
- [17] CHATTOPADHYAY, A., MCCARTHY, T., and PAGALDIPTI, N., "Multilevel decomposition procedure for efficient design optimization of helicopter rotor blades," *AIAA Journal*, vol. 33, no. 2, pp. 223–230, 1995.
- [18] COELLO, C. A., "Theoretical and numerical constraint handling techniques used with evolutionary algorithms: A survey of the state of the art," *Computer Methods in Applied Mechanics and Engineering*, vol. 191, no. 11-12, pp. 1245–1287, 2002.
- [19] DEGRIECK, J. and VAN, P. W., "Fatigue damage modelling of fibre-reinforced composite materials: Review," *Applied Mechanics Reviews*, vol. 54, no. 4, pp. 279–300, 2001.
- [20] D'IPPOLITO, R., DONDEERS, S., HACK, M., TZANNETAKIS, N., LINDEN, G. V. D., and VANDEPITTE, D., "Reliability-based design optimization of composite and steel aerospace structures," in *Proceedings of the 47th AIAA/ASME/ASCE/AHS/ASC Structures, Structural Dynamics, and Materials Conference*, (Newport, RI), May 1-4, 2006. AIAA 2006-2153.
- [21] DOVRAKAND, G.J.AND LAWS, N., "Analysis of progressive matrix cracking in composite laminates ii first ply failure," *Journal of Composite Materials*, no. 21, pp. 309–329, 1987.
- [22] FANJOY, D. W. and CROSSLEY, W. A., "Using a genetic algorithm for structural topology design of helicopter rotor blades," in *Proceedings of the 42nd AIAA/ASME/ASCE/AHS/ASC Structures, Structural Dynamics and Materials Conference and Exhibit*, vol. 5, (Seattle, Washington), pp. 3110–3118, American Inst. Aeronautics and Astronautics Inc., Apr. 16-19, 2001. AIAA 2001-1605.

- [23] FLAGGS, D. and LAWS, N., "Prediction of tensile matrix failure in composite laminates," *Journal of Composite Materials*, vol. 19, no. 1, pp. 29–50, 1985.
- [24] FRIEDMANN, P. P., "Helicoptervibration reduction using structural optimization with aeroelastic/multidisciplinary constraintsa survey," *Journal of Aircraft*, vol. 28, no. 1, pp. 8–21, 1991.
- [25] GANGULI, R. and CHOPRA, I., "Aeroelastic optimization of a helicopter rotor with two-cell composite blades," *AIAA Journal*, vol. 34, no. 4, pp. 835–854, 1996.
- [26] GANGULI, R., "Survey of recent developments in rotorcraft design optimization," *Journal of Aircraft*, vol. 41, no. 3, pp. 493–510, 2004.
- [27] GARNICH, M. R. and KARAMI, G., "Localized fiber waviness and implications for failure in unidirectional composites," *Journal of Composite Materials*, vol. 39, no. 14, pp. 1225–1245, 2005.
- [28] GUERDAL, Z., TAMASINO, A. P., and BIGGERS, S. B., "Effects of processing induced defects on laminate response: Interlaminar tensile strength," *SAMPE Journal*, vol. 27, pp. 3–49, 1991.
- [29] GÜRDAL, Z., HAFTKA, R. T., and HAJELA, P., *Design and Optimization of Laminated Composite Materials*. New York: John Wiley Sons, Inc., 1999.
- [30] HAJELA, P., "Nongradient methods in multidisciplinary design optimization-status and potential," *Journal of Aircraft*, vol. 36, no. 1, pp. 255–265, 1999.
- [31] HALE, R. D. and VILLA, M., "Influence of opposing wave nesting in compression-loaded composites," *Journal of Composite Materials*, vol. 37, no. 13, pp. 1149–1166, 2003.
- [32] HAUGEN, E. B., *Probabilistic Mechanical Design*. New York: Wiley, 1980. pp. 91–188.
- [33] HODGES, D. H., ATILGAN, A. R., CESNIK, C. E. S., and FULTON, M. V., "On a simplified strain energy function for geometrically nonlinear behaviour of anisotropic beams," *Composites Engineering*, vol. 2, no. 5-7, pp. 513–526, 1992.
- [34] HODGES, D. H., *Nonlinear Composite Beam Theory*. Reston, Virginia: AIAA, 2006. Chapter 4.
- [35] HODGES, D., "A review of composite rotor blade modeling," *AIAA Journal*, vol. 28, no. 3, pp. 561–565, 1990.
- [36] HOEPFER, M., LAURENDEAU, B., MISHRA, S., SHROTRI, K., SIRIROJVISUTH, A., SUHR, C. S., THEEL, T., WU, L., and YANG, J., *23rd AHS Annual Student Design Competition Report–Rambler*. Georgia Institute of Technology, 2006.

- [37] HOGG, R. V., MCKEAN, J. W., and CRAIG, A. T., *Introduction to Mathematical Statistics*. Upper Saddle River, NJ: Pearson Education, sixth ed., 2004.
- [38] HOLLAND, J., *Adaptation in Natural and Artificial Systems*. Ann Arbor: University of Michigan Press, 1975.
- [39] HONG, X., *Three-Dimensional Strain and Stress Recovery Theory for Initially Curved and Twisted Composite Beams*. M.S., Georgia Institute of Technology, 2001.
- [40] HUANG, H. and TALREJA, R., “Effects of void geometry on elastic properties of unidirectional fiber reinforced composites,” *Composites Science and Technology*, vol. 65, no. 13, pp. 1964–1981, 2005.
- [41] HUGHES, G. W. and MCINNES, C. R., “Solar sail hybrid trajectory optimization for non-keplerian orbit transfers,” *Journal of Guidance, Control, and Dynamics*, vol. 25, no. 3, pp. 602–604, 2002.
- [42] HYPERWORKS7.0, *Altair OptiStruct: Concept Design Using Topology and Topography Optimization*. Altair Engineering, Inc., 2004.
- [43] JEN, M.-H. and LEE, C.-H., “Strength and life in thermoplastic composite laminates under static and fatigue loads. part II: formulation,” *International Journal of Fatigue*, vol. 20, no. 9, pp. 617–629, 1998.
- [44] JOHNSON, W., *Helicopter Theory*. New York: Dover publications, Inc., 1994.
- [45] KIM, J.-E. and SARIGUL-KLIJN, N., “Structural optimization for light-weight articulated rotor blade,” in *Proceedings of the 41st AIAA/ASME/ASCE/AHS/ASC Structures, Structural Dynamics, and Materials Conference*, (Atlanta, GA), Apr. 3-6, 2000. AIAA 2000-1520.
- [46] KIM, J.-E. and SARIGUL-KLIJN, N., “Elastic-dynamic rotor blade design with multiobjective optimization,” *AIAA Journal*, vol. 39, no. 9, pp. 1652–1661, 2001.
- [47] KIM, T. K. and HWANG, I. H., “Reliability analysis of composite wing subjected to gust loads,” *Composite Structures*, vol. 66, no. 1-4, pp. 527–531, 2004.
- [48] KOTTEGODA, N. T. and ROSSO, R., *Statistics, Probability, and Reliability for Civil and Environmental Engineers*. McGraw-Hill, 1997.
- [49] KU, J., *Hybrid Optimization of Aeromechanical Stability for Rotorcraft with Composite Blades*. Ph.D., Georgia Institute of Technology, 2007.
- [50] K.W, G. and E., B. J., “Multiple transverse fracture in 90 crossply laminates of a glass fibre-reinforced polyester,” *Journal of Material Science*, no. 12, pp. 157–168, 1977.

- [51] LAND, A. and DOIG, A., "An automatic method for solving discrete programming problems," *Econometrica*, vol. 28, pp. 497–520, 1960.
- [52] LAWLER, E. and WOOD, D., "Branch-and-bound methods: A survey," *operations research*, vol. 14, pp. 699–719, 1966.
- [53] LEE, J. and HAJELA, P., "Parallel genetic algorithm implementation in multidisciplinary rotor blade design," *Journal of Aircraft*, vol. 33, no. 5, pp. 962–969, 1996.
- [54] LEMANSKI, S. L., WEAVER, P. M., and HILL, G. F. J., "Design of composite helicopter rotor blades to meet given cross-sectional properties," *Aeronautical Journal*, vol. 109, no. 1100, pp. 471–475, 2005.
- [55] LI, J., "Flange delamination prediction in composite structures with ply waviness," *AIAA Journal*, vol. 38, no. 5, pp. 893–897, 2000.
- [56] LI, L., VOLOVOI, V. V., and HODGES, D. H., "Cross-sectional design of composite rotor blades considering manufacturing constraints," in *Proceedings of the 63rd Annual Forum of the American Helicopter Society*, (Virginia Beach, Virginia), 2007.
- [57] LIAN, Y. and KIM, N.-H., "Reliability-based design optimization of a transonic compressor," in *Proceedings of the 41st AIAA/ASME/SAE/ASEE Joint Propulsion Conference and Exhibit*, (Tucson, Arizona), Jul. 10-13, 2005. AIAA 2005-4021.
- [58] LINDSLEY, N. J., BERAN, P. S., and PETTIT, C. L., "Effects of uncertainty on nonlinear plate aeroelastic response," in *Proceedings of the 43rd AIAA/ASME/ASCE/AHS/ASC Structures, Structural Dynamics, and Materials Conference*, (Denver, Colorado), Apr. 22-25, 2002. AIAA 2002-1271.
- [59] LIU, B. and LESSARD, L. B., "Fatigue and damage-tolerance analysis of composite laminates: Stiffness loss, damage-modelling, and life prediction," *Composites Science and Technology*, vol. 51, pp. 43–51, 1994.
- [60] LUO, Y.-Z., TANG, G.-J., WANG, Z.-G., and LI, H.-Y., "Optimization of perturbed and constrained fuel-optimal impulsive rendezvous using a hybrid approach," *Engineering Optimization*, vol. 38, no. 8, pp. 959–973, 2006.
- [61] MELCHERS, R. E., *Structural Reliability Analysis and Prediction*. John Wiley and Sons, Inc., second ed., 1999. Chapter 3 and 5.
- [62] MIURA, H., "Applications of numerical optimization methods to helicopter design problems a survey," *Vertica*, vol. 9, no. 2, pp. 141–154, 1985.
- [63] MURUGAN, S., GANGULI, R., and HARURSAMPATH, D., "Aeroelastic response of composite helicopter rotor with random material properties," *Journal of Aircraft*, vol. 45, no. 1, pp. 306–322, 2008.

- [64] ORR, S. A. and HAJELA, P., “A comprehensive model for multi-disciplinary design of a tiltrotor configuration,” in *Proceedings of the 46th AIAA/ASME/ASCE/AHS/ASC Structures, Structural Dynamics, and Materials Conference*, (Austin, Texas), Apr. 18 - 21, 2005. AIAA 2005-2284.
- [65] OZBAY, S., *Extension-twist Coupling Optimization in Composite Rotor Blades*. Ph.D., Georgia Institute of Technology, 2006.
- [66] PAEPEGEM, W. V. and DEGRIECK, J., “Modelling damage and permanent strain in fibre-reinforced composites under in-plane fatigue loading,” *Composites Science and Technology*, vol. 63, no. 5, pp. 677–694, 2003.
- [67] PAIK, J., VOLOVOI, V. V., and HODGES, D. H., “Cross-sectional sizing and optimization of composite blades,” in *Proceedings of the 43rd AIAA/ASME/ASCE/AHS/ASC Structures, Structural Dynamics, and Materials Conference*, (Denver, Colorado), pp. 601–610, Apr. 22-25, 2002. AIAA 2002-1322.
- [68] PATIL, M. J. and JOHNSON, E. R., “Cross-sectional analysis of anisotropic, thin-walled, closed-section beams with embedded strain actuation,” in *Proceedings of the 46th AIAA/ASME/ASCE/AHS/ASC Structures, Structural Dynamics and Materials Conference*, (Austin, Texas), Apr. 18-21, 2005. AIAA 2005-2037.
- [69] PETERS, D. and BARWEY, D., “A general theory of rotorcraft trim,” in *Proceedings of the 36th AIAA/ASME/ASCE/AHS/ASC Structures, Structural Dynamics, and Materials Conference and AIAA/ASME Adaptive Structures Forum*, (New Orleans, LA), pp. 2558–2590, 1995.
- [70] PETERS, D. and HE., C., “Finite state induced flow models. part II: Three-dimensional rotor disk,” *Journal of Aircraft*, vol. 32, no. 2, pp. 323–333, 1995.
- [71] PETERS, D., KARUNAMOORTHY, S., and CAO, W., “Finite state induced flow models. part I: Two dimensional thin airfoil,” *Journal of Aircraft*, vol. 32, no. 2, p. 313322, 1995.
- [72] PETTIT, C. L., “Uncertainty quantification in aeroelasticity: Recent results and research challenges,” *Journal of Aircraft*, vol. 41, no. 5, pp. 1217–1229, 2004.
- [73] PETTIT, C. L. and BERAN, P. S., “Effects of parametric uncertainty on airfoil limit cycle oscillation,” *Journal of Aircraft*, vol. 40, no. 5, pp. 1004–1006, 2003.
- [74] PIATAK, D. J., NIXON, M. W., and KOSMATKA, J. B., “Stiffness characteristics of composite rotor blades with elastic couplings,” Tech. Rep. TP-3641, NASA, 1997.
- [75] PIEGL, L. and TILLER, W., *The Nurbs Book*. Berlin, New Jersey: Springer-Verlag, 2nd ed., 1997.

- [76] PIGGOTT, M., "The effect of fiber waviness on the mechanical properties of unidirectional fiber composites – a review," *Composites Science Technology*, vol. 53, pp. 201–205, 1995.
- [77] PRADLWARTER, H. J., PELLISSETTI, M. F., SCHENK, C. A., SCHULLER, G. I., KREIS, A., FRANSEN, S., CALVI, A., and KLEIN, M., "Realistic and efficient reliability estimation for aerospace structures," *Computer Methods in Applied Mechanics and Engineering*, vol. 194, no. 12-16, pp. 1597–1617, 2005.
- [78] RAIS-ROHANI, M. and XIE, Q., "Probabilistic structural optimization under reliability, manufacturability, and cost constraints," *AIAA Journal*, vol. 43, no. 4, pp. 864–873, 2005.
- [79] REIFSNIDER, K. L. and CASE, S. W., *Damage Tolerance and Durability of Material Systems*. New York: John Wiley & Sons, Inc., 2002.
- [80] ROSEN, J. B., "The gradient projection method for nonlinear programming, part one," *Journal SIAM*, vol. 8, pp. 181–217, 1960.
- [81] ROZVANY, G., *Topology Optimization in Structural Mechanics*. New York: Springer, 1997.
- [82] SCHAFF, J. R. and DAVIDSON, B., "Life prediction methodology for composite structures. part I - constant amplitude and two-stress level fatigue," *Journal of Composite Materials*, vol. 31, no. 2, 1997.
- [83] SCHAFF, J. R. and DAVIDSON, B., "Life prediction methodology for composite structures. part II - spectrum fatigue," *Journal of Composite Materials*, vol. 31, no. 2, 1997.
- [84] SCHAFF, J. R., "Fatigue analysis of helicopter tail rotor spar," in *39th AIAA/ASME/ASCE/ASC Structures, Structural Dynamics, and Materials Conference*, (Long Beach, CA), 1998.
- [85] SMITH, E. and CHOPRA, I., "Formulation and evaluation of an analytical model for composite box beams," *Journal of the American Helicopter Society*, vol. 36, no. 3, pp. 23–35, 1991.
- [86] SOBIESZCZANSKI-SOBIESKI, J. and HAFTKA, R., "Multidisciplinary aerospace design optimization: Survey of recent developments," in *Proceedings of the 34th Aerospace Sciences Meeting and Exhibit*, (Reno, NV.), Jan., 1996. AIAA 96-0711.
- [87] SOYKASAP, O., *Aeroelastic Optimization of a Composite Tilt Rotor*. Ph.D., Georgia Institute of Technology, 1999.

- [88] TALREJA, R., “Effects of manufacturing induced defects on composite damage and failure,” in *Proceedings of the 27th Riso International Symposium on Materials Science: Polymer Composite Materials for Wind Power Turbine* (LILHOLT, H., MADSEN, B., ANDERSEN, T., MIKKELSEN, L., and THYGESEN, A., eds.), (Roskilde, Denmark), Sep. 11-17, 2006.
- [89] TAN, S. and NUISMER, R., “A theory for progressive matrix cracking in composite laminates,” *Journal of Composite Materials*, vol. 23, no. 10, pp. 1029–1047, 1989.
- [90] THOMSEN, O. T., “Sandwich materials for wind turbine blades,” in *Proceedings of the 27th Riso International Symposium on Materials Science: Polymer Composite Materials for Wind Power Turbine* (LILHOLT, H., MADSEN, B., ANDERSEN, T., MIKKELSEN, L., and THYGESEN, A., eds.), (Roskilde, Denmark), Sep. 11–17, 2006.
- [91] TROSSET, M. W., “What is simulated annealing?,” *Optimization and Engineering*, vol. 2, no. 2, pp. 201–213, 2001.
- [92] TSAI, S. W., *Composites Design*. Think composites, 3rd ed., 1987.
- [93] VALLONS, K., ZONG, M., LOMOV, S. V., and VERPOEST, I., “Carbon composites based on multi-axial multi-ply stitched preforms - part 6. fatigue behaviour at low loads: Stiffness degradation and damage development,” *Composites Part A: Applied Science and Manufacturing*, vol. 38, no. 7, pp. 1633–1645, 2007.
- [94] VANDERPLAATS, G. N., *Numerical Optimization Techniques for Engineering Design*. Colorado Spring, Co.: Vanderplaats Research & Development, Inc., 4th ed., 2005. Chapter 9.
- [95] VOLOVOI, V. V. and HODGES, D. H., “Theory of anisotropic thin-walled beams,” *Journal of Applied Mechanics*, vol. 67, no. 3, pp. 453–459, 2000.
- [96] VOLOVOI, V. V., HODGES, D. H., CESNIK, C. E. S., and POPESCU, B., “Assessment of beam modeling methods for rotor blade applications,” *Mathematical and Computer Modelling*, vol. 33, no. 10-11, pp. 1099–1112, 2001.
- [97] VOLOVOI, V. V., KU, J., and HODGES, D. H., “Coupling global and local aspects of cross-sectional optimization for rotor blades,” in *Proceedings of the 47th AIAA/ASME/ASCE/AHS/ASC Structures, Structural Dynamics and Materials Conference*, vol. 4, (Newport, RI), pp. 2808–2821, American Inst. Aeronautics and Astronautics Inc., Reston, VA 20191-4344, United States, 2006.
- [98] VOLOVOI, V. V., LI, L., KU, J., and HODGES, D. H., “Multi-level structural optimization of composite rotor blades,” in *Proceedings of the 46th AIAA/ASME/ASCE/AHS/ASC Structures, Structural Dynamics, and Materials Conference*, (Austin, Texas), Apr. 18–21, 2005.

- [99] VOLOVOI, V. V., YOON, S., LEE, C.-Y., and HODGES, D. H., “Structural optimization of composite rotor blades,” in *Proceedings of the 45th AIAA/ASME/ASCE/AHS/ASC Structures, Structural Dynamics, and Materials Conference*, (Palm Springs, California), Apr. 19-22, 2004.
- [100] WALSH, J. L., YOUNG, K. C., PRITCHARD, J. I., ADELMAN, H. M., and MANTAY, W. R., “Integrated aerodynamic/dynamic/structural optimization of helicopter rotor blades using multilevel decomposition,” Tech. Rep. 3465, NASA, Jan., 1995.
- [101] WÖRNDLE, R., “Calculation of the cross section properties and the shear stresses of composite rotor blades,” *Vertica*, vol. 6, pp. 111–129, 1982.
- [102] WU, C. F. J. and HAMADA, M., *Experiments: Planning, Analysis, and Parameter Design Optimization*. New York: John Wiley & Sons, Inc., 2000.
- [103] YADAV, D. and VERMA, N., “Buckling of composite circular cylindrical shells with random material properties,” *Composite Structures*, vol. 37, no. 3-4, pp. 385–391, 1997.
- [104] YU, W., *Variational Asymptotic Modeling of Composite Dimensionally Reducible Structures*. Ph.D., Georgia Institute of Technology, 2002.
- [105] YU, W., HODGES, D. H., VOLOVOI, V. V., and CESNIK, C. E. S., “On timoshenko-like modeling of initially curved and twisted composite beams,” *International Journal of Solids and Structures*, vol. 39, no. 19, pp. 5101–5121, 2002.
- [106] YU, W., HODGES, D. H., VOLOVOI, V. V., and HONG, X., “Validation of the variational asymptotic beam sectional analysis (VABS),” *AIAA Journal*, vol. 40, no. 10, pp. 2105–2112, 2002.
- [107] YUAN, K.-A. and FRIEDMANN, P. P., “Aeroelasticity and structural optimization of composite helicopter rotor blades with swept tips,” Tech. Rep. CR 4665, NASA, May, 1995.